Characterization and modelling of sea breeze cooling in coastal cities

By

Yifei Zhou

Thesis
Submitted to Flinders University
for the doctoral degree of

Doctor of Philosophy

College of Science and Engineering

Flinders University of South Australia
August 2022

Table of Contents

Abstract

With the combined effects of climate change and enhanced urban heat island, the intensity and frequency of heatwave events in cities are increasing rapidly over the world. This is deemed to lead to negative effects on environment and society of urban areas, such as restricted growth of vegetations and increased health risks for residents. Therefore, there is an increasing need of improving thermal environment in urban areas. In addition to the traditional mitigation measures such as adding vegetations and the use of high-albedo materials for building surfaces, emphasizes have been placed on the natural cooling sources, such as urban waterbodies and ventilation. The sea breeze, which is a typical mesoscale ventilation process of coastal cities, can significantly change the temperature pattern in coastal areas. However, there is limited understanding of the cooling effects of sea breezes. In this study, I propose to explore the cooling magnitudes of sea breezes and their influencing factors at different spatial scales.

Sea Breeze Cooling Capacity (SBCC) is firstly proposed with the definition being the difference of temperature between a sea breeze day and the average of non-sea breeze days. With this definition, I have displayed the temporal and spatial patterns of SBCC and calculated their associations with environmental variables (weather background, topography and urban structure) using data from the Adelaide urban heat island monitoring network in summer days during December 2010 - March 2013 (Chapter 2). Results show that the SBCC values averaged over all sea breeze days range from 733.9 to 858.7 °C·h per season (from 19.0 to 22.2 °C·h per event) for individual sites in the Adelaide Central Business District, which can primarily be explained by Frontal Area Index (FAI), Terrain Ruggedness Index (TRI), distance towards the coast and temperature prior to the sea breeze onset. Meanwhile, the variability of SBCC among all sea breeze events is significantly related to specific humidity and wind speed. Based on the relationship between urban structure and SBCC, I predicted the potential changes of mean SBCC induced by the projected change of building heights ranging from −195 to 143 °C·h per season (from −5.0 to 3.7 °C·h per event).

I have also evaluated the basic characteristics of sea breeze cooling across the metropolitan Adelaide to investigate the penetration process of this cooling effect (Chapter 3). An inland delaying trend of arrival time (9:29 - 10:36) and an advanced trend of cessation time (18:36 - 16:14) of cooling are revealed. There is also a decreasing trend of SBCC during the penetration with the spatial average SBCC of 21.3 °C·h per event. Hot sea breeze days here are defined as

sea breeze days with maximum temperatures above the 75th percentile of all sea breeze days (32.8 °C). SBCC values are particularly smaller in hot sea breeze days compared to that in other sea breeze days and the contrasts increase when cooling fronts go inland. Correspondently, the penetration distance of sea breeze cooling is estimated to drop from 42 to 29 km from the period of all sea breeze days to hot sea breeze days. This difference can be explained by a higher frequency of synoptic systems with directional flows from east or south-east in hot sea breeze days of Adelaide. Overall, this result is helpful for understanding the whole sea breeze penetration process.

In the analysis of sea breezes across major Australian cities in Chapter 4, a large diversity of sea breeze frequency is found among the five cities (Perth, Adelaide, Melbourne, Brisbane and Sydney), which ranges from 17% to 56%. This contrast is significantly related to the frequency of days with anti-cyclone synoptic types. In Sydney and Brisbane, the characteristics of sea breezes are less significant compared to those of other three cities and this can be explained by complex topography of the two cities. Differences of SBCC exist among the three cities with flat surfaces (Perth, Adelaide and Melbourne). In coastal areas, frequency of days with anti-cyclone systems can explain most of the SBCC variability among these three cities.

In Chapter 5, I have estimated the quantitative effects of urban structure and wind speed on air temperature and thermal comfort in a typical sea breeze day of Adelaide based on ENVI-met. The comparison among 48 scenarios shows the critical roles of building height, canyon orientation and wind speed in shaping urban microclimate during a sea breeze event. Results show a reduction of averaged early afternoon air temperature from 27.16 °C to 26.92 °C with an increase of building height from 4 metres to 12 metres. It is also interesting to note that the mean cooling magnitude induced by increasing wind speed (from 2 m/s to 4 m/s) is negatively related to the averaged building height. With 4-metre buildings, the cooling is 0.28 °C, the corresponding value drops to 0.17 °C with 12-metre buildings. This demonstrates the contrasting aspects of building height in shaping urban thermal environment. On one hand, increasing building height is considered to cool the local environment by providing more shading areas. On the other hand, wind cooling can be weakened with higher buildings.

Declaration

I certify that this thesis does not incorporate without acknowledgment any material previously submitted for a degree or diploma in any university; and that to the best of my knowledge and belief it does not contain any material previously published or written by another person except where due reference is made in the text.

Signed  .

Date 28, Feb, 2022

Acknowledgement

During the period of my PhD study, I have got assistances from many people. The completion of my PhD thesis largely relies on supports and suggestions from them.

Firstly, I am extremely grateful to my major supervisor Prof. Huade Guan. In the early stage of my PHD study, he gave me many chances for field works from different projects, such as the use and installation of eddy-covariance systems and sap flow tools. Thanks to these experiences, I have learned a lot of technical skills in operating experimental tools and equipment. Although most of these skills are not used in my PhD studies, they are helpful for my research career. In addition, his extensive knowledge and deep insights in scientific problems during the academic discussions always inspire me with my research. Overall, Huade has spent a lot of time supervising me and it is helpful for my progress.

Many thanks should also be given to my co-supervisors Okke Batelaan and Craig Simmons. We have meetings every month. Discussions with them are exciting experiences as I not only get useful suggestions from them but also get encouragement when I am not confident enough.

The Adelaide urban heat island network was funded by Government of South Australia, Adelaide City Council, Goyder Institute for Water Research, and South Australia Water Corporation. John Bennett, Cecilia Ewenz, Vinokumar, and Chris Kent made great contributions in collecting the field data. I am grateful to them for their supports for the study. The comments from Prof. Roger Clay and Prof. Jochen Kaempf are extremely important. As assessors for my milestone presentations, they have proposed multiple interesting questions that inspire me. During the final thesis review, they give detailed suggestions on my thesis. I want to give many thanks to my colleges: Na Liu, Zidong Luo, Rose Deng, Ajiao Chen, Xanthia Gleeson and Wenjie Liu, Lanre.Abiodun and the visiting scholars in our research group: Lingli Fan, Jiawen Zhu, Lihui Tian, and Jinmei Zhao. We have worked together many times for field works. Your assistances for my PhD research are essential. The happy time with you is also unforgettable.

Finally, I want to thank China Scholarship Council and Flinders University who provide the funding during my PhD study.

List of Figures

List of Tables

Glossary

Notation (Variables)	Description
CBD	Central Business District
CFD	Computational Fluid Dynamics
DEM	Digital Elevation Model
dT_{max}	Maximum temperature reduction of the sea breeze
dx	Distance towards the coast
FAI	Frontal Area Index
LAD	Leaf Area Density
LAI	Leaf Area Index
LST	Land Surface Temperature
PET	Physiological Equivalent Temperature
q	Specific Humidity
R^2	Coefficient of Determination
RMSE	Root Mean Square Error
SBCC	Sea Breeze Cooling Capacity
SST	Sea Surface Temperature
T_0	Temperature prior to the sea breeze onset
TRI	Terrain Ruggedness Index
UHI	Urban Heat Island
UHIC	Urban Heat Island Circulation
U	Wind Speed

Chapter 1 Introduction

1.1 Research Background

1.1.1 Global warming

Human-induced climate change is mainly characterized by a universal trend of warming and the corresponding changes in climatic systems over the world. The warming magnitude since pre-industrial era can reach 1.5 °C before 2052 (Ogunbode et al., 2020). These changes can pose profound impacts on ecosystems, human health and agricultural production. For example, the unprecedented frequency and intensity of extreme weather events in the first decade of 21st century have been confirmed to be strongly related to global warming (Coumou et al., 2012). Therefore, climate change has become an important social agenda for national governments, academia and the public. Scientific researches on climate change have lasted several decades and most of them focus on the temporal evolutions, spatial differences and the effects on environment and society at different scales.

The widespread warming trend over the world is considered to be resulted from emissions of greenhouse gases from human activities, such as carbon dioxide. During the period of 1750 - 2019, the concentration of carbon dioxide in the atmosphere has increased from 277 ppm to 409.85 ± 0.1 ppm mainly resulted from human activities, such as the use of fossil fuel and deforestation (Friedlingstein et al, 2020). The increased emissions of methane and oxynitride have also been confirmed to contribute to this warming (Kiesgen et al., 2013). With respect to the temporal and spatial changes, heterogeneous patterns of warming trends are detected. At high latitudes of Northern Hemisphere, the magnitudes of temperature increase are larger than areas of the same latitudes in the Southern Hemisphere, which is considered to be caused by the heat uptake of oceans at high latitudes in the Southern Hemisphere (Flato et al., 2001). There are also contrasts of warming between daytime and nighttime and the corresponding differences vary with locations (Solomon, 2007).

An interesting phenomenon is observed from multiple sources during 1998 - 2012 when the increasing trend of air temperature is only 0.05 ± 0.08 °C over the world, much lower than the averaged warming trend over the 53 years of 1970 - 2012. This phenomenon is called the

global warming hiatus (Fyfe et al., 2013). It is particularly reflected in winter of Northern Hemisphere, which is attributed to the changed ocean currents resulted from variations in atmospheric circulations and surface winds (Trenberth et al., 2014). However, the hiatus of warming in a certain period is not rare. During 1900s and 1960s, the warming rates have also decreased (Hegerl et al., 2018). According to the simulations from CMIP5 models, the earth will continue to get hotter by the end of 21st century. Even under the scenarios with controlled greenhouse gas emissions (RCP 4.5), the 40-year change rate of air temperature is still higher than 0.15 °C/decade in the following decades (Smith et al., 2015).

1.1.2 Urban heat island

In addition to climate change which has been described in the last section, residents in urban areas are also exposed to the effects of urban heat island. Urban heat island is a phenomenon that urban areas tend to be warmer than the surrounding rural areas. It is considered to have led to a variety of environmental and social problems. Statistics show that 4.22 billion people lived in urban areas by 2018 and the number is estimated to be 6.6 billion in 2050 (UNPD, 2019). Correspondently, much attention has been given to researches of urban heat island and its effects on local environment in many aspects.

Urban heat island intensity and its temporal and spatial patterns are controlled by multiple factors. Among these factors, much attention has been paid on the land cover inside or around cities. Impervious surfaces are covered by water-resistant materials such as asphalt, concrete and brick. They occupy a large proportion of urban surfaces and play significant roles in affecting urban climate. According to observations in many cities, the percentage of impervious area in the city is positively related to UHI intensity (Yang et al., 2017; Henits et al., 2017). The key roles of vegetations (e.g., trees, grasslands) in cooling air and land surface of urban areas have also been widely investigated (Zhou et al., 2014; Taheri et al., 2016). In addition, the effects of basic characteristics of a city are non-negligible. For example, a remote sensing study in Shanghai demonstrates that the land surface temperature is positively related to population density (Chen et al., 2016). By comparing countries with different levels of development, it is discovered that urban population has a relatively stronger effect on urban heat island at the early stage of urbanization, while the role of gross domestic product (GDP) becomes critical once a certain urbanization level is achieved (Cui et al., 2016). There are also seasonal changes of urban heat island intensity in cities. Normally, UHI intensity is higher in

spring and summer as these seasons are growing seasons of most vegetations. Reduced sensible heat transfer from the surface of relatively strong evapotranspiration can enlarge the temperature difference between rural and urban areas (Zipper et al., 2016).

In heatwave days, distinct intensities of urban heat island have been observed. In some coastal cities, high temperatures in urban areas can lead to intensified secondary circulations and correspondingly reduce the temperature difference between urban and rural areas (Lebassi et al., 2009). Meanwhile, some other researchers have detected enhanced UHI intensity in heatwave events, especially for big cities (Ramamurthy et al., 2017). This is expected to be mainly caused by increased difference of latent heat and absorption of heat by impervious surfaces (e.g., buildings, roads…) between urban and rural areas (He et al., 2020; Li et al., 2015). This strengthened UHI effect can even continue for several days after heatwave episodes, which is confirmed by a simulation study in the metropolitan area of Baltimore and Maryland-Washington, D.C., metropolitan area (Li et al., 2013). Therefore, the potential heat stress can be more severe in cities compared to that in the surrounding rural areas (He et al., 2020).

Combined with global warming, increased UHI magnitudes resulted from the urbanization process have risen the frequency and intensity of heatwave events in urban areas for many countries. For example, increasing trends of extremely high-temperature days from 1955 to 2014 exist in most of the provincial capital cities of China, especially those located in the eastern and southern regions (Li et al., 2020). An increase of ~3 °C in the maximum temperature of the hottest southern Australian heatwaves is also projected by the end of 21st century (Cowan et al., 2014).

1.1.3 Heat effects on environment and society

With the increasing frequency and intensity of heatwaves, the negative effects of heatwaves on natural and urban ecosystems have received much attention. With respect to vegetations, the function of water retention capacity of soil could be destroyed and thus vegetation growth could be worse during heatwaves (Poumadere, et al., 2003). In addition, heatwaves can also affect human health, especially for those living in cities. These effects are primarily embodied in the aspects of sunstroke, cardiovascular disease and excess mortality rate, which have been confirmed by studies over the world. In the Chicago heatwave events of July 1995, 696 excess deaths are reported (Whitman et al., 1997). In Italy, about 20000 excess deaths

were recorded during the 2003 European heatwaves (Kosatsky,2005). In fact, the effects of heatwaves on mortality and morbidity rely on personal basic health condition and lifestyle. Those who live in low socioeconomic status or live by themselves are more likely to suffer. Furthermore, although the maximum air temperatures are relatively lower at high latitudes, studies still show the existence of substantial heat-related health risks in these areas. In the US, the largest impacts of heatwaves on mortality appear in cities with milder summers. This is supposed to be resulted from the shortage of adaptation to extreme heat for these cities (Medina-Ramon et al., 2007). It should also be noted that excessively high temperatures not only affect physical health, but also worsen the mental health of urban residents, which has been reflected in increased suicide rate and hospital admissions for mental, cognitive and behavioural disorders (Hansen et al., 2008; Ajdacic-Gross et al., 2007).

Heatwave events also exert a certain influence on water use and energy demand of a city. In the Adelaide CBD, electricity demand of office buildings is estimated to increase 50% during heatwaves (Guan et al., 2014). The continuous high temperature can even bring about damage to concretes by reducing the strengths and masses of materials, which is not beneficial for the maintenance of road facilities.

The frequency of traffic accidents has also been observed to be tightly linked to excessive high temperature. For example, Park et al. (2021) observed that there is an increase of probability of traffic accidents by about 0.59% for 1 °C rise in daily maximum temperature above the threshold (30 °C) in four major cities of South Korea. This is supposed to be primarily resulted from the deterioration of psychological states at high temperatures. Similar relationships have also been found in other cities of the world (Deschenes et al., 2009).

1.1.4 Mitigation of excessive urban heat

As heatwaves pose threats to urban residents and the society in many aspects, the mitigation of excessive urban heat is particularly important. Among the multiple measures developed, planting vegetation is widely recognized as a simple and efficient approach in cooling air of urban areas. Shading effect of trees is one of the major reasons of this cooling. In summer when leaf area density is the largest in the year, only a small portion of solar radiation can reach the ground surface. Gordon (1986) revealed that a mid-sized tree can reduce the solar radiation by about 80% in sunny days when leaves grow well. The reduced shortwave radiation from this shading effect can mitigate excessive heat of land surfaces and further

contribute to the decreased emission of longwave radiation. In addition to tree shading, evapotranspiration of vegetations also plays roles in cooling air. Evapotranspiration consists of transpiration from the plants and evaporation from soil and leaf surfaces. By strengthening the release of excess radiation budget in the form of water vapor, evapotranspiration can suppress the emission of sensible heat. Based on an on-site measurement in Shenzhen, a significant negative relation between urban heat island and evapotranspiration is presented (Qiu, et al., 2017).

Properties of materials used at road and building surfaces take obvious effects on thermal environment of urban areas. In order to relieve excessive heat, the surfaces should remain relatively cooler to limit the emission of longwave radiation to the air. Light coloured materials generally present higher albedo than deep coloured materials. Consequently, there is a reduction of air temperature due to the less sensible heat flux from the cooler surface. In a measurement in Athens (Greece), the average surface temperature of asphalts pavements with the albedo being 0.12 is about 36 °C, while marble pavements with the albedo being 0.38 present the average temperature of about 28 °C (Gaitani et al., 2017). The proposed replacement of conventional materials by "cool" ones would result in the reduction of maximum air temperature by 1.39 °C at noon of the warmest day in Florina, Greece (Zoras et al., 2014).

In addition to the mitigation measures mentioned above, methods such as decreasing the release of anthropogenic heat and construction of grey infrastructures (facilities for shading) have also been proposed in recent studies. By using multiple solutions such as high-performance insulation layers of external walls and air to air heat ex-changers, Yang et al. (2017) estimated a reduction of the campus anthropogenic heat by up to 22 W/m^2 in the National University of Singapore. In Guangzhou, an analysis demonstrates a decrease of daily mean temperature by 0.63 °C and 0.26 °C for squares and parks respectively when grey infrastructures are configurated (Jing et al., 2020).

1.1.5 Natural cooling resources

In addition to the application of mitigation measures of urban heat island, it should be noted that land covers and weather characteristics inside or near cities can be potential cooling sources. Understanding their roles in coping with heat stress in urban areas is important as they can be helpful for the decision making on the utilization of these natural resources in

urban design. In some cities, forests are located inside the metropolitan area and they are expected to provide cooling for these cities. From a study in Nanjing, a reduction of air temperature by more than 8 °C is observed in the surrounding area of an urban forest. The temperature gradually increases with the increasing outward distance from the forest (Yin et al., 2022). Forests with dense vegetations are found to show stronger cooling ability than that with sparse vegetations (Jonsson, 2004).

Wind from surrounding areas is another potential cooling source. The negative relation between wind speed and UHI has been reported with different urban structures (Morris et al., 2001). It is also observed that when wind speed exceeds a threshold, the UHI would completely disappear. With observations, the thresholds are estimated to be 11.1 m/s at 1.5-metre height in Seoul and 12 m/s at 6-metre height in London (Park et al., 1986, Kolokotroni et al., 2008). In addition, the increased cloud coverage of sky has been found to mitigate UHI at different magnitudes (Yow et al., 2006).

Water bodies include rivers, lakes, seas, reservoirs and wetlands and a large number of them are located inside or near cities. Mainly induced by a large amount of evaporation from water surfaces and heat transfer between air above cooler water surfaces and that above warmer land areas, water bodies are regarded as important cooling sources of urban areas. In an observation analysis of three lakes in the city of Chongqing, China, Li et al. (2014) concluded that the cooling magnitude near the lakeside can be up to 3 °C. In Tel Aviv, Israel (Csa), a small pond with an area of only 40,000 m^2 has been observed to cool the ambient air by approximately 1 °C at midday (Saaroni et al., 2003). This indicates that cooling power can be even generated from a very small water surface. It has also been found that the cooling effect varies with time. According to the observation in Sheffield, UK, the maximum cooling magnitude of water body is estimated to be 2 °C, which appears at noon. However, during nighttime it is much decreased (Hathway et al., 2012). There are also differences in cooling among different types of water bodies. A comparative analysis of water cooling in Shanghai demonstrated that the cooling intensity of lakes are much stronger than that of rivers of similar sizes (Du et al., 2016). In addition, the effects of characteristics and locations of water bodies on the heat mitigation have received much attention. According to the ASTER images of ten lakes/reservoirs and five rivers in Beijing, Sun et al. (2012) demonstrated a negative correlation between land shape index (LSI) and cooling of water bodies. The distance of a water body towards the city centre is also shown to affect the cooling effect on the city. Syafii et al. (2017) revealed a positive relation between the sizes of water bodies and cooling potential in a simulation study. It is

worth noting that water bodies do not always provide cooling. For example, a warming of more than 5 ° C was identified in the afternoon near a river of Amsterdam (Klok et al., 2019). During the nighttime, water surfaces can be warmer than the overlying air. This can lead to an enhanced urban heat island, particularly in later summer (Steeneveld et al., 2014; Van Hove et al., 2015). Therefore, it is still questionable whether water bodies can provide the cooling effect with respect to the average over a day.

For a coastal city, the sea located nearby is a huge waterbody and can be a potential cooling source primarily because of the cooling effect of sea breezes. Investigations on the sea breeze characteristics have become the focus of many researchers as they can be helpful in mitigating urban heat.

1.1.6 Sea breezes

Observations of sea breezes have a history of more than two thousand years (Miller et al., 2003). In recent decades, precise measurements of sea breeze characteristics have been performed with the help of measuring equipment, such as meteorological balloons, meteorological towers and weather radars. So far, sea breeze observations have been performed in many coastal areas over the world, primarily in Australia, East Asia, Europe and North America. Initially, the observations focused on dynamic structures and thermal properties of sea breezes. Combining thermographs and meteorological balloons, the vertical cross-sections of wind fields during sea breeze events were investigated in north-eastern US (Fisher, 1960). Finkele et al. (1995) observed completed land-sea breeze circulations in the southern part of Australia. It is revealed that the circulation is asymmetrical, and the sea breeze component is much stronger than the land breeze one. With the help of the Doppler radar, Banta et al. (1993) observed the details on the horizontal variability of the sea breeze resulting from inland topography. It is found that the topography leads to an asymmetry of the sea breeze between land and sea and the persistence of south-westerly airflow into later hours.

The interaction between land-sea breezes and other types of synoptic systems with various spatial scales can lead to complex weather conditions. For example, if a city is located in the coastal area, the urban heat island can strengthen sea breeze intensity in daytime and decrease land breeze intensity in nighttime (Lin et al., 2008). In addition, humidification of the low-level air can be detected when different sea breeze systems converge. This could promote the

possibility of convective rainfall events (Comin et al., 2015). Complicated topography in the coastal area may generate other thermally driven breezes which may affect the structures of sea breezes, such as the river breeze. In eastern Florida, the convergence of sea breezes with river breezes from Indian River which is parallel to the coast is helpful in formulating convergence zone near the riverbank (Zhong et al., 1992). In addition, if a sea-facing hillside is near the coast, the uphill airflow can contribute to the inland penetration of the sea breeze, and consequently intensify the sea breeze circulation. In contrast, if hills are in shadows, the intensities of sea breezes are weakened (Mahrer et al., 1977; Miller et al., 2003). For urban canyons with different structures, the directions and intensities of airflows are also shaped by the widths and depths of canyons. For example, when successive buildings are closely placed, there is a stable circulatory vortex inside the canyon by momentum transfer and the bulk of the airflow cannot go into the canyon. When there are large spaces between building blocks, the flow fields of consecutive buildings are relatively isolated (Erell et al., 2012).

1.1.7 Sea breeze cooling

An important role of sea breezes is the cooling of coastal areas. This happens because of the contrast between air temperature over sea surfaces and that over coastal land areas during sea breezes. It has been confirmed by a variety of studies of coastal cities based on observations and simulations. Sakakibara et al. (2005) found that inland cities present higher UHI intensity than coastal cities, which can be attributed to the infiltration of cooler sea breezes. On the eastern coast of central Greece, a temperature reduction of 4 °C was observed during a sea breeze event in summer (Papanastasiou et al., 2010). Meanwhile, the temperature of the sea breeze has been found to increase as the wind blows inland (Katayama et al.,1991), which confirms the interaction of the air above the sea with that above the warmer land. Wind characteristics are important factors in influencing cooling intensity of sea breezes. In Hania, Greece, air temperature is approximately 26 °C with westerly sea breezes, while it increases to 30 °C with sea breezes of the same wind speed conditions from the north primarily because of the resistance from the old city's walls (Kolokotsa et al., 2009). There is also a significant negative relation between wind speed and air temperature in sea breeze events, which has been confirmed in Sydney (He et al., 2020). With respect to the land covers of coastal areas, Katayama et al. (1991) observed that air temperatures above river surfaces are significantly lower than those above streets. The gaps are narrowed downstream of the sea

breeze penetration path. This shows that open space can improve the penetration of sea breezes and promote the corresponding cooling effects.

Although many observation and simulation studies have explored the temperature patterns during sea breeze events, there is not particular research that focuses on the systematic analysis of the cumulative magnitudes of sea breeze cooling effects and their influencing factors at different spatial scales.

1.2 Objectives

Most Australian cities are in coastal areas and the occurrences of sea breezes have been detected in these cities with different frequencies. Particularly, the cooling effects of sea breezes can mitigate heat stress during hot days. Therefore, it is important to have a better understanding of the cooling magnitudes of sea breezes and their influencing factors at different spatial scales.

Adelaide is near St Vincent Gulf to the west and the topography of this city is relatively flat. The characteristics of sea breezes are typical in this city. A a metric of sea breeze cooling capacity is developed and used to analyse its temporal and spatial patterns of sea breeze cooling effect based on observations. In addition, the comparisons of sea breezes and their cooling magnitudes of Adelaide with those of other Australian cities are also performed to have a more comprehensive understanding of sea breeze cooling in different cities. Specific scientific questions in this study include:

(1) What is the magnitude of sea breeze cooling in the Adelaide CBD? What are the roles of urban structure and meteorological variables on it? Here I hypothesize that the cooling ability of sea breezes in an urban area is negatively correlated with the average building height and positively dependent on the diversity of building heights.
(2) How does sea breeze cooling penetrate inside the metropolitan area of Adelaide? What is the difference of the behaviour of sea breeze cooling penetration between hot sea breeze days and the average of all sea breeze days?
(3) What are the main factors that lead to the diversity of sea breeze frequency and sea breeze cooling magnitudes of coast areas among cities?
(4) How do building height, canyon orientation and wind speed affect air temperature and thermal comfort during sea breezes at micro-scale? How does urban structure affect wind cooling during sea breezes?

1.3 Thesis structure

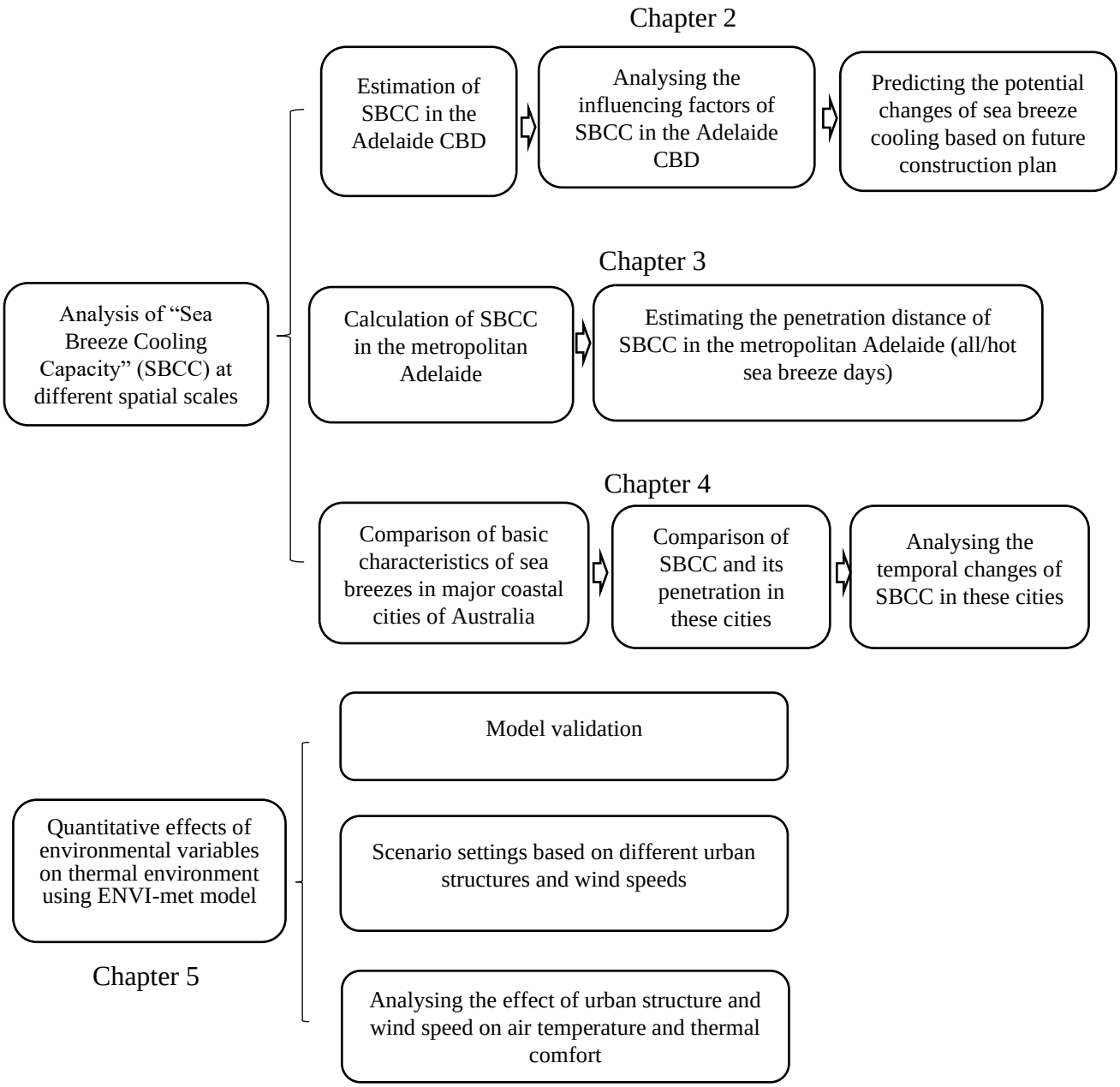

In Chapter 2, the Sea Breeze Cooling Capacity (SBCC) is firstly defined as the metric for quantifying the cumulative cooling effect of the sea breeze. Then, the temporal and spatial patterns of sea breeze cooling in the Adelaide CBD are analysed and attributed. After establishing the relationship between building height characteristics and sea breeze cooling, I also estimate the potential changes in sea breeze cooling with the future development plan of

the Adelaide CBD. Results in this chapter answer Question (1) in Sect. 1.2. The hypothesis of this question is also tested in this Chapter.

In Chapter 3, I focus on the whole metropolitan area of Adelaide. Firstly, the diurnal temperature patterns of selected sites in an example of sea breeze day are investigated to demonstrate the attenuation process of sea breeze cooling along the penetration path. Then, I also estimate the penetration distance of sea breeze cooling on the basis of the relation between SBCC and distance towards the coast. The difference between SBCC pattern of heatwave days and that of all sea breeze days is also analysed and attributed. Results in this chapter answer Question (2) in Sect. 1.2.

In Chapter 4, five major coastal cities in Australia are concerned. I firstly compare and attribute the frequencies of sea breezes of these cities. With the analysis of wind patterns during sea breezes days, three cities with regular sea breeze characteristics are selected for the further analysis of sea breeze cooling. For these three cities, I investigate the spatial patterns and penetration distances of SBCC. Finally, the temporal trends of SBCC and their relations with large-scale synoptic patterns are analysed. Results in this chapter answer Question (3) in Sect. 1.2.

In Chapter 5, ENVI-met, a commonly used micro-climate model, is utilized to simulate the quantitative effects of building height, canyon orientation and background wind speed on air temperatures and thermal comfort levels inside an urban area at micro-scale. The cooling induced by increased wind speed is also investigated and attributed. Results in this chapter answer Question (4) in Sect. 1.2.

References

Ajdacic-Gross V, Lauber C, Sansossio R, Bopp M, Eich D, Gostynski M, Gutzwiller F, Rössler W. Seasonal associations between weather conditions and suicide—evidence against a classic hypothesis. American journal of epidemiology. 2007 Mar 1;165(5):561-9.

Banta RM, Olivier LD, Levinson DH. Evolution of the Monterey Bay sea-breeze layer as observed by pulsed Doppler lidar. Journal of Atmospheric Sciences. 1993 Dec 15;50(24):3959-82.

Cao X, Onishi A, Chen J, Imura H. Quantifying the cool island intensity of urban parks using ASTER and IKONOS data. Landscape and urban planning. 2010 Jun 30;96(4):224-31.

Change IP. Climate change 2007: the physical science basis. Agenda. 2007 May 31;6(07):333. New York, USA: Cambridge University Press, 2007.

Chen L, Jiang R, Xiang WN. Surface heat island in Shanghai and its relationship with urban development from 1989 to 2013. Advances in Meteorology. 2016 Jan 1;2016.

Comin AN, Miglietta MM, Rizza U, Acevedo OC, Degrazia GA. Investigation of sea-breeze convergence in Salento Peninsula (Southeastern Italy). Atmospheric Research. 2015 Jun 15;160:68-79.

Coumou D, Rahmstorf S. A decade of weather extremes. Nature climate change. 2012 Jul;2(7):491-6.

Coumou D, Robinson A. Historic and future increase in the global land area affected by monthly heat extremes. Environmental Research Letters. 2013 Aug 14;8(3):034018.

Cowan T, Purich A, Perkins S, Pezza A, Boschat G, Sadler K. More frequent, longer, and hotter heat waves for Australia in the twenty-first century. Journal of Climate. 2014 Aug 1;27(15):5851-71.

Cui Y, Xu X, Dong J, Qin Y. Influence of urbanization factors on surface urban heat island intensity: A comparison of countries at different developmental phases. Sustainability. 2016 Aug;8(8):706.

Deschenes O, Moretti E. Extreme weather events, mortality, and migration. The Review of Economics and Statistics. 2009 Nov 1;91(4):659-81.

Du H, Cai W, Xu Y, Wang Z, Wang Y, Cai Y. Quantifying the cool island effects of urban green spaces using remote sensing Data. Urban Forestry & Urban Greening. 2017 Oct 1;27: 24-31.

Du H, Song X, Jiang H, Kan Z, Wang Z, Cai Y. Research on the cooling island effects of water body: A case study of Shanghai, China. Ecological indicators. 2016 Aug 1;67: 31-8. Flato GM, Boer GJ. Warming asymmetry in climate change simulations. Geophysical research letters. 2001 Jan 1;28(1):195-8.

Erell, E., Pearlmutter, D., & Williamson, T. (2012). Urban microclimate: designing the spaces between buildings. Routledge.

Finkele K, Hacker JM, Kraus H, Byron-Scott RA. A complete sea-breeze circulation cell derived from aircraft observations. Boundary-layer meteorology. 1995 Mar;73(3):299-317.

Friedlingstein P, O'sullivan M, Jones MW, Andrew RM, Hauck J, Olsen A, Peters GP, Peters W, Pongratz J, Sitch S, Le Quéré C. Global carbon budget 2020. Earth System Science Data. 2020 Dec 11;12(4):3269-340.

Fyfe JC, Gillett NP, Zwiers FW. Overestimated global warming over the past 20 years. Nature Climate Change. 2013 Sep;3(9):767-9.

Gaitani N, Burud I, Thiis T, Santamouris M. High-resolution spectral mapping of urban thermal properties with Unmanned Aerial Vehicles. Building and Environment. 2017 Aug 15;121: 215-24.

Guan H, Soebarto V, Bennett J, Clay R, Andrew R, Guo Y, Gharib S, Bellette K. Response of office building electricity consumption to urban weather in Adelaide, South Australia. Urban Climate. 2014 Dec 1;10: 42-55.

Hansen A, Bi P, Nitschke M, Ryan P, Pisaniello D, Tucker G. The effect of heat waves on mental health in a temperate Australian city. Environmental health perspectives. 2008 Oct;116(10):1369-75.

Hathway EA, Sharples S. The interaction of rivers and urban form in mitigating the Urban Heat Island effect: A UK case study. Building and Environment. 2012 Dec 1;58: 14-22.

He BJ, Ding L, Prasad D. Outdoor thermal environment of an open space under sea breeze: A mobile experience in a coastal city of Sydney, Australia. Urban Climate. 2020 Mar 1;31: 100567.

He X, Wang J, Feng J, Yan Z, Miao S, Zhang Y, Xia J. Observational and 13odelling study of interactions between urban heat island and heatwave in Beijing. Journal of cleaner production. 2020 Feb 20;247: 119169.

Heaviside C, Vardoulakis S, Cai XM. Attribution of mortality to the urban heat island during heatwaves in the West Midlands, UK. Environmental health. 2016 Dec;15(1):49-59.

Hegerl GC, Brönnimann S, Schurer A, Cowan T. The early 20th century warming: Anomalies, causes, and consequences. Wiley Interdisciplinary Reviews: Climate Change. 2018 Jul;9(4):e522.

Heisler GM. Effects of individual trees on the solar radiation climate of small buildings. Urban ecology. 1986 Jun 1;9(3-4):337-59.

Henits L, Mucsi L, Liska CM. Monitoring the changes in impervious surface ratio and urban heat island intensity between 1987 and 2011 in Szeged, Hungary. Environmental monitoring and assessment. 2017 Feb;189(2):1-3.

Jonsson P. Vegetation as an urban climate control in the subtropical city of Gaborone, Botswana. International Journal of Climatology: A Journal of the Royal Meteorological Society. 2004 Aug;24(10):1307-22.

Katayama T, Hayashi T, Shiotsuki Y, Kitayama H, Ishii A, Nishida M, Tsutsumi JI, Oguro M. Cooling effects of a river and sea breeze on the thermal environment in a built-up area. Energy and buildings. 1991 Jan 1;16(3-4):973-8.

Kiesgen de_Richter R, Ming T, Caillol S. Fighting global warming by photocatalytic reduction of CO2 using giant photocatalytic reactors. Renewable and Sustainable Energy Reviews. 2013 Mar 1;19:82-106.

Klok, L., Rood, N., Kluck, J., & Kleerekoper, L. (2019). Assessment of thermally comfortable urban spaces in Amsterdam during hot summer days. International journal of biometeorology, 63(2), 129-141.Kolokotroni M, Giridharan R. Urban heat island intensity in London: An investigation of the impact of physical characteristics on changes in outdoor air temperature during summer. Solar energy. 2008 Nov 1;82(11):986-98.

Kolokotsa D, Psomas A, Karapidakis E. Urban heat island in southern Europe: The case study of Hania, Crete. Solar Energy. 2009 Oct 1;83(10):1871-83.

Kosatsky T. The 2003 European heat waves. Eurosurveillance. 2005 Jul 1;10(7):3-4.

Lebassi B, González J, Fabris D, Maurer E, Miller N, Milesi C, Switzer P, Bornstein R. Observed 1970 – 2005 cooling of summer daytime temperatures in coastal California. Journal of Climate. 2009 Jul 1;22(13):3558-73.

Li C, Yu CW. Mitigation of urban heat development by cool island effect of green space and water body. InProceedings of the 8th International Symposium on Heating, Ventilation and Air Conditioning 2014 (pp. 551-561). Springer, Berlin, Heidelberg.

Li D, Bou-Zeid E. Synergistic interactions between urban heat islands and heat waves: The impact in cities is larger than the sum of its parts. Journal of Applied Meteorology and Climatology. 2013 Sep;52(9):2051-64.

Li, D., Sun, T., Liu, M., Yang, L., Wang, L., & Gao, Z. (2015). Contrasting responses of urban and rural surface energy budgets to heat waves explain synergies between urban heat islands and heat waves. Environmental Research Letters, 10(5), 054009.

Li J, Wang Y, Ni Z, Chen S, Xia B. An integrated strategy to improve the microclimate regulation of green-blue-grey infrastructures in specific urban forms. Journal of Cleaner Production. 2020 Oct 20;271:122555.

Li K, Amatus G. Spatiotemporal changes of heat waves and extreme temperatures in the main cities of China from 1955 to 2014. Natural Hazards and Earth System Sciences. 2020 Jul 2;20(7):1889-901.

Lin CY, Chen F, Huang JC, Chen WC, Liou YA, Chen WN, Liu SC. Urban heat island effect and its impact on boundary layer development and land – sea circulation over northern Taiwan. Atmospheric Environment. 2008 Jul 1;42(22):5635-49.

Mahrer, Y & Pielke, RA 1977. The Effects of Topography on Sea and Land Breezes in a Two-

Dimensional Numerical Model. Monthly Weather Review, 105, 1151-1162,DOI:

10.1175/1520-0493(1977)105<1151:teotos>2.0.co;2.

Medina-Ramon M, Schwartz J. Temperature, temperature extremes, and mortality: a study of acclimatisation and effect modification in 50 US cities. Occupational and environmental medicine. 2007 Dec 1;64(12):827-33.

Miller ST, Keim BD, Talbot RW, Mao H. Sea breeze: Structure, forecasting, and impacts. Reviews of geophysics. 2003 Sep;41(3).

Morris CJ, Simmonds I, Plummer N. Quantification of the influences of wind and cloud on the nocturnal urban heat island of a large city. Journal of Applied Meteorology and Climatology. 2001 Feb 1;40(2):169-82.

Ngarambe J, Oh JW, Su MA, Santamouris M, Yun GY. Influences of wind speed, sky conditions, land use and land cover characteristics on the magnitude of the urban heat island in Seoul: An exploratory analysis. Sustainable Cities and Society. 2021 Aug 1;71:102953.

Ogunbode CA, Doran R, Böhm G. Exposure to the IPCC special report on 1.5 C global warming is linked to perceived threat and increased concern about climate change. Climatic Change. 2020 Feb;158(3):361-75.

Oke TR. Initial guidance to obtain representative meteorological observations at urban sites.

Papanastasiou DK, Melas D, Bartzanas T, Kittas C. Temperature, comfort and pollution levels during heat waves and the role of sea breeze. International journal of biometeorology. 2010 May;54(3):307-17.

Park HS. Features of the heat island in Seoul and its surrounding cities. Atmospheric Environment (1967). 1986 Jan 1;20(10):1859-66.

Park J, Choi Y, Chae Y. Heatwave impacts on traffic accidents by time-of-day and age of casualties in five urban areas in South Korea. Urban Climate. 2021 Sep 1;39:100917.

Poumadere M, Mays C, Le Mer S, Blong R. The 2003 heat wave in France: dangerous climate change here and now. Risk Analysis: an International Journal. 2005 Dec;25(6):1483-94.

Qiu GY, Zou Z, Li X, Li H, Guo Q, Yan C, Tan S. Experimental studies on the effects of green space and evapotranspiration on urban heat island in a subtropical megacity in China. Habitat international. 2017 Oct 1;68:30-42.

Ramamurthy P, Bou‐Zeid E. Heatwaves and urban heat islands: a comparative analysis of multiple cities. Journal of Geophysical Research: Atmospheres. 2017 Jan 16;122(1):168-78.

Saaroni H, Ziv B. The impact of a small lake on heat stress in a Mediterranean urban park: the case of Tel Aviv, Israel. International journal of Biometeorology. 2003 May;47(3):156-65.

Stocker T, editor. Climate change 2013: the physical science basis: Working Group I contribution to the Fifth assessment report of the Intergovernmental Panel on Climate Change. Cambridge university press; 2014 Mar 24.

Steeneveld, G. J., Koopmans, S., Heusinkveld, B. G., & Theeuwes, N. E. (2014). Refreshing the role of open water surfaces on mitigating the maximum urban heat island effect. Landscape and Urban Planning, 121, 92-96.

Syafii NI, Ichinose M, Kumakura E, Jusuf SK, Chigusa K, Wong NH. Thermal environment assessment around bodies of water in urban canyons: A scale model study. Sustainable cities and society. 2017 Oct 1;34:79-89.

Taheri Shahraiyni H, Sodoudi S, El-Zafarany A, Abou El Seoud T, Ashraf H, Krone K. A comprehensive statistical study on daytime surface urban heat island during summer in urban areas, case study: Cairo and its new towns. Remote Sensing. 2016 Aug;8(8):643.

Tan J, Zheng Y, Tang X, Guo C, Li L, Song G, Zhen X, Yuan D, Kalkstein AJ, Li F, Chen H. The urban heat island and its impact on heat waves and human health in Shanghai. International journal of biometeorology. 2010 Jan;54(1):75-84.

Trenberth KE, Fasullo JT, Branstator G, Phillips AS. Seasonal aspects of the recent pause in surface warming. Nature Climate Change. 2014 Oct;4(10):911-6.

United Nations, Department of Economic and Social Affairs, Population Division. World Urbanization Prospects: the 2018 Revision. 2019

Van Hove, L. W. A., Jacobs, C. M. J., Heusinkveld, B. G., Elbers, J. A., Van Driel, B. L., & Holtslag, A. A. M. (2015). Temporal and spatial variability of urban heat island and thermal comfort within the Rotterdam agglomeration. Building and Environment, 83, 91-103.

Whitman S, Good G, Donoghue ER, Benbow N, Shou W, Mou S. Mortality in Chicago attributed to the July 1995 heat wave. American Journal of public health. 1997 Sep;87(9):1515-8.

Yang C, He X, Yan F, Yu L, Bu K, Yang J, Chang L, Zhang S. Mapping the influence of land use/land cover changes on the urban heat island effect—A case study of Changchun, China. Sustainability. 2017 Feb;9(2):312.

Yang J, Tham KW, Lee SE, Santamouris M, Sekhar C, Cheong DK. Anthropogenic heat reduction through retrofitting strategies of campus buildings. Energy and buildings. 2017 Oct 1;152:813-22.

Yin, S., Peng, L. L., Feng, N., Wen, H., Ling, Z., Yang, X., & Dong, L. (2022). Spatial-temporal pattern in the cooling effect of a large urban forest and the factors driving it. Building and Environment, 209, 108676.

Yow DM, Carbone GJ. The urban heat island and local temperature variations in Orlando, Florida. Southeastern geographer. 2006 Nov 1;46(2):297-322.

Yu K, Chen Y, Wang D, Chen Z, Gong A, Li J. Study of the seasonal effect of building shadows on urban land surface temperatures based on remote sensing data. Remote sensing. 2019 Jan;11(5):497.

Zhong S, Takle ES. An observational study of sea-and land-breeze circulation in an area of complex coastal heating. Journal of Applied Meteorology and Climatology. 1992 Dec;31(12):1426-38.

Zhou W, Qian Y, Li X, Li W, Han L. Relationships between land cover and the surface urban heat island: seasonal variability and effects of spatial and thematic resolution of land cover data on predicting land surface temperatures. Landscape ecology. 2014 Jan;29(1):153-67.

Zipper SC, Schatz J, Singh A, Kucharik CJ, Townsend PA, Loheide SP. Urban heat island impacts on plant phenology: intra-urban variability and response to land cover.

Zoras S, Tsermentselis A, Kosmopoulos P, Dimoudi A. Evaluation of the application of cool materials in urban spaces: A case study in the centre of Florina. Sustainable Cities and Society. 2014 Oct 1;13:223-9.

Chapter 2 Sea breeze cooling capacity and its influencing factors in a city centre

Abstract

The sea breeze is a common phenomenon in coastal cities, but its cooling effect has not been well investigated. In this research, I firstly propose a metric of sea breeze cooling capacity (SBCC) to quantify the cooling effect of sea breezes in a coastal city, Adelaide, Australia. Based on data from the Adelaide urban heat island monitoring network in 2010 – 2013, I reveal the temporal and spatial patterns of SBCC in summer days in the Adelaide Central Business District (CBD) and examine their associations with environmental variables. The results show that the variability of SBCC among sea breezes events is explained by specific humidity and wind speed, while the spatial variability of SBCC is explained by distance towards the coast, frontal area index (FAI), terrain ruggedness index (TRI) and temperature prior to the sea breeze onset. Specifically, SBCC is negatively correlated with FAI and positively correlated with TRI. Future development of high-rise buildings in the Adelaide CBD can lead to changes in both FAI and TRI. It is estimated that the projected building development in Adelaide may cause a change of SBCC ranging from −195 to 143 °C·h over an average summer.

In the thesis, this chapter makes the contribution on the quantification and attribution of sea breeze cooling in high-density urban areas, taking the Adelaide CBD as an example. The major component in Chapter 2 is already published in 'Building and Environment':

Zhou Y, Guan H, Huang C, Fan L, Gharib S, Batelaan O, Simmons C. Sea breeze cooling capacity and its influencing factors in a coastal city. Building and Environment. 2019 Dec 1;166:106408. *https://doi.org/10.1016/j.buildenv.2019.106408*

Author contribution:

Zhou Y performed the analysis and wrote the paper. Guan H conceived the analysis. Huang C and Gharib S contributed to the data collection and data analysis. Fan L contributed to the interpretation of the results. Batelaan O and Simmons C contribute to review the paper.

2.1 Introduction

Urban heat island (UHI) is a phenomenon in which the urban area tends to be warmer than its surrounding rural area. The mechanisms leading to UHI have been well investigated and are largely understood (Oke, 2006). UHI can cause multiple problems, particularly in a warming climate. For example, previous studies have shown that energy consumption for summer cooling is temperature dependent (Guan et al., 2014; Lowe, 2016). According to a study in the city centre of Tokyo, an increase of peak-time electricity consumption used for cooling can be up to 6% when the outdoor environment warms up by 1 ℃ (Kikegawa et al., 2003). Thus, UHI can lead to an increasing demand for energy. In addition, urban heat island exacerbates heatwaves which reduce human comfort level and health (Ma et al., 2011; Patz et al., 2005).

Multiple ways of mitigating urban heat island effects have been proposed and undertaken. These solutions include modification of land surface albedo (Synnefa et al., 2007), increasing vegetation cover (Sugawara et al., 2016; Jamei et al., 2016) and enhancing urban ventilation (Takebayashi, 2015). Among them, the idea of urban ventilation utilizes cooler wind from surrounding areas to mitigate urban heat. Common environmental resources for urban ventilation include land and sea breezes, mountain and valley winds, and cool air flowing from parks and green areas (Takebayashi et al., 2015; Gunawardena et al.,2017).

In coastal cities throughout the world, the sea breeze is a widespread phenomenon. Sea breezes happen mostly on clear days when there is no significant synoptic wind. Because of different specific heat capacity of land and sea, there is usually a temperature contrast between the two sides: land warms up stronger than sea during the daytime. This difference causes a pressure gradient that makes the low-level marine air move towards the land. The inland penetration distances of sea breezes vary and can be up to 200 km in mid-latitudes (Simpson, 1994). Sea breezes can change the atmospheric conditions on land, including initializing storms, increasing moisture, changing air quality, and mitigating the urban heat island (Grossi et al., 2000; Kala et al, 2011; Baker et al., 2001).

Previous studies have investigated the effects of urban structure on the characteristics of sea breeze circulation in coastal cities (Shen et al., 2018; Varquez et al., 2015; Cenedese et al., 2003). Specifically, Chen et al. demonstrated that the stagnation of sea breeze circulation tended to occur in Houston (Chen et al., 2011). Quantitatively, Wong et al. used the concept of frontal area index to map urban horizontal ventilation paths and validate the usefulness of the frontal area index in Hong Kong (Wong et al., 2010). Other studies showed that roughness and shape of the urban area had impacts on sea breeze intensity (Thompson et al., 2007; Martilli et al., 2003). In many cities over the world, construction of high-rise buildings is underway. Such development can have potential impacts on urban ventilation. Therefore, investigating the potential influences of urban construction on sea breezes has significant implications, especially in understanding the sea breeze cooling effect in urban areas.

Several studies have investigated the effects of sea breezes on temperature inside cities. Papanastasiou et al. demonstrated that sea breeze development led to a maximum temperature reduction of 4 °C in Greek cities (Papanastasiou et al., 2010). In Japan, Sasaki et al. used Weather Research and Forecasting Model to map the distribution of temperature during sea breeze events which appeared to be helpful for mitigating urban warming in the coastal area (Sasaki et al., 2018). However, the effect of sea breezes on cooling is still poorly understood. Firstly, previous studies only focused on maximum temperature reduction rather than cumulative temperature reduction. Like the metric of cooling degree-days with the unit of °C-day, cumulative temperature reduction represents the cumulative difference between real temperature and a prescribed temperature curve during a certain period. This is important for estimating the changes in energy consumption (Emmanuel et al., 2006; Masuda et al., 2005; Katayama et al., 1991). For example, by combining meteorological data and population data, a monthly aggregated model has been applied for estimating variations in electricity consumption induced by climate change in eight energy-intensive states of the US (Sailor, 2001). Secondly, it is not well understood what factors significantly influence sea breeze cooling inside a city and how much the influence is. To be specific, there is no study that applies 3D building data to explore and explain the sea breeze cooling effect. Generally, it is supposed that the sea breeze cooling effect decreases as building heights increase. However, the diversity of building heights can also be regarded as a positive factor for cooling as the vertical convection caused by diverse building heights can enhance land surface cooling (Allegrini et al., 2017). Therefore, I hypothesize that the cooling ability of sea breezes in an urban area is negatively correlated with average building height and positively dependent on

the diversity of building heights. Adelaide is a typical coastal city where daytime temperature distribution is strongly affected by sea breezes in summer (Guan et al., 2016). To fill research gaps, I propose a new metric to quantify the cumulative cooling effect of the sea breeze and test this hypothesis in this study, taking Adelaide as an example. The research objectives are: (1) to propose a new metric to quantify sea breeze cooling effect and explore its spatial distribution in the Adelaide Central Business District (CBD); (2) to investigate the influencing factors of sea breeze cooling in this city; (3) to evaluate the potential effect of urban development on sea breeze cooling.

2.2 Sea breeze cooling capacity

In order to quantify the cooling ability of sea breezes, I need to estimate the difference between observed temperature pattern of each sea breeze day and that of sea breeze-free days during a similar weather condition, that is to say, how much the temperature would increase if there is no sea breeze during a sea breeze day. For this purpose, a reference temperature curve and an adjusted reference temperature curve are proposed to be used. They are plotted according to the temperature observations in days without sea breezes (Gharib, 2017).

The reference temperature curve is assumed to be the diurnal temperature pattern of the corresponding month averaged by days when there are no sea breeze events and the diurnal temperature ranges are larger than 6 °C. Here a diurnal pattern is any cycle that recurs every 24 hours. By doing so, I assume that the reference curve represents the typical pattern of temperature time course of a sea breeze day, particularly during daytime when the curve is used to quantify the sea breeze cooling effect. The threshold of 6 °C is set based on the minimum diurnal range of sea breeze days in order to exclude the effects of other meteorological variables (e.g., rain, cloud …) on air temperature in sea breeze-free days of Adelaide. For other cities, this threshold should be adjusted.

For different sea breeze days, the initial temperatures before the sea breeze onset time vary. Thus, the reference temperature curve needs to be adjusted to match the initial temperature when the temperature starts to drop, and consequently I derive the adjusted reference temperature curve (Figure 2.1).

The difference between the observed temperature and the adjusted reference temperature curve during the sea breezes tells the sea breeze cooling capacity (SBCC). SBCC (°C·h) is

defined as the product of sea breeze cooling and the cooling duration (the shaded area in Figure 2.1). The calculation is described in Eq. (2.1).

$$\mathrm{SBCC} = REF - OBS \tag{2.1}$$

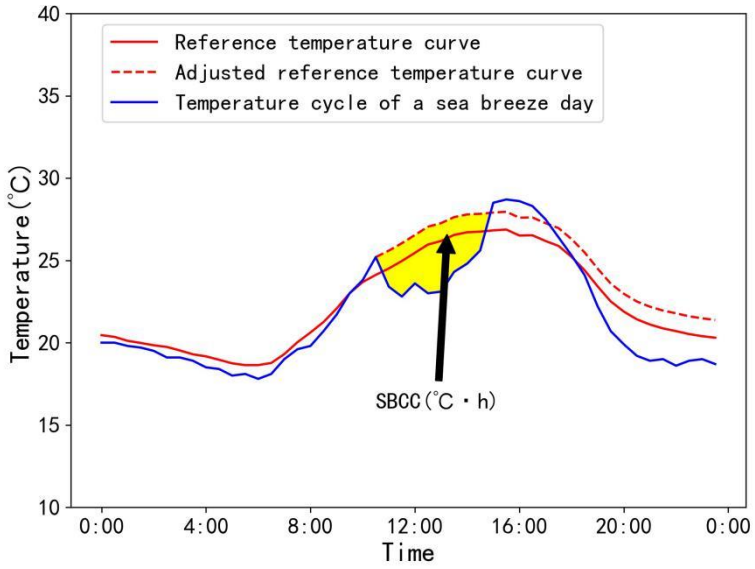

Figure 2. 1 Illustration of the reference temperature curve, adjusted reference temperature curve and diurnal temperature cycle, respectively at Corner Halifax/King William (site 8) of Adelaide urban heat island monitoring network in an example of sea breeze day (16_{th}, Feb, 2012). The yellow shaded part represents the sea breeze cooling capacity.

where *REF* is the time integral of the estimated adjusted reference curve of temperature and *OBS* is the time integral of the curve of observed temperature. They are defined by Eqs. (2.2) and (2.3):

$$REF = \sum_{i=2}^{n} \frac{(T_{ref\,(i-1)} + T_{ref\,(i)}) \times \Delta t}{2} \tag{2.2}$$

$$OBS = \sum_{i=2}^{n} \frac{(T_{obs(i-1)} + T_{obs(i)}) \times \Delta t}{2} \quad (2.3)$$

where $T_{ref(i)}$ and $T_{obs(i)}$ are temperatures of the adjusted reference curve and observed curve at the time stamp of i, respectively, Δt is the time interval between neighbouring time stamps and n is the number of time intervals in the calculation during a sea breeze event. Correspondingly, the unit of SBCC is °C·h.

According to the definition, SBCC accounts for the cumulative cooling effect of the sea breeze. Unlike the average or maximum value, it considers both the intensity and duration of the sea breeze. Like the metric of cooling degree-days with a unit of °C-day, this metric is also helpful for estimating the reduction of energy consumption caused by the sea breeze by combining other local socioeconomic data. Therefore, SBCC is used in the further analysis of sea breeze cooling in this study.

2.3 Data and Methods

2.3.1 Study area

Adelaide is the capital city of South Australia. Located on the south coast of the Australian continent, the metropolitan Adelaide is built on the Adelaide Plain bounded by the Mount Lofty Ranges to the east and by Gulf St. Vincent on the west (Figure 2.2). The major part of the metropolitan area spreads over the Adelaide Plain, extending about 60 km from north to south. The east-west distance varies, wider in the north and narrower in the south, forming a triangular shape (Guan et al., 2013b).

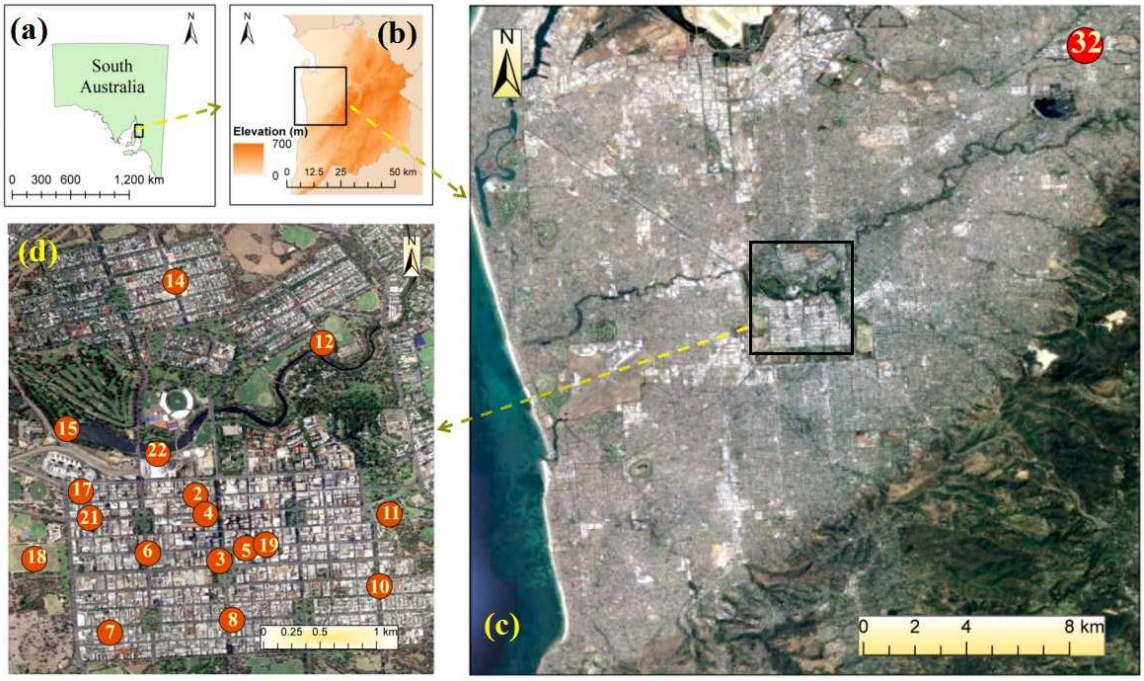

Figure 2. 2 Location of Adelaide (a,b) and the distribution of sensors for the analysis of sea breeze cooling in the Adelaide CBD (c,d). The sensors were installed at 4-m height recording data at a temporal resolution of 30 min.

Adelaide has a temperate Mediterranean climate with scorching summers and mild winters. This region occasionally suffers from excessively hot weather with temperature up to 46 ˚C in summer caused by anti-cyclone systems centred within the range of 35 ˚ - 40 ˚S. According to the data from Bureau of Meteorology, Australia, the number of days with maximum air temperatures being higher than 35 °C is more than 14 in a year on average. It is predicted that the annual mean temperature will rise by more than 3 ˚C by 2070 in Adelaide (Suppiah et al., 2006) and this can inevitably worsen the living conditions of residents.

The prevailing winds in winter are the large-scale synoptic flows that mostly come from north, while in summer the prevailing daytime winds are mostly south-westerly, especially in sea breeze days (Figure 2.3). It as explained by Physick originates from the Gulf St Vincent (Physick et al., 1977). The winds actively influence air temperature in Adelaide and the surrounding area (Guan et al., 2016). According to the on-site measurement, there is a clear temperature gradient from coast to inland in summer daytime and this phenomenon is supposed to be generated from prevailing sea breezes (Guan et al., 2016).

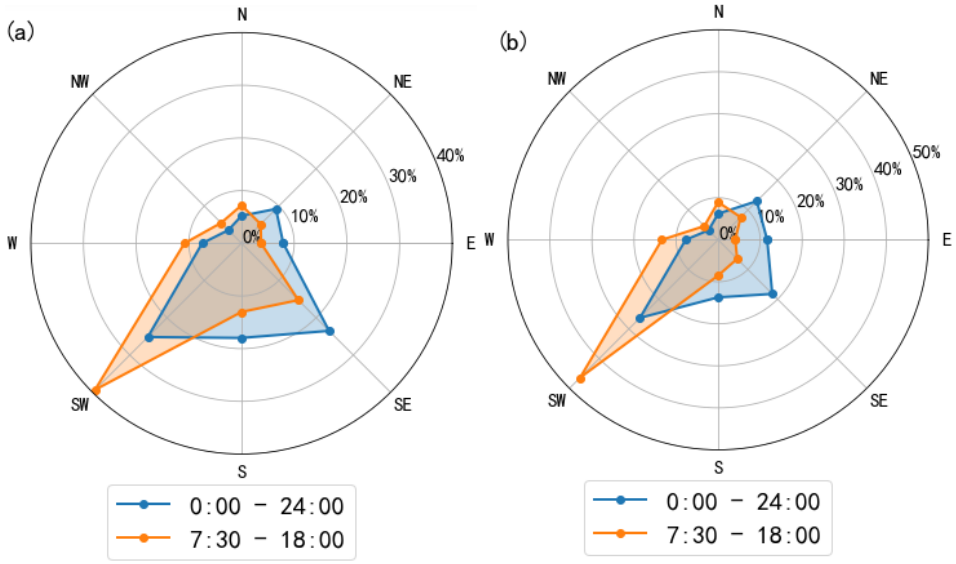

Figure 2. 3 Distribution of wind direction at the Adelaide coast during daytime (7:30 - 18:00, local standard time) and the whole day (0:00 - 24:00) in all summer days (a) and sea breeze days (b) from Dec 2010 to Mar 2013 (Selection of sea breeze days is based on a set of criteria described in Sect. 2.3.3). The abbreviations of wind directions are described as follows (0° from north, clockwise): N: northerly (0° - 22.5° and 337.5° - 360°), NE: northeasterly (22.5° - 67.5°), E: easterly (67.5° - 112.5°), SE: southeasterly (112.5° - 157.5°), S: southerly (157.5° - 202.5°), SW: southwesterly (202.5° - 247.5°), W: westerly (247.5° - 292.5°), NW: northwesterly (292.5° - 337.5°).

In this chapter, the Adelaide CBD is concerned. Located in the centre of the metropolitan Adelaide, the Adelaide CBD is an area of <10 km^2 consisting of different urban landscapes with building heights varying from 3 metres for single-story residential houses to 130 metres for office buildings (Figure 2.4). The major part of the CBD is completely surrounded by a unique green belt of parkland with an average width of 500 m, designed by Colonel William Light in 1837 (Figure 2.2 (d)). The parkland belt around the Adelaide CBD exhibits lower temperatures than the built-up area (Guan et al., 2015; Clay et al., 2020). Green roofs have also been found to cool the nearby area in central Adelaide (Razzaghmanesh et al., 2016). However, these cooling sources take effects at a limited spatial scale with a cost of water, electricity and maintenance. The sea breeze, in contrast, can influence a much larger area.

Figure 2. 4 Typical view in the Adelaide CBD (up) and the metropolitan Adelaide (down)

2.3.2 Data

Because sea breezes are most common in the warm season (Pazandeh Masouleh, 2015), I only consider summer days in this research. Commonly, December, January and February in the Southern Hemisphere are considered as the summer months. However, historical records show that abnormally high temperature or heatwaves (> 35 °C) can occur in March, this month is also included in this study. Totally, there are 364 days selected from December 2010 to March 2013. Appendix A2 shows the comparisons of air temperature between our study period and a 15-year period (summer months from Dec 2002 to Mar 2017) for sea breeze days and non-sea breeze days. The result indicates the representativeness of our study period for the climate of Adelaide.

Meteorological data at Adelaide Airport weather station are selected to identify sea breeze days and to analyse the climate in Adelaide. The Adelaide Airport weather station (34.95°S, 138.52°E) is located only 1.5 km eastwards from the coast with measurement heights being

1.2 m for the temperature sensor, 6.2 m for the barometer and 10 m for the anemometer. The surrounding area of this station is flat without high-rise buildings, so the information provided by this station is supposed to represent the local weather condition. The weather condition at this station also provides appropriate information to identify land-sea breezes. Meteorological variables recorded include air temperature, specific humidity, wind direction, air pressure and wind speed. It is important to note that specific humidity rather than relative humidity is utilized here. This is because specific humidity is directly related to the moisture in a volume of air, while relative humidity can also be affected by air temperature. These variables were all collected instantaneously with a time interval of 10 min. These data are provided from Bureau of Meteorology, Australia (BOM). Physically, sea breezes result from a temperature contrast between land surface and the nearby sea surface, which is often used as a common quantity to identify the existence of sea breezes. For this purpose, I use daily sea surface temperature data at Gulf St Vincent from NOAA/NCEI (https://www.ncei.noaa.gov/products/optimum-interpolation-sst) with the spatial resolution being 0.25° and MODIS/ Aqua land surface temperature (MYD11A1) data (1×1 km^2 spatial resolution and 1-day time interval) sampled at 13:30 as representatives of the sea and land surface temperature, respectively. For simplicity, time interpreted below is local standard time in Adelaide (GMT +9:30).

Air temperature data from the Adelaide urban heat island monitoring network are adopted to investigate the temperature reduction inside the Adelaide CBD during sea breeze days. The network consisted of 39 stations equipped with Maxim Thermochron Ibutton Sensors (Model: DS1922) (Guan et al., 2013a) (Figure 2.5). The sensors were datalogger sensors, and they were installed at 4-metre height above the ground in locations with free airflow and away from building walls to avoid the local effects on measurements. The sensors were covered by ventilated radiation shields to be protected from the effects of rain and sunlight. They recorded the ambient air temperature and relative humidity instantaneously at a time interval of 30 min with the accuracies of ±0.1 °C and ±0.1 %, respectively. The detailed information of the sites in this network is shown in Table 2.1.

In this study, I obtain data from 18 sensors of this network. Among them, 17 sensors were installed inside the Adelaide CBD and surrounding parklands and the remaining one (Site 32) was installed at Modbury. The Modbury site is about 21 km away from the coast showing very minor sea breeze cooling. The data at this site are used to check the consistency of

daytime temperature course between the two groups (sea breeze days vs. non-sea breeze days). The distribution of these sensors is shown in Figure 2.2(c,d).

Figure 2. 5 Photographs showing how a radiation shield is installed on a light pole (left). Bottom view and major components of a radiation shield (right).

Table 2. 1 Information of measurement sites of the Adelaide urban heat island monitoring network.

Site ID	Location	Latitude	Longitude
1	Rundle Mall near Stephens Place	34°55'22"S	138°36'3"E
2	Corner Hindley/Bank	34°55'23"S	138°35'52"E
3	Victoria Square	34°55'42"S	138°35'59"E
4	Currie Street	34°55'28"S	138°35'55"E
5	Flinders Street(South)	34°55'38"S	138°36'6"E
6	Corner Franklin/Morphett	34°55'39"S	138°35'38"E
7	Little Sturt Street	34°56'2"S	138°35'27"E
8	Corner Halifax/King William	34°55'58"S	138°36'2"E
9	Oval across from Pultney Grammer	34°56'14"S	138°36'9"E
10	Hutt Street	34°55'49"S	138°36'44"E
11	Rymill Park	34°55'28"S	138°36'47"E
12	Adelaide Uni Sports Ground	34°54'39"S	138°36'28"E
13	Park near Adelaide Aquatic Centre	34°53'59"S	138°35'35"E
14	Corner O'Connell/Tynte	34°54'22"S	138°35'46"E
15	Torrens Weir	34°55'4"S	138°35'15"E
16	Netball Courts on ANZAC Highway	34°56'24"S	138°35'12"E
17	Newmarket Street	34°55'22"S	138°35'19"E
18	Parklands off Sir Donald Bradman Drive	34°55'41"S	138°35'6"E
19	Flinders Street	34°55'37"S	138°36'12"E
20	Park near intersection Port Rd/Park Tce	34°54'27"S	138°34'51"E
21	Currie street West	34°55'29"S	138°35'21"E

22	Torrens River behind Convention Centre	34°55'11"S	138°35'41"E
23	Adelaide Airport	34°57'9"S	138°31'13"E
24	Eyre Street	35°1'53"S	138°32'10"E
25	Talisman Avenue	34°59'4"S	138°34'18"E
26	Harding Street	34°59'32"S	138°31'31"E
27	Kent Avenue	34°54'43"S	138°30'45"E
28	Foot Aventue	34°53'35"S	138°31'14"E
29	Francis Road	34°50'46"S	138°32'51"E
30	Duncan Road	34°50'31"S	138°35'9"E
31	Northcote Street	34°51'35"S	138°35'5"E
32	Modbury	34°49'50"S	138°41'52"E
33	Clarence Avenue	34°52'47"S	138°38'23"E
34	Roberts Street	34°56'45"S	138°36'10"E
35	Mitcham Avenue	34°59'6"S	138°36'14"E
36	Clifton Street	34°58'0"S	138°36'20"E
37	Colarado Avenue	34°57'47"S	138°33'2"E
38	Winara Drive	34°49'48"S	138°38'20"E
39	Beatrice Road	34°52'53"S	138°35'22"E

To investigate how urban structure influences sea breeze cooling in the Adelaide CBD and predict the change of SBCC in the future, I obtain Digital Elevation Model (DEM) data with current building heights and projected building heights (1-m resolution) in the Adelaide CBD from Adelaide City Council. DEM data with current building heights in the Adelaide CBD is shown in Figure 2.6. I also use the DEM data in metropolitan Adelaide for the calculation of distance towards the coast along the wind path for each site.

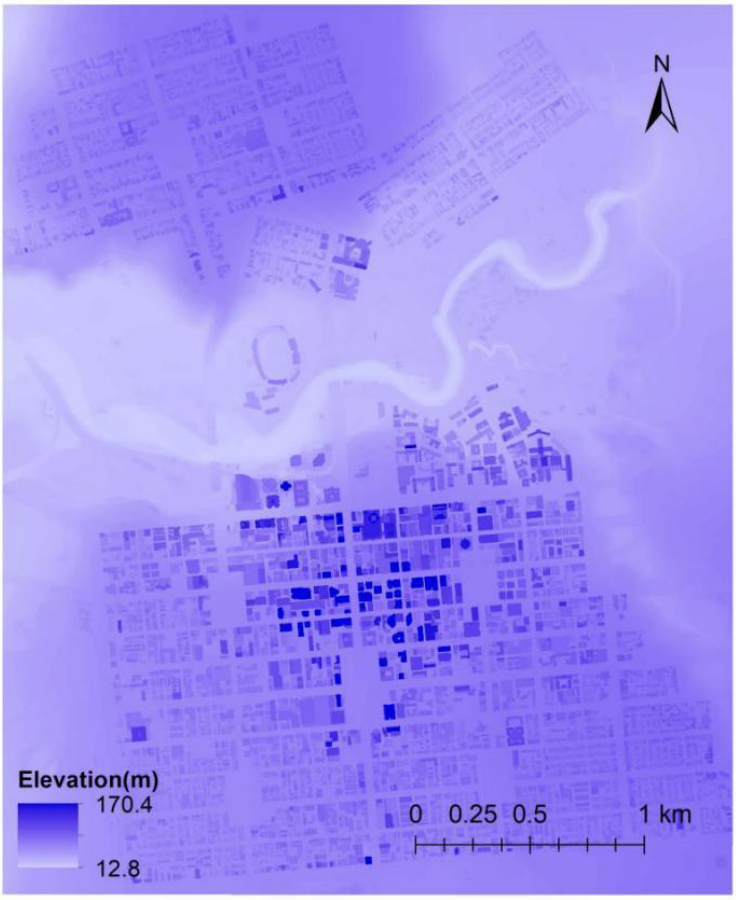

Figure 2. 6 DEM with current building heights in the Adelaide CBD.

2.3.3 Identification of sea breezes

Selection of sea breeze days using background weather information is important as it strongly influences the result of sea breeze analysis (Azorin-Molina et al., 2011). Previous studies have shown different methods in detecting sea breeze days by considering the effects and the mechanisms of them. The most significant surface characteristic is wind direction as in most cases there is an abrupt transition from offshore to onshore wind direction (Borne et al., 1998; Azorin-Molina et al., 2009; Azorin-Molina et al., 2011). In Adelaide, it was found that magnitude of change in wind direction is mostly larger than 45° within half an hour at the sea breeze onset. According to the past study on seafront wind near Adelaide (Crooks et al., 1987), sea breezes are considered blowing from 180° to 320° (0° from north, clockwise). Therefore, the above characteristics of wind direction are considered as the major criteria for sea breeze identification in this study.

Sea breezes are accompanied by a decrease of temperature and an increase of specific humidity (Abbs et al., 1986). In Adelaide, our data show that it takes almost 1 h for air temperature and specific humidity to stabilize after the sea breeze onset (Figure A.3). In addition, a positive difference between land and sea surface temperatures should exist in sea breeze days.

With the above-mentioned characteristics of sea breezes in Adelaide, I propose the screening criteria for sea breeze days in Adelaide in summer as below:

1. Wind blows onshore (180° - 320°) for at least 2 h after the sea breeze onset.

2. There is a rapid shift (> 45°) in wind direction within half an hour at the sea breeze onset.

3. Decreased air temperature last for at least 1 h after the sea breeze onset.

4. Increased specific humidity last for at least 1 h after the sea breeze onset.

5. Sea breeze onset occurs between 6:00 and 16:00.

6. Positive temperature difference exists between the land and sea surface during sea breezes.

According to the criteria, a sea breeze event is configurated once the breeze is active for at least 2 hours.

2.3.4 Calculation of SBCC

SBCC in the Adelaide CBD is calculated based on the definition in Sect. 2.2 for all 17 sites. During its calculation, the onset time is set when the temperature starts to drop, while the sea breeze cessation time is set to be whichever earliest of the following three time points: (1) the intercept of the actual temperature curve and the adjusted reference temperature curve, (2) the time offshore wind starts, or (3) a fixed time point of 23:00. It should be noted that the measured sites are distributed relatively widely inside the Adelaide CBD, so the temperature reduction may not occur simultaneously among all the sites. The example of reference temperature curve, adjusted reference temperature curve, SBCC, maximum temperature reduction during a selected sea breeze day (16_{th}, Feb 2012) at one site (site 8: Corner Halifax/ King William) is shown in Figure 2.1, where the yellow area showed is SBCC. Because the time interval of measured temperature is half an hour, I set half an hour as Δt of Eqs. (2.2) and (2.3) in this study. The cumulative seasonal SBCC is the summation of SBCC of all sea breeze events over the whole season.

2.3.5 Frontal area index (FAI) and terrain ruggedness index (TRI)

Frontal area index (FAI) is defined as the ratio of total facet area perpendicular to the wind direction over the total plain area (Wong et al., 2010). In this study, it aims to quantify the averaged building density in urban areas. In addition, vertical convection caused by the diversity of building heights is supposed to dissipate heat from surface to the air when the air at the lower level is warmer than that at the upper level. Accordingly, Terrain ruggedness index (TRI), originally defined as the heterogeneity of elevations inside an area, is adopted to quantify the diversity of building heights in the Adelaide CBD. The two indexes represent different characteristics of urban structure. With the changes of these two indexes, both positive and negative effects of building height related factors on sea breeze cooling can be achieved. Therefore, their potential relationships with SBCC are investigated here.

In this study, FAI and TRI are calculated based on the building heights of surrounding square areas of individual sites. To select the optimal square sizes of FAI and TRI, I conduct stepwise regressions of spatial variation of time-averaging SBCC with FAI, TRI, T_0, dx, where FAI and TRI are calculated by 1-m DEM over several square sizes (50 m, 70 m, 90 m, 110 m) centred at each site. From the result shown in Table A.1, SBCC is best explained by urban structure and weather conditions when the square sizes are both set as 70 m in the calculation of FAI and TRI. Therefore, the square size of 70 m is selected. The detailed calculations of the two indexes are shown in Appendices.

2.3.6 Calculation of the distance from the coast

In order to analyse the penetration process of sea breeze cooling, I have calculated distances from the coast for individual sites along the prevailing wind path. Specifically, the coastline is detected by using DEM data. For each site, the corresponding landing location of sea breeze cooling front can be identified as the intersection between the prevailing wind path for this site and coastline. Therefore, the distance from the coast is calculated as the length from this landing location to the corresponding site. According to the wind patterns in Adelaide, 225° is set as the prevailing sea breeze direction.

2.4 Results

2.4.1 Basic characteristics of sea breeze events in Adelaide summer

From December 2010 to March 2013, 116 among 364 summer days are selected as sea breeze days altogether based on weather data from Adelaide Airport station, accounting for 31.9%. The distribution of onset time of sea breeze events is shown in Figure 2.7. It shows that most sea breeze events start between 8:00 and 12:00 (Australian Central Standard Time), distributed slightly more in 10:00 - 12:00 compared to 8:00 - 10:00. Only 11 in 116 sea breeze events start before 8:00. The result demonstrates the reliability of criteria in the identification of sea breeze days proposed in Sect. 3.3.

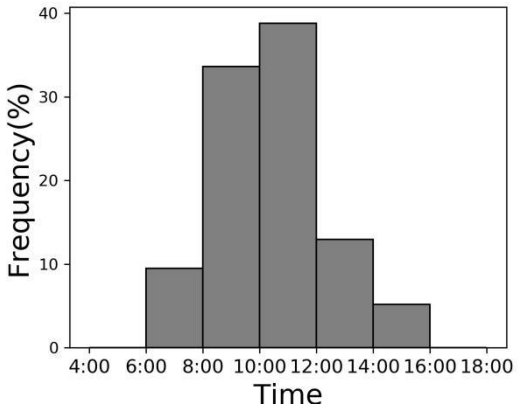

Figure 2. 7 Distribution of onset time of sea breeze events in summer days from Dec 2010 to Mar 2013 at Adelaide Airport weather station

2.4.2 Summer temperature diurnal pattern at a site of little sea breeze cooling

The Modbury site, located 21 km away from the coast, is nearly beyond the reach of sea breeze cooling (Figure 2.2 (c)). It is chosen to examine how similar the diurnal temperature courses are between two group of days (sea breeze vs non-sea breeze) identified in this study. The diurnal temperature patterns in sea breeze and non-sea breeze days during the study period at Modbury site are shown in Figure 2.8. There is a good consistency between the two groups of days with $R^2 > 0.99$. This high similarity forms the basis for using the reference temperature curve obtained from the non-sea breeze days to estimate SBCC for sites within the influence of sea breeze cooling. It is observed that at this site, the mean air temperature in the days without sea breezes is lower than that with sea breezes. This is consistent with our understanding that sea breezes result from thermal contrast between land and sea. In a hot day, the land-sea temperature contrast tends to be larger. Thus, to calculate SBCC, the

reference curve needs to be adjusted to match the sea breeze day temperature at the onset time.

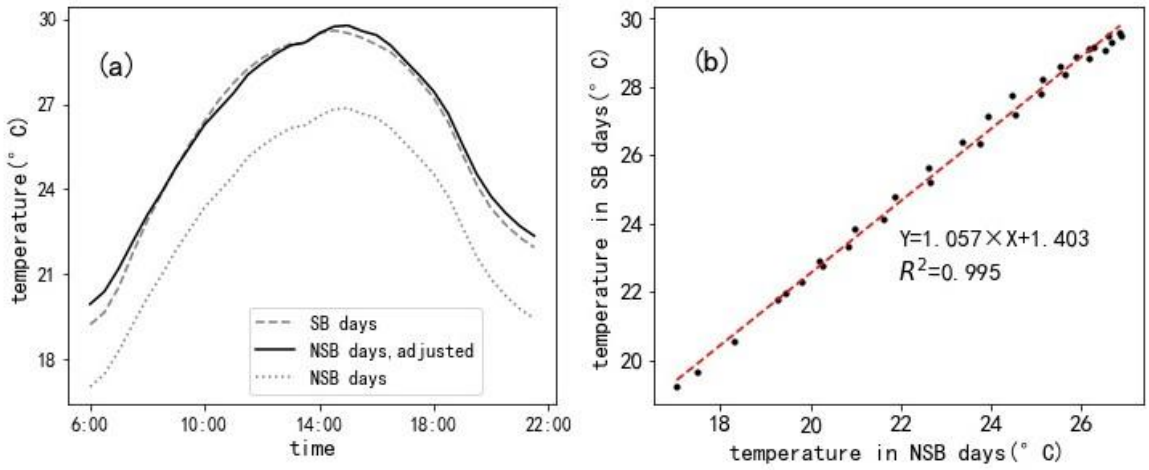

Figure 2. 8 (a) The averaged diurnal temperature fluctuations of sea breeze (SB, dashed) and non-sea breeze (NSB, dotted) days at Modbury during the study period. In order to clearly compare the diurnal changes of temperature between SB days and NSB days, I have adjusted the curve of NSB days to match the SB curve at 9:00 (solid line); (b) The relation of average temperature at different time of a day (from 6:00 to 22:00, with the interval of 30 min) between sea breeze and non-sea breeze days at Modbury.

2.4.3 Basic characteristics of SBCC in Adelaide summer

For the identified sea breeze days, I have calculated the magnitudes of SBCC of individual events averaged over all 17 sites in the Adelaide CBD. On a monthly basis, the event SBCC is strongest in December being 25.4 °C·h, while in January it is the weakest, being 17.0 °C·h (Figure 2.9(a)). Adding SBCC together for all sea breeze events in each month, I find that December has the largest magnitude of cumulative SBCC, followed by February (Figure 2.9(b)). The relatively weak SBCC in January is likely due to the prevailing controlling synoptic conditions in Adelaide during midsummer.

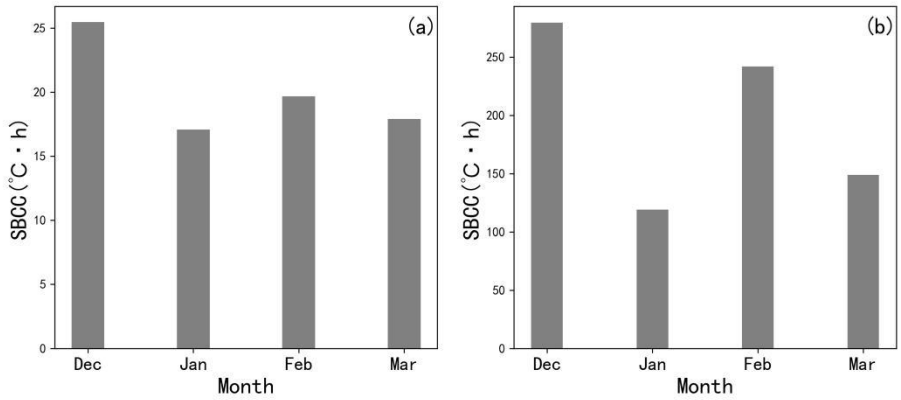

Figure 2. 9 Basic characteristics of SBCC averaged over all sites in the Adelaide CBD for each summer month. (a) Average magnitude *of SBCC for individual events. (b) Average monthly cumulative SBCC.*

The SBCC accumulated over all observed sea breeze events in summer for individual sites ranges from 733.9 to 858.7 °C·h per season (from 19.0 to 22.2 °C·h per event), with an average of 789.6 °C·h per season (20.4 °C·h per event). The SBCC at North Adelaide and the western part of the CBD are generally stronger than that at the other part of the CBD (Figure 2.10). In particular, the strongest cooling is observed at site 14 (Corn'r O'Connell/Tynte) located in the North Adelaide, while the weakest cooling is observed at site 2 (Corner Hindley/Bank) which is at the centre of the Adelaide CBD.

There is a large contrast in SBCC between western and eastern part of the Adelaide CBD. To be specific, the western part which is closer to the coastal area experiences a larger magnitude of sea breeze cooling, while in the central and eastern part, the SBCC is lower than average. The boundary is roughly along the area with high FAI and perpendicular to the major wind direction (Figure 2.10). It indicates a deterioration of the cooling capacity as it passes around high-rise buildings. It should be noted that even for places located inside eastern parkland, the temperature reduction is still below the average which proves the blocking effect of skyscrapers in CBD.

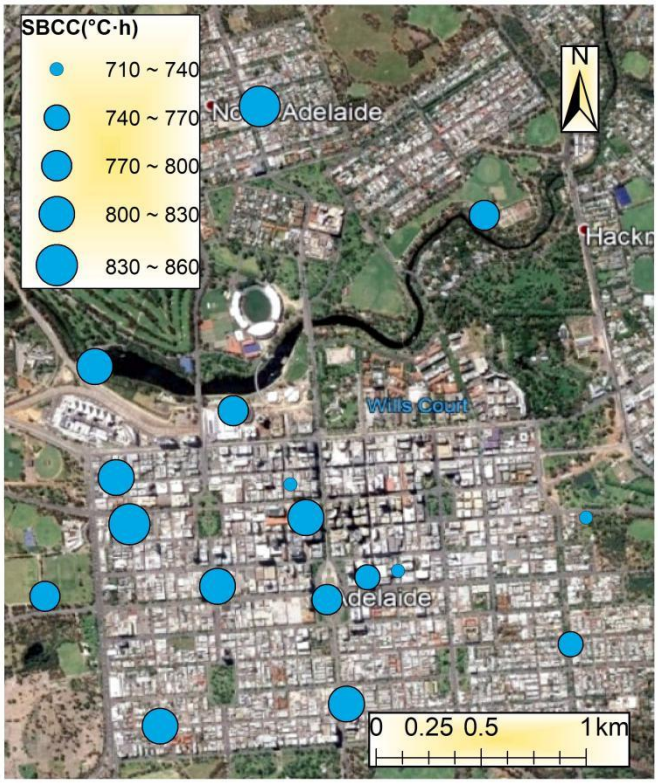

Figure 2. 10 Spatial distribution of summer SBCC per season from Dec 2010 to Mar 2013 for all sites in the Adelaide CBD.

2.4.4 Exploring the contribution of different environmental variables on SBCC

2.4.4.1 Multiple linear regression of temporal variation of SBCC

Stepwise regression analysis is conducted to identify the statistical association between space averaging SBCC and selected environmental variables. I select wind speed (U), specific humidity(q) at Adelaide Airport weather station during sea breezes and the temperature difference between Adelaide Airport station and CBD prior to the sea breeze onset (dT) as independent variables in this regression (Table 2.2). The temperature in the Adelaide CBD is calculated as the average among 17 sites. The variable of dT is chosen because it reflects the temperature contrast between the Adelaide CBD and the coast. The regression indicates that temperature difference between Adelaide Airport and CBD is a statistically insignificant parameter while wind speed and specific humidity are both significantly contributing to interpret the temporal variability of SBCC with the p-values both being 0.000. The regression coefficients for the two variables are 325.8 °C ·h·s·m^{-1} and 201.7 °C ·h·kg·g^{-1}, respectively. Totally, the two variables explain the inter-event variability of SBCC with an R^2 of 0.33.

Table 2. 2 Results of stepwise regression between temporal variability of SBCC and environmental variables.

	U(m/s)	*dT(°C)*	*q(g/kg)*	R^2
Coefficients	325.8	/	201.7	0.33
p-value	0.000	0.318	0.000	

Note: *U* represents wind speed, *dT* represents temperature difference between Adelaide Airport station and CBD prior to the sea breeze onset, *q* represents specific humidity. Red colour in characters of p-values means the corresponding variable does not pass the significance level of $p < 0.05$. Slash here means the variable is not significantly correlated with SBCC.

2.4.4.2 Multiple linear regression of spatial variation of SBCC

In the multiple regression of the spatial SBCC variability, four variables are used as independent variables, including frontal area index (FAI), terrain ruggedness index (TRI), mean temperature prior to the sea breeze onset (T_0), distance towards the coast (dx) of individual sites, where T_0 and SBCC are the values averaged over all sea breeze events. In this regression, linear relations are assumed between SBCC and four independent variables. Through statistical analysis (Table 2.3), the four independent variables are statistically significant in interpreting the cooling effect of sea breezes and the p-values are 0.001, 0.002, 0.002 and 0.049, respectively. It should be noted that the significance of distance towards the coast with SBCC is weaker than the remaining three variables. The corresponding regression coefficients are −498.4 °C·h, 12.0 °C·h/m, 36.4 h and $-1.1*10^{-2}$ °C·h/m. They together explain 79% spatial variability of SBCC in the Adelaide CBD.

Table 2. 3 Results of stepwise regression between spatial variability of SBCC and environmental variables.

	FAI	*TRI(m)*	$T_0(^\circ C)$	*dx(m)*	R^2
Coefficients	-498.4	12.0	36.4	$-1.1*10^{-2}$	0.79
p-value	0.001	0.002	0.002	0.049	

Note: T_0 represents temperature prior to the sea breeze onset, *dx* represents distance towards the coast.

2.4.5 Prediction of the influence of building development on SBCC

Adelaide city council recently released the regulation on maximum building heights in the Adelaide CBD (Guan et al., 2013a) and projected an increase of future building heights up to 150 m (Figure 2.11(a)). This projected development will lead to a change in sea breeze cooling capacity. Because there is a significant relationship between SBCC and urban structure (indicated by FAI and TRI), I can derive a relationship shown in Eq. (2.4) by assuming linear relations of SBCC with FAI and TRI:

$$\Delta SBCC = k_1 \times \Delta FAI + k_2 \times \Delta TRI \quad (2.4)$$

In this case, k_1 = −498.4 °C·h, k_2 = 12.0 °C·h/m, derived from regression coefficients in the regression above. Using this equation, I predict the potential change of SBCC inside the Adelaide CBD according to the regulated maximum building heights. As is shown in Figure 2.11(b), the potential change of mean SBCC caused by projected maximum building heights range from −195.0 - 143.0 °C·h per season (from −5.0 - 3.7 °C·h per event). With projected changes in building height, both positive and negative impacts on sea breeze cooling are revealed. With respect to the spatial pattern, the reduction of mean SBCC is mostly distributed in the western and eastern part where there is a large area that is for the future construction.

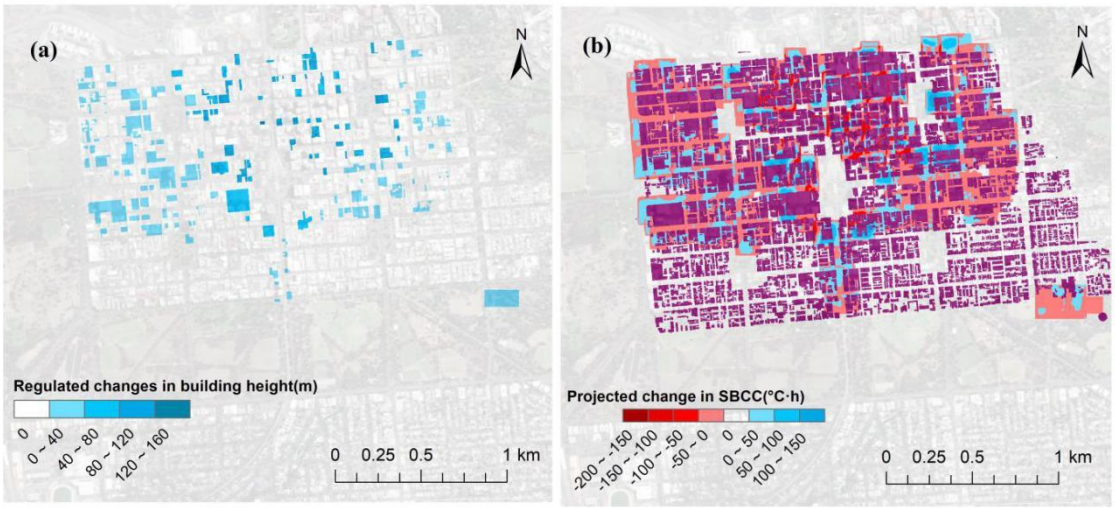

Figure 2. 11 (a) Projected change of building heights and (b) potential change of mean SBCC per season caused by projected maximum building heights in the future in the Adelaide CBD. The grey area in (b) shows the distribution of buildings in the Adelaide CBD where SBCC is not calculated.

2.5 Discussion

2.5.1 Influencing factors on the sea breeze cooling effect

Among the influencing factors of sea breeze cooling, wind speed is certainly a significant variable. As for specific humidity, it can be considered as an indicator of the magnitude of the sea breeze. The positive relation between specific humidity and SBCC confirms that the stronger cooling induced by the sea breeze is caused by the intensified sea breeze. TRI and FAI are more significant in explaining spatial variability of SBCC than distance towards the coastline. It indicates that in cities with dense buildings, the distribution of buildings with different heights cannot be ignored to estimate sea breeze cooling. FAI is an effective parameter to describe the resistance and thus contributes to depict the near-surface horizontal

wind environment (Chen et al., 2011; Grimmond et al., 1999; Liu et al., 2009). Studies show that the negative correlation between FAI and wind speed is significant in Hong Kong (Ng et al., 2011; Wong et al., 2013). Here I find that FAI also has a significant relationship with temperature reduction during sea breezes in Adelaide, which supports previous understanding of the relationship between building structure and urban ventilation. However, it does not mean that high-rise buildings always reduce SBCC. In fact, high-density buildings may also form a highly uneven plane composed of rooftops with non-uniform building heights. With an increased diversity of building heights, more vertical convective movements are generated and the exchanges of hot air mass near surface with the cool air mass at the upper level are boosted. As a result, it is easier for winds to penetrate into urban canopies. Consequently, the cooling power from the sea breeze can be stronger. In this study, I find the positive relationship between SBCC and terrain ruggedness index. It is similar to the results of previous studies. For example, Allegrini et al. (2017) suggested that the block with uniform building height shows higher temperature compared to that with non-uniform building heights. In Niigata City, the negative relationship between building height heterogeneity and air temperature is displayed (Tominaga, 2012). Compared to the above-mentioned studies which use traditional indexes such as air temperature, this study focuses on sea breeze cooling. Overall, the complex relationship between urban structure and microclimate is clarified (Zhu et al., 2013).

2.5.2 Implication for further studies and applications

With the ongoing urbanization over the world, more buildings will be built, and they can have potential effects on urban thermal environment. The results of this study provide useful information for urban designers to incorporate the distribution of buildings of various heights into policy making on urban planning. The relationships found in this study contribute to understanding the mechanism of sea breeze cooling in coastal cities. However, due to the uniqueness of urban structure and climate background in the Adelaide CBD, respective contributions of environmental factors may be different in other cities. More researches in other coastal cities are required to examine that the mechanisms found in this study are transferable and contribute to a universal rule of the impacts of environmental factors on SBCC.

2.6 Conclusions

In coastal cities, sea breeze is an important ventilation mechanism that can mitigate urban heat island, especially during summer. This study proposes a new metric of sea breeze cooling capacity (SBCC) to quantify the cooling induced by sea breezes and to investigate relevant factors using data collected from the Adelaide urban heat island monitoring network in 2010 - 2013.

The results show that sea breezes occur in 32% of summer days in Adelaide. From the map of spatial distribution of SBCC over the Adelaide CBD, there is a large contrast in SBCC between western and eastern parts which indicates the deterioration of the cooling capacity as it passes around high-rise buildings. The results from the stepwise regression analysis show that inter-event variability of SBCC is explained by specific humidity and wind speed, while spatial variability of SBCC is explained by FAI, TRI, distance towards the coast and temperature prior to the sea breeze onset. It is found that the diversity of building heights can increase SBCC, while mean building height, as intuitively expected, reduces SBCC.

Based on the relationship between SBCC and indexes about urban structure (FAI and TRI), I derive a simple equation to predict the potential change of SBCC due to future building construction. The result shows that the projected development of high-rise buildings in the Adelaide CBD may cause a change of SBCC in a range from −195 to 143 °C·h over an average summer. These results have important implications for urban management regarding issues such as energy consumption, public health and urban planning.

References

Abbs DJ. Sea-breeze interactions along a concave coastline in southern Australia: Observations and numerical modeling study. Monthly weather review. 1986 May;114(5):831-48.

Allegrini J, Carmeliet J. Coupled CFD and building energy simulations for studying the impacts of building height topology and buoyancy on local urban microclimates. Urban Climate. 2017 Sep 1;21:278-305.

Azorin-Molina C, Chen D. A climatological study of the influence of synoptic-scale flows on sea breeze evolution in the Bay of Alicante (Spain). Theoretical and applied climatology. 2009 May;96(3):249-60.

Azorin-Molina C, Tijm S, Chen D. Development of selection algorithms and databases for sea breeze studies. Theoretical and applied climatology. 2011 Dec;106(3):531-46.

Baker RD, Lynn BH, Boone A, Tao WK, Simpson J. The influence of soil moisture, coastline curvature, and land-breeze circulations on sea-breeze-initiated precipitation. Journal of Hydrometeorology. 2001 Apr 1;2(2):193-211.

Borne K, Chen D, Nunez M. A method for finding sea breeze days under stable synoptic conditions and its application to the Swedish west coast. International Journal of Climatology: A Journal of the Royal Meteorological Society. 1998 Jun 30;18(8):901-14.

Cenedese A, Monti P. Interaction between an inland urban heat island and a sea-breeze flow: A laboratory study. Journal of Applied Meteorology and Climatology. 2003 Nov 1;42(11):1569-83.

Chen F, Miao S, Tewari M, Bao JW, Kusaka H. A numerical study of interactions between surface forcing and sea breeze circulations and their effects on stagnation in the greater Houston area. Journal of Geophysical Research: Atmospheres. 2011 Jun 27;116(D12).

Clay R, Guan H. The urban-parkland nocturnal temperature interface. Urban Climate. 2020 Mar 1;31:100585.

Gharib S. Sea Breeze Cooling Power in the Adelaide Metropolitan Area (Master dissertation, Flinders University, School of the Environment.), 2017.

Crooks G, Brooks B, Sea Front Winds Near Adelaide, Aust. Bureau of Meteorology, 1987.

Emmanuel R, Johansson E. Influence of urban morphology and sea breeze on hot humid microclimate: the case of Colombo, Sri Lanka. Climate research. 2006 Apr 26;30(3):189-200.

Grimmond CS, Oke TR. Aerodynamic properties of urban areas derived from analysis of surface form. Journal of Applied Meteorology and Climatology. 1999 Sep 1;38(9):1262-92.

Grossi P, Thunis P, Martilli A, Clappier A. Effect of sea breeze on air pollution in the greater Athens area. Part II: Analysis of different emission scenarios. Journal of Applied Meteorology and Climatology. 2000 Apr 1;39(4):563-75.

Guan H, Bennett J, Ewenz C, Benger S, Zhu S, Clay R, Soebarto V, Characterisation, Interpretation and Implication of the Adelaide Urban Heat Island, 2013a.

Guan H, Kumar V, Clay R, Kent C, Bennett J, Ewenz C, Hopkins G, Simmons CT. Temporal and spatial patterns of air temperature in a coastal city with a slope base setting. Journal of Geophysical Research: Atmospheres. 2016 May 27;121(10):5336-55.

Guan H, McGrath AJ, Clay R, Ewenz C, Benger S, Bennett J. Effective surface areas for optimal correlations between surface brightness and air temperatures in an urban environment. Journal of Applied Remote Sensing. 2015 Apr;9(1):096059.

Guan H, Soebarto V, Bennett J, Clay R, Andrew R, Guo Y, Gharib S, Bellette K. Response of office building electricity consumption to urban weather in Adelaide, South Australia. Urban Climate. 2014 Dec 1;10:42-55.

Guan H, Zhang X, Makhnin O, Sun Z. Mapping mean monthly temperatures over a coastal hilly area incorporating terrain aspect effects. Journal of Hydrometeorology. 2013b Feb;14(1):233-50.

Gunawardena KR, Wells MJ, Kershaw T. Utilising green and bluespace to mitigate urban heat island intensity. Science of the Total Environment. 2017 Apr 15;584:1040-55.

Jamei E, Rajagopalan P, Seyedmahmoudian M, Jamei Y. Review on the impact of urban geometry and pedestrian level greening on outdoor thermal comfort. Renewable and Sustainable Energy Reviews. 2016 Feb 1;54:1002-17.

Kala J, Lyons TJ, Nair US. Numerical simulations of the impacts of land-cover change on cold fronts in south-west Western Australia. Boundary-layer meteorology. 2011 Jan;138(1):121-38.

Katayama T, Hayashi T, Shiotsuki Y, Kitayama H, Ishii A, Nishida M, Tsutsumi JI, Oguro M. Cooling effects of a river and sea breeze on the thermal environment in a built-up area. Energy and buildings. 1991 Jan 1;16(3-4):973-8.

Kikegawa Y, Genchi Y, Yoshikado H, Kondo H. Development of a numerical simulation system toward comprehensive assessments of urban warming countermeasures including their impacts upon the urban buildings' energy-demands. Applied Energy. 2003 Dec 1;76(4):449-66.

Liu G, Sun J, Jiang W. Observational verification of urban surface roughness parameters derived from morphological models. Meteorological Applications: A journal of forecasting, practical applications, training techniques and modelling. 2009 Jun;16(2):205-13.

Lowe SA. An energy and mortality impact assessment of the urban heat island in the US. Environmental Impact Assessment Review. 2016 Jan 1;56:139-44.

Ma W, Xu X, Peng L, Kan H. Impact of extreme temperature on hospital admission in Shanghai, China. Science of the total environment. 2011 Sep 1;409(19):3634-7.

Martilli A. A two-dimensional numerical study of the impact of a city on atmospheric circulation and pollutant dispersion in a coastal environment. Boundary-Layer Meteorology. 2003 Jul;108(1):91-119.

Masuda Y, Ikeda N, Seno T, Takahashi N, Ojima T. A basic study on utilization of the cooling effect

of sea breeze in waterfront areas along Tokyo Bay. Journal of Asian Architecture and Building Engineering. 2005 Nov 1;4(2):483-7.

Monson R, Baldocchi D. Terrestrial biosphere-atmosphere fluxes. Cambridge University Press; 2014 Mar 6.

Ng E, Yuan C, Chen L, Ren C, Fung JC. Improving the wind environment in high-density cities by understanding urban morphology and surface roughness: A study in Hong Kong. Landscape and Urban planning. 2011 May 15;101(1):59-74.

Oke TR. Towards better scientific communication in urban climate. Theoretical and Applied Climatology. 2006 Feb;84(1):179-90.

Papanastasiou DK, Melas D, Bartzanas T, Kittas C. Temperature, comfort and pollution levels during heat waves and the role of sea breeze. International journal of biometeorology. 2010 May;54(3):307-17.

Patz JA, Campbell-Lendrum D, Holloway T, Foley JA. Impact of regional climate change on human health. Nature. 2005 Nov;438(7066):310-7.

Pazandeh Masouleh Z. Identification of sea breezes, their climatic trends and causation, with application to the Adelaide coast (Doctoral dissertation). 2015.

Razzaghmanesh M, Beecham S, Salemi T. The role of green roofs in mitigating Urban Heat Island effects in the metropolitan area of Adelaide, South Australia. Urban Forestry & Urban Greening. 2016 Jan 1;15:89-102.

Riley SJ, DeGloria SD, Elliot R. Index that quantifies topographic heterogeneity. intermountain Journal of sciences. 1999 Dec;5(1-4):23-7.

Physick WL, Byron‐Scott RA. Observations of the sea breeze in the vicinity of a gulf. Weather. 1977 Oct;32(10):373-81.

Sailor, D. J. (2001). Relating residential and commercial sector electricity loads to climate—evaluating state level sensitivities and vulnerabilities. Energy, 26(7), 645-657.

Sasaki Y, Matsuo K, Yokoyama M, Sasaki M, Tanaka T, Sadohara S. Sea breeze effect mapping for mitigating summer urban warming: For making urban environmental climate map of Yokohama and its surrounding area. Urban climate. 2018 Jun 1;24:529-50.

Shen L, Sun J, Yuan R. Idealized large-eddy simulation study of interaction between urban heat island and sea breeze circulations. Atmospheric Research. 2018 Dec 1;214:338-47.

Simpson JE. Sea breeze and local winds. cambridge university press; 1994 Jun 2.

Suppiah R, Preston B, Whetton PH, McInnes KL, Jones RN, Macadam I, Bathols J, Kirono D. Climate change under enhanced greenhouse conditions in South Australia. Australia: CSIRO. 2006 Jun.

Sugawara H, Shimizu S, Takahashi H, Hagiwara S, Narita KI, Mikami T, Hirano T. Thermal influence of a large green space on a hot urban environment. Journal of Environmental Quality. 2016 Jan;45(1):125-33.

Synnefa A, Santamouris M, Apostolakis K. On the development, optical properties and thermal performance of cool colored coatings for the urban environment. Solar energy. 2007 Apr 1;81(4):488-97.

Takebayashi H. Improvement measures of urban thermal environment. InImprovement Measures of Urban Thermal Environment 2015 (pp. 1-40). Springer, Cham.

Thompson WT, Holt T, Pullen J. Investigation of a sea breeze front in an urban environment. Quarterly Journal of the Royal Meteorological Society: A journal of the atmospheric sciences, applied meteorology and physical oceanography. 2007 Apr;133(624):579-94.

Tominaga, Y. (2012). Visualization of city breathability based on CFD technique: case study for urban blocks in Niigata City. Journal of visualization, 15(3), 269-276.

Varquez AC, Nakayoshi M, Kanda M. The effects of highly detailed urban roughness parameters on a sea-breeze numerical simulation. Boundary-layer meteorology. 2015 Mar;154(3):449-69.

Wong MS, Nichol JE. Spatial variability of frontal area index and its relationship with urban heat island intensity. International Journal of Remote Sensing. 2013 Feb 10;34(3):885-96.

Wong MS, Nichol JE, To PH, Wang J. A simple method for designation of urban ventilation corridors and its application to urban heat island analysis. Building and Environment. 2010 Aug 1;45(8):1880-9.

Zhu S, Guan H, Bennett J, Clay R, Ewenz C, Benger S, Maghrabi A, Millington AC. Influence of sky temperature distribution on sky view factor and its applications in urban heat island. International journal of climatology. 2013 Jun 15;33(7):1837-43.

Chapter 3 Cooling power of sea breezes and its inland penetration in dry-summer Adelaide, Australia

Abstract

Extreme high-temperature events pose a threat to human beings on Earth. In coastal cities, the sea breeze is widely known as a prevailing wind that has a cooling effect on local environment. However, the cumulative cooling effect and its attenuation process during the sea breeze penetration have not been well investigated. In this study, I analyse sea breeze cooling capacity (SBCC) and propose a new method in estimating the penetration distance of sea breeze cooling in metropolitan Adelaide during summer using data from the Adelaide urban heat island monitoring network. The results show that during a sea breeze day, wind direction rapidly changes from southeast to southwest in the morning, and it gradually returns to southeast in the afternoon. It takes 67 min on average for the sea breeze cooling fronts to penetrate inside metropolitan Adelaide. The SBCC value is 21.3 °C·h per event averaged spatially in Adelaide summer. During the penetration process, the SBCC values decrease at a rate of 0.7 and 0.9 °C·h per kilometre from coast to inland on an average sea breeze day and a hot sea breeze day, respectively. Correspondingly, the mean cooling penetration distances are 42 and 29 km along the prevailing wind path. A multiple linear regression analysis indicates that the distance from the coast and elevation at the onshore point together explain 88% of the spatial variability of the temporally average SBCC in the study area.

In the thesis, this chapter makes the contribution on the spatial pattern and inland penetration of sea breeze cooling in low-density metropolitan areas, taking the metropolitan Adelaide as an example. The spatial pattern and penetration distance of the cumulative sea breeze cooling effect contribute to a better understanding of this common cooling source for heat mitigation in coastal cities where a large number of people reside.

The major component in Chapter 2 is already published in ‘Atmospheric Research:

Zhou Y, Guan H, Gharib S, Batelaan O, Simmons CT. Cooling power of sea breezes and its inland penetration in dry-summer Adelaide, Australia. Atmospheric Research. 2021 Mar 1;250:105409. *https://doi.org/10.1016/j.atmosres.2020.105409*

Author contribution:

Zhou Y performed the analysis and wrote the paper. Guan H conceived the analysis. Gharib S contributed to the data collection and data analysis. Batelaan O and Simmons C contribute to review the paper.

3.1 Introduction

Different thermal properties between land and sea lead to a contrast of air temperature for both sides. This phenomenon can generate a low-level atmospheric inland or ocean-directed airflow, generally described as a sea-land breeze. In the nighttime when the land is cooler than the nearby sea, wind blows from the land to the sea forming the land breeze. During the daytime when air temperature over the land is higher, wind direction reverses, forming the sea breeze. The sea-land breeze is a mesoscale atmospheric phenomenon recurring on a diurnal cycle along about 2/3 of coasts in the world, especially in tropical and subtropical zones (Pattiaratchi and Gould, 1997). It has attracted high attention for highly populated coastal areas, as it influences the thermodynamic structure of air and changes the atmospheric environment by dispersion effect inside the boundary layer (Yamamoto and Ishikawa, 2020; Zhang et al., 2019).

Multiple studies have analysed the roles of different temporal and spatial variables in explaining the intensity, coverage and key time points of sea-land breeze events (Chen et al., 2011; Meir et al., 2013; Arrillaga et al., 2016). These influencing factors can be generally classified into meteorological variables, local geographical variables and anthropogenic factors. The time-varying meteorological variables mainly consist of cloud fraction, atmospheric stability, direction and intensity of synoptic wind. For example, large cloudiness in the sky can lead to a relatively cool land surface, which is unfavourable for the formation of a sea breeze at daytime (Kala et al., 2010). As for the synoptic background, Azorin-Molina and Chen (2009) found that offshore synoptic flows contributed to a delay of sea breeze arrival on land while onshore synoptic flows had an opposite effect. In Yokohama, Japan, patterns with southwestern synoptic wind were revealed to have stronger effects on air temperature compared to other background patterns in sea breeze events (Sasaki et al., 2018). Other characteristics of sea breezes, such as maximum wind speed, height of sea breeze front, and shape of sea breeze circulation have also been found to be significantly influenced by synoptic flows (Miller et al., 2003; Poljak et al., 2014). Generally, local geographical variables, such as land use pattern, terrain and shape of the coast are time-invariant with respect to atmospheric processes. The location of the Durance Valley (Marseille area, France) was reported to impair sea-land breeze circulation by decreasing the temperature gradient along the wind path (Bastin et al., 2005). In addition, curvature of shoreline has been found to

determine convergence or divergence of sea breezes according to a study in Israel (Neumann, 1951). Anthropogenic factors of sea breezes include aerosol particles, urban structure, and urban heat island, etc. For example, emission of aerosol particles can decrease solar radiation and thus reduce the magnitude of wind speed during sea breezes in coastal areas (Shen and Zhao, 2020). In Sydney, observations have found a positive relationship between sky view factor and wind speed during the sea breeze, while wind can be enhanced in street canyons (He et al., 2020).

For coastal cities, the urban environment can significantly interact with the sea-breeze circulation. The Urban Heat Island Circulation (UHIC) is a small atmospheric circulation caused by the temperature difference between urban and rural areas. In Tokyo, UHIC has been found to delay the arrival of inland propagation of sea breezes and contribute to an upward convergence at the sea breeze front due to wind shear (Ado, 1992). In addition, increased surface roughness caused by urbanization could contribute to the weakening of sea breezes which has been found in cities such as Athens and Shanghai (Dandou et al., 2009; Shen et al., 2019). On the other hand, in large cities at a distance from the coast, such as Sao Paulo, sea breezes can be strengthened by the existence of UHIC resulting from a strong convergence zone in the city centre (Freitas et al., 2007). The sea breeze onset time could be earlier if there is an enhanced urban heat island effect in the morning (Khan and Simpson, 2001). This interaction can also change the urban climate inside the city. The height of urban boundary layer has been found to be reduced due to the passage of a sea breeze front (Ribeiro et al., 2018). Ohashi and Kida (2002) revealed the shift in the centre of UHIC towards the inland suburbs during sea breeze events. More importantly, sea breezes have been found to mitigate urban heat island in many cities globally (Guan et al., 2016; Kim and Baik, 2004; He, 2018). There is no doubt that sea breeze cooling can improve human's comfort level and is beneficial in reducing energy consumption during heatwave days (Lopes et al., 2011).

The last decades have witnessed noteworthy increases in intensity and duration of heatwave events globally (Coumou and Rahmstorf, 2012; Wang and Zhu, 2020). For example, Trewin and Vermont (2010) revealed that there were significantly increasing trends for both daily maximum temperature and minimum temperature from 1957 to 2009 in Australia ($p < 0.05$). These increases in intensity and duration of heatwaves have resulted in some adverse consequences such as increasing mortality and excessive energy consumption in summer (Lapola et al., 2019; Smoyer- Tomic et al., 2003). The sea breeze could be a potential cooling source for coastal cities where a large number of people reside. It can be helpful for

addressing the negative effects of heatwaves. Some studies have already explored the characteristics of sea breezes and their impacts on air temperature using observations and numerical simulations (Furberg et al., 2002; Huang et al., 2016; Naor et al., 2017). Particularly investigated are the spatial patterns of air temperature during sea breeze events. For example, with the help of a high-density temperature observation network, Yamato et al. (2017) noted a significantly lower air temperature in central Tokyo than that in the leeward suburbs during a sea breeze. However, no study has examined the cumulative cooling effect of sea breezes inside the whole metropolitan area and estimated its penetration distance, which is the focus of this study based on Adelaide, a coastal city in South Australia.

In the previous chapter, I proposed the metric of sea breeze cooling capacity (SBCC) for quantifying the cumulative cooling effect of sea breezes, and analysed its temporal and spatial patterns for the Central Business District (CBD) of Adelaide, Australia. The Adelaide CBD study focuses on a relatively small dense area (<10 km^2) with many high buildings. Therefore, Chapter 2 pays more attention on the effects of building characteristics such as building heights. In contrast to the Adelaide CBD, the metropolitan Adelaide is a much larger area (> 300 km^2) mostly composed of residential houses being less than 10 metres. Although the dense area of the Adelaide CBD is included in the metropolitan area, it only occupies a small proportion (<4%). Therefore, topography and location play much larger roles and are considered as the potential main influencing factors. Therefore in this chapter, I continue to use this proposed metric to perform a quantitative analysis of sea breeze cooling in metropolitan Adelaide and propose a new method to estimate its inland penetration distance. Additionally, the basic climatological characteristics of sea breezes are investigated because they are helpful in understanding how sea breeze cooling forms and varies.

The objectives of this study are:

(1) To determine the major climatological characteristics of sea breezes in the coastal area of Adelaide during summer.

(2) To illustrate, quantify and attribute the spatial patterns of sea breeze cooling during all sea breeze days and hot sea breeze days and explain their difference.

(3) To estimate the penetration distance of sea breeze cooling in the Adelaide metropolitan area.

3.2 Data and methods

3.2.1 Data

The same as Chapter 2, 364 summer days during December 2010 - March 2013 are selected for the sea breeze cooling analysis in the metropolitan Adelaide. Using the same criteria as that in Chapter 2, observed data from Adelaide Airport weather station, MODIS/Aqua land surface temperature and daily sea surface temperature near the Adelaide coast provided by NOAA/NCEI are used for identifying sea breeze days.

In addition, data from the Adelaide urban heat island monitoring network are utilized for the analysis of sea breeze cooling in the metropolitan Adelaide. In this chapter, most of the sites in the Adelaide CBD and northern Adelaide are excluded to eliminate the effects of high-rise buildings to the maximum extent and therefore the selected sites distribute relatively uniformly over the metropolitan Adelaide. Overall, data from 20 sites are used (Figure 3.1). Site 3 is selected to represent the weather condition in the Adelaide CBD as this site is in an open area with less interference of high-rise buildings compared to other sites. According to the result in Chapter 2, the SBCC at this site is close to the average over the surrounding area.

In addition, I have used DEM data in the metropolitan Adelaide with 30-metre resolution to calculate relevant geographic quantities such as the distance from the coast. This DEM data is provided by Department for Environment and Water, South Australia. NCEP/NCAR reanalysis data with the spatial resolution being $2.5^{\circ} \times 2.5^{\circ}$ have also been used for the analysis of synoptic background during sea breeze days (https://psl.noaa.gov/data/gridded/).

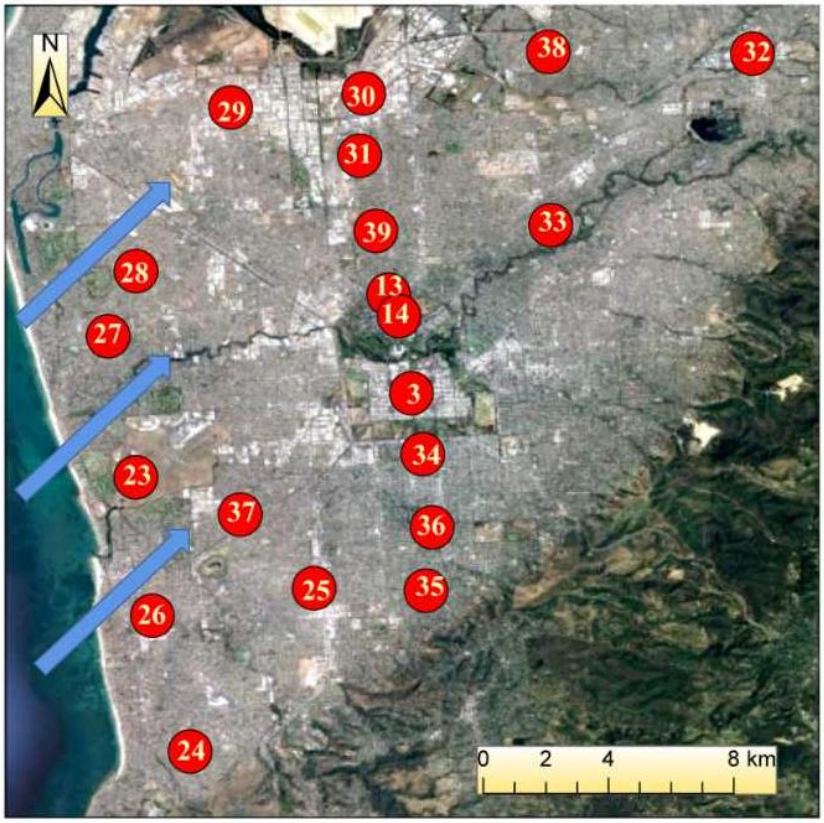

Figure 3. 1 The distribution of temperature sensors used in this study (circles). The blue arrows represent the mean prevailing wind direction (southwesterly) during sea breezes.

3.2.2 Definition of hot sea breeze days

It is interesting and relevant to examine sea breeze cooling during hot days as it is directly related to the mitigation of excessive heat stress. This is of great concern for local residents. In this study, hot sea breeze days are defined as sea breeze days with maximum temperatures above the 75th percentile of all sea breeze days (32.8°C).

3.2.3 Jenkinson and Collison classification

The Jenkinson and Collison (hereafter, JC) classification is a widely used objective classification method in identifying synoptic types with data of sea level pressure (Sarricolea et al., 2018). With this classification method, patterns of atmospheric circulations are revealed and therefore their relationships with sea breeze occurrences can be investigated. The JC method is designed to identify 27 synoptic types that can be classified into four groups: (1) anti-cyclonic (A) and cyclonic (C); (2) directional flows in eight wind directions (N; NE; E; SE; S; SW; W; NW); (3) hybrid types combining directional flows and cyclonic

types (AN; ANE; AE; ASE; AS; ASW; AW; ANW; CN; CNE; CE; CSE; CS; CSW; CW; CNW); (4) the unclassified type (U). This method has been used in multiple fields such as analysis of atmospheric circulations, mechanism of extreme events and synoptic background of sea breeze events (Broderick and Fealy, 2015; Pattison and Lane, 2012; Khan et al., 2018). In this study, I analyse the synoptic types during sea breeze days using the JC method to see how synoptic background influences sea breeze cooling. The analysis is performed with NCEP/NCAR sea level pressure data of an area centred on Adelaide with 5° resolution in latitude and 10 °C·h resolution in longitude (25° - 45° S, 125° - 155° E).

3.3 Results and discussion

According to the criteria proposed above, I have identified 116 (31.9%) sea breeze days from 364 summer days during December 2010 - March 2013. This is similar to findings in other places in the world (Azorin-Molina et al., 2011; Shen et al., 2019). When compared with the sea breeze frequency of about 60% in Perth, which is located on the west coast of the Australian continent, this percentage is lower. A higher sea breeze frequency in Perth is probably because of the West Coast Trough moving onshore on the west coast of Australia (Masselink and Pattiaratchi, 2001). Using the criteria in Sect. 3.2.2, 29 days are identified as hot sea breeze days in Adelaide.

3.3.1 Case study of a sea breeze event

In order to explain the spatial pattern of sea breeze cooling within metropolitan Adelaide, the diurnal patterns of air temperature at different sites are compared during an example of sea breeze day (6_{th}, Mar, 2013). This day is selected because clear contrasts exist in the diurnal cycles of air temperatures at different sites. In this study, two transects are defined. Site 23 (Adelaide Airport), 39 (Beatrice Road) and 38 (Winara Drive) are selected as the northern transect, while site 24 (Eyre Street), 25 (Talisman Avenue) and 34 (Roberts Street) are selected as the southern transect. The two transects are chosen because they are distributed along the prevailing wind path of sea breezes. The three sites along the northern transect are 2, 11 and 17 km from coast along the prevailing wind path, while the corresponding distances are 5, 9 and 11 km for the southern transect.

Diurnal changes of air temperature during this sea breeze day are shown in Figure 3.2. The transgressions and regressions of cooling fronts along both transects are distinctly demonstrated. For the northern transect, all three sites experience significant temperature drops during the daytime. The earliest arrival of the cooling front appears at Adelaide Airport at about 11:30. With the penetration of the sea breeze inland, cooling is observed at Beatrice Road half an hour later and at Winara Drive one hour later. Correspondingly, the retreat time follows a reversed order. There are also clear gradients of maximum cooling and SBCC among the three sites. Specifically, SBCC values are 29.9 ˚C·h, 15.6 ˚C·h and 9.7 ˚C·h, respectively. As for the three sites along the southern transect, the diurnal patterns of air temperature are similar and the corresponding SBCC values are 16.8 ˚C·h, 10.8 ˚C·h and 9.6 ˚C·h, respectively. From the comparison between the two transects, I can see that the magnitude of the sea breeze cooling along the southern transect is significantly smaller than that along the northern transect with a similar distance from the coast. For example, SBCC at site 39 is 6 ˚C·h larger than that at site 34 although both sites are about 11 km from coast. From the diurnal variations of air temperatures, it can be derived that the distance towards the coast is a major factor in affecting sea breeze cooling in Adelaide. Other factors, such as topography, also take some effects.

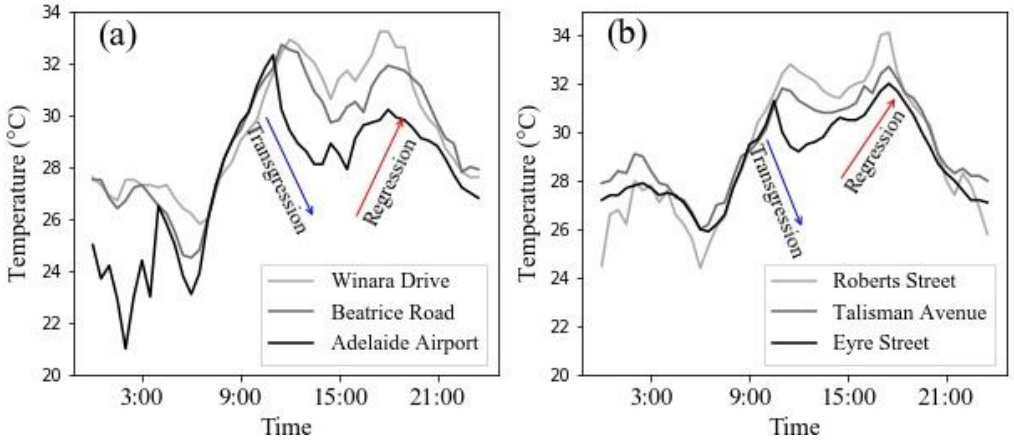

Figure 3. 2 Temperature patterns of a sea breeze day (6th, Mar, 2013) along the northern (a) and southern (b) transects of metropolitan Adelaide. For the northern transect, site 23 (Adelaide Airport), 39 (Beatrice Road) and 38 (Winara Drive) are selected, while for the southern transect, site 24 (Eyre Street), 25 (Talisman Avenue) and 34 (Roberts Street) are selected. The arrows on both subplots show the processes of transgression and regression of sea breeze cooling fronts.

3.3.2 Wind condition of sea breeze days

Wind direction and wind speed are major characteristics in explaining the dynamics of sea breezes. Therefore, I have analysed the two variables during sea breezes using wind data at Adelaide Airport station (10 m) as the reference. The hodograph in Figure 3.3(a) shows the mean diurnal evolutions of both variables averaged over all sea breeze days. It is clear that there is a transition between offshore and onshore wind. At 8:00 in the morning, there is a rapid shift in wind direction from southeast to southwest. In the afternoon, it returns to southeast until about 20:00 when winds have stabilized. The average turning point is 233° at 12:00. It should be noted that winds mostly come from the south during sea breezes and this is different from cases in autumn and winter when northerly and westerly winds dominate. This shows that that sea breezes mostly appear in summer rather than autumn and winter in Adelaide. As for wind speed, it is mostly lighter than 4 m/s from 0:00 to 8:00. The wind speed gradually increases after sunrise to 6.3 m/s on average at 16:00. Overall, afternoon wind speed is higher than morning wind speed. This phenomenon agrees well with other sea breeze observations in mid-latitudes (Huang et al., 2016; Papanastasiou and Melas, 2009).

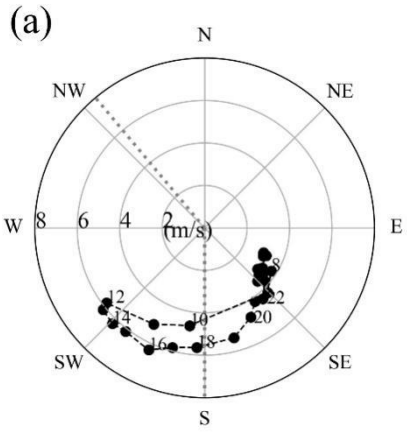

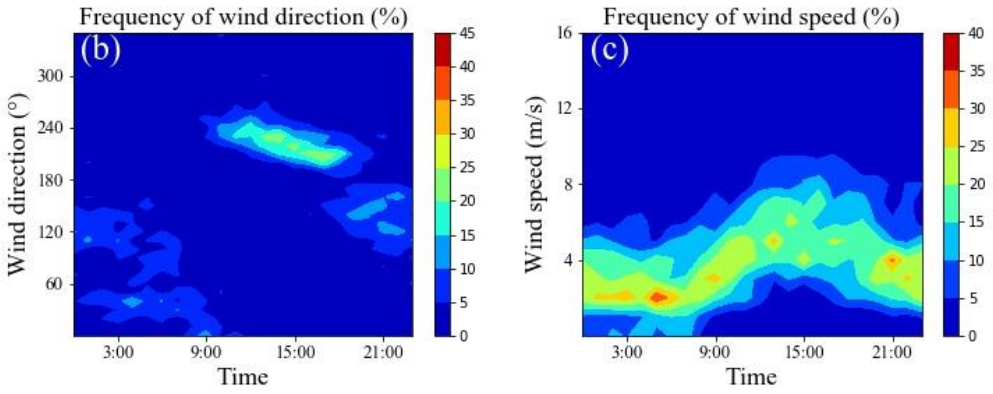

Figure 3. 3 (a) Wind hodograph averaged over sea breeze days. The two dotted lines represent the range of wind directions during sea breezes (180° - 320°). The values on the horizontal axis indicate wind speed and the values on the dashed line indicate time of the day (hours); (b) Pattern of hourly wind direction frequencies (%) during sea breeze days with an interval of 10°; (c) Pattern of hourly wind speed frequencies (%) during sea breeze days with an interval of 1 m/s.

Wind pattern can also be further explained by the diurnal distribution of wind direction frequency during sea breeze days, which clearly demonstrates the contrast between daytime and nighttime. More than 68% of the winds blow within the range of 200 - 250° during 12:00 - 18:00, while a relatively higher percentage of wind directions between 0 and 180° occur during nighttime (Figure 3.3(b)). As for wind speed, the magnitudes are much higher during 12:00 - 18:00. This is consistent with the time when wind directions are concentrated within 200 - 250° (Figure 3.3(c)). The results demonstrate that sea breezes play important roles in influencing wind conditions in Adelaide.

3.3.3 Arrival time, retreat time and duration of sea breeze cooling

The arrival time and retreat time of a sea breeze cooling front are influenced by local topography and synoptic background (Ookouchi and Wakata, 1984; Estoque, 1962), while the duration of sea breeze cooling (time span between its arrival and retreat) can indicate the cooling strength. These variables are estimated here based on the Adelaide urban heat island monitoring network for a better understanding of the basic characteristics of sea breeze climatology.

The mean arrival time of sea breeze cooling fronts in metropolitan Adelaide is shown in Figure 3.4(a). A clear delaying pattern from coast to inland can be identified and site 24 (Eyre Street) is the site cooled the earliest by the sea breeze. Averaged over 116 sea breeze days, the cooling front arrival time is 9:29 am at this site. In contrast, the averaged arrival time is

10:36 at site 32 (Modbury), which is about 24 km from the coast along the prevailing wind path. This result demonstrates that it commonly takes more than one hour (67 min on average) for the sea breeze cooling front to penetrate over metropolitan Adelaide. In order to clearly compare the differences in key time points of a sea breeze cooling, I separate the sites into three groups according to their distances from the coast along the prevailing wind path. The detailed classification is demonstrated in Table 3.1. Arrival time, retreat time and duration classified by the three groups are shown in Figure 3.5 in which the numerical distributions are calculated by values averaged over all sea breeze days of individual sites. From Figure 3.5(a), the mean arrival time is 9:44, 10:09 and 10:26 for group 1, 2 and 3, respectively. This clearly shows the transgression of sea breezes.

Table 3. 1 Classification of sites according to the distances from the coast along the prevailing wind path.

	Site number	Distance from the coast along the prevailing wind path
Group 1	23, 24, 25, 26, 27, 28, 29, 37	< 10 km
Group 2	3, 13, 14, 30, 31, 34, 36, 39	10 - 16 km
Group 3	32, 33, 35, 38	> 16 km

Sea breeze cooling fronts normally retreat before sunset. Opposite to the spatial pattern of arrival time, retreats happen earlier at inland sites (Figure 3.4(b)). On average, the earliest is found to be 16:14 (site 32), while the latest is 18:36 at a coastal site (site 27, Kent Avenue). This is not surprising as the sea breeze is weakened during the penetration inside the city and its cooling effect could disappear halfway when its intensity is discounted. For the three groups of sites, the mean values of corresponding retreat time are 17:49, 17:17 and 16:41, respectively (Figure 3.5 (b)).

Time durations of sea breeze cooling for individual sites have also been estimated by the intervals between arrival and retreat time of cooling fronts. The all-site mean duration is 7.3 h. There is a significantly decreasing trend from coast to inland ranging from 9.0 (site 27) to 5.6 (site 32) hours (Figure 3.4(c)). For the three groups of sites, the mean durations are 8.1, 7.1 and 6.3 h, respectively (Figure 3.5(c)). It can also be identified that durations of sea breeze cooling of the southernmost sites are shorter than other sites. More specifically, the

mean daily duration of cooling is only 7.3 h at site 24 (Eyre Street), while the corresponding values are more than 8 h for other coastal sites.

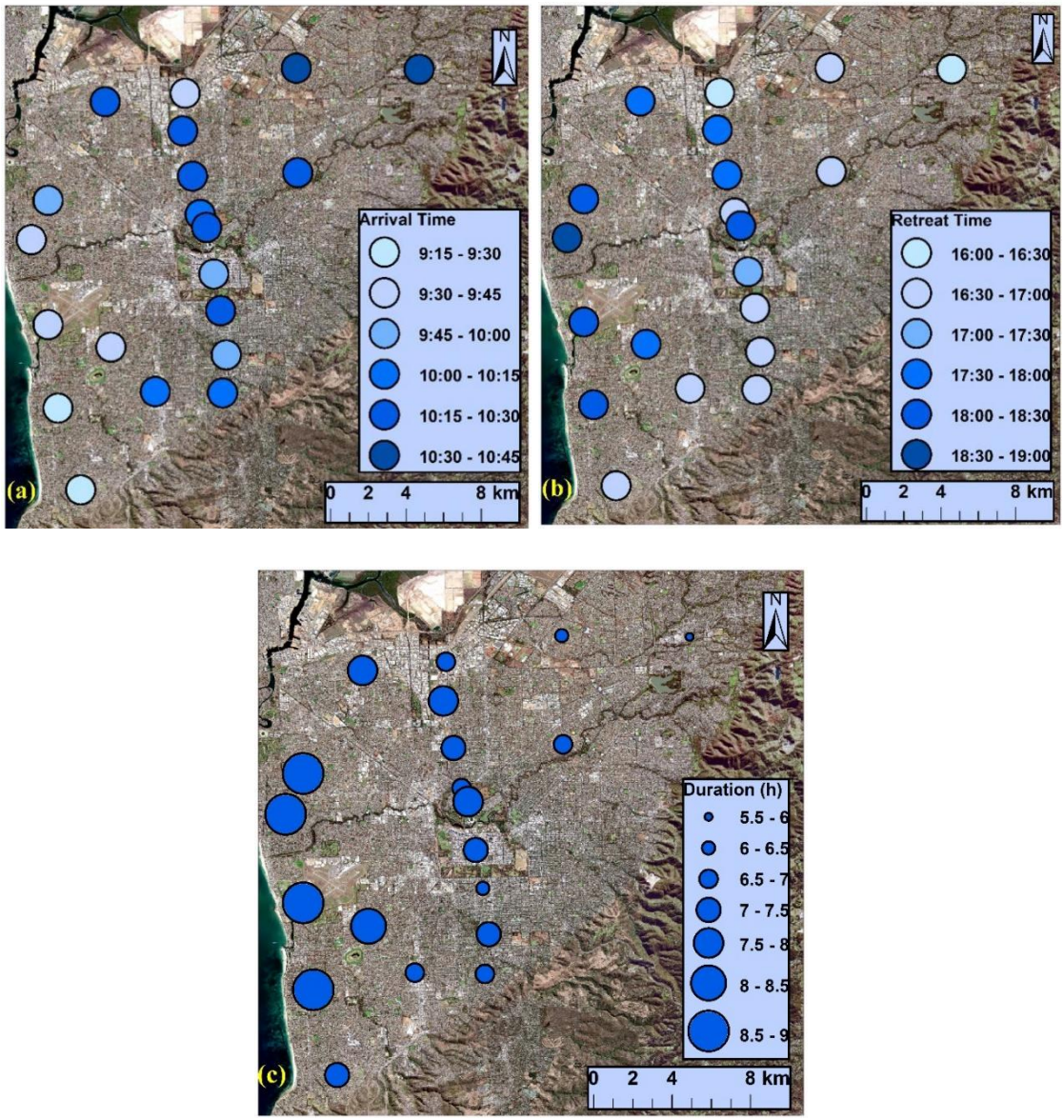

Figure 3. 4 Spatial patterns of arrival time (a), retreat time (b) and duration (c) of sea breeze cooling in the metropolitan Adelaide averaged over all sea breeze events during summer days from December 2010 to March 2013.

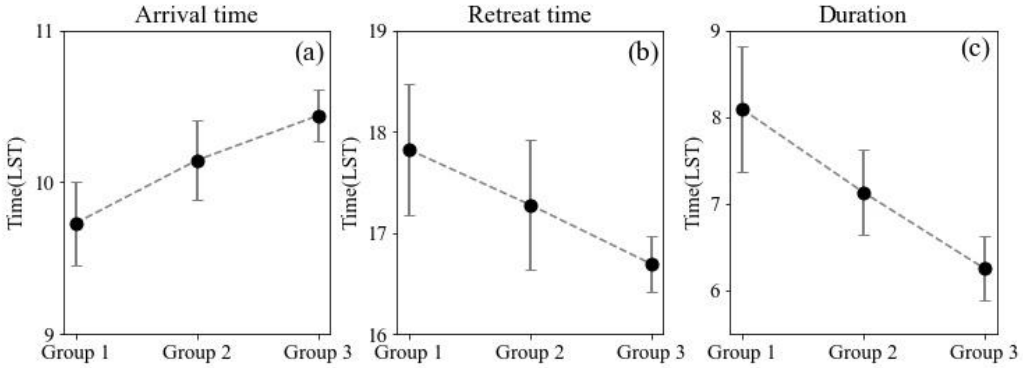

Figure 3. 5 Mean values and standard errors of arrival time (a), retreat time (b) and duration (c) of sea breeze cooling classified by three groups according to distances from the coast along the prevailing wind path. Mean values are indicated by solid dots, while standard errors are indicated by error bars. The numerical distributions are calculated by values averaged over all sea breeze days of individual sites.

3.3.4 Sea breeze cooling capacity in metropolitan Adelaide during summer

The spatial patterns of calculated SBCC and maximum cooling (dT_{max}) in metropolitan Adelaide averaged over all sea breeze days and hot sea breeze days are presented in Figure 3.6. The SBCC values range from 11.5 to 28.4 ˚C·h per event (444.1 - 1098.1 ˚C·h per season) during summer days and the average is 21.3 ˚C·h per event (824.5 ˚C·h per season). As expected, the cooling power is evidently weakened from coast to inland mainly due to the roughness of urban surface and heat exchange of sea breezes with the local atmosphere. The largest cooling appears at site 27 (Kent Avenue). This site is only 2.2 km from the coast (Figure 3.6(a)). Its surrounding area is relatively flat with only single-story residential housing. Therefore, sea breeze cooling at this site is less influenced by frictional effects from the urban surface. Similar magnitudes of SBCC appear at site 23 and 26, which are also near the coast.

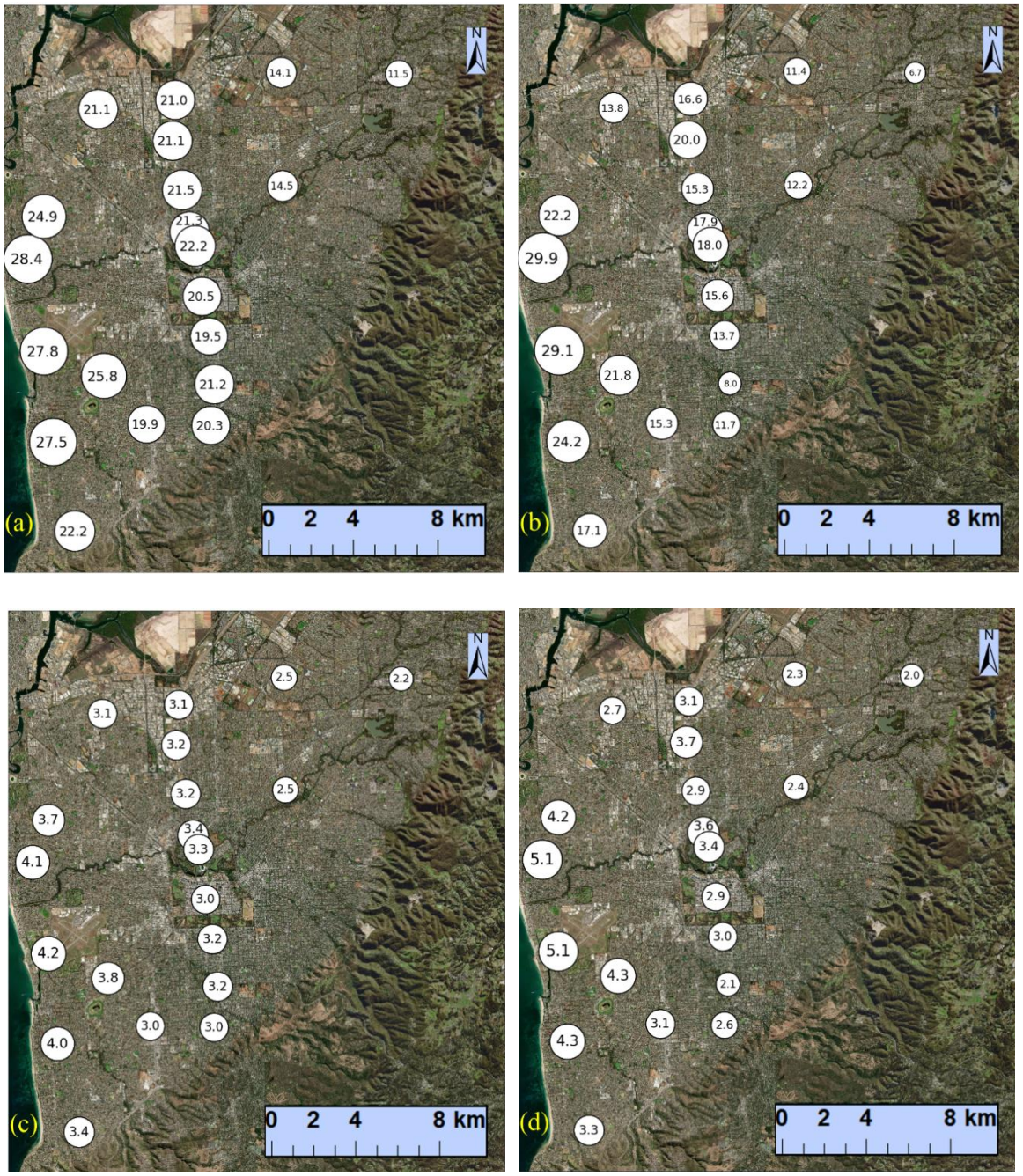

Figure 3. 6 The spatial patterns of SBCC (°C·h) (a,b) and dT_{max} (°C) (c,d) per event averaged from December 2010 to March 2013 in the metropolitan Adelaide for all sea breeze days (a,c) and hot sea breeze days (b,d), respectively .

Averaged over hot sea breeze days, there is also an inland decreasing pattern of SBCC with the largest one presented at site 27 and the smallest one at the most inland site (site 32, Modbury) (Figure 3.6(b)). However, the corresponding SBCC values are apparently smaller in most sites when compared to other sea breeze days and the differences are gradually

becoming larger from coast to inland. Therefore, the range across sites is larger from 6.7 to 29.9 ˚C·h per event (64.3 - 289.4 ˚C·h per season).

Similar spatial patterns and characteristics are also identified for dT_{max} (Figure 3.6(c), (d)). Averaged over all sea breeze days, dT_{max} values are over 4 ˚C at Adelaide Airport and Kent Avenue, which are less than 2.5 km from coast. The values are even larger in hot sea breeze days (5.1 ˚C·h for both sites). However, when focusing on the inland sites, the magnitudes are smaller in hot sea breeze days than those in other sea breeze days, which further confirms the faster weakening rate during inland penetration under heatwave conditions. Linearly interpolated, the decreasing rates of dT_{max} values along the prevailing wind path are 0.08 ˚C/km and 0.13 ˚C/km over all sea breeze days and hot sea breeze days, respectively.

In previous studies, there is no quantitative analysis of temperature reduction during sea breezes. However, similar gradients of air temperature at specific time points have been revealed in some studies. For example, in metropolitan Tokyo, there is a temperature difference of about 4 ˚C between the coastal area and Kawagoe which is 40 km inland during a sea breeze event (Yamato et al., 2017). The transgression relies on the local topography and the background synoptic system. Therefore, similar studies in other places are important for a better understanding of the effect of sea breeze cooling on heat mitigation with different topographical and climatic settings in future work.

Consistent with the spatial pattern of cooling duration discussed in Sect. 3.3.3, the magnitudes of sea breeze cooling are evidently smaller at the southernmost sites than the sites of similar distances from the coast in the north. This phenomenon is more pronounced in the coastal area. Averaged over all sea breeze days, SBCC is only 22.2 °C·h per event at site 24 (Eyre Street), while the corresponding values are mostly larger than 27 °C·h at other coastal sites (site 23: 27.8 °C·h; site 26: 27.5 °C·h; site 27: 28.4 °C·h). In southern Adelaide, elevation along the prevailing wind path is higher than that in other parts of Adelaide. According to Figure 3.6, the southern sites are located closer to the Mount Lofty compared to the northern sites. The Mount Lofty can resist the inland penetration of the sea breeze and weaken the cooling power. Therefore, the complicated topography in southern Adelaide is likely to explain this lower cooling capacity.

3.3.5 Inland penetration distance of sea breeze cooling in metropolitan Adelaide

Because SBCC values negatively correlate to distances from the coast in metropolitan Adelaide, the penetration distance of the cooling front can be calculated based on the location where SBCC drops to zero from this spatial relation. In this study, linear regression (better than higher order polynomial fits according to the Bayesian information criterion) between SBCC and the distance from the coast, is adopted to describe the sea breeze cooling penetration (Figure 3.7). It demonstrates that the weakening rate of SBCC values during the penetration is 0.7 °C·h/km per event averaged over all sea breeze days. Based on this rate, the estimated penetration distance of cooling front along the prevailing wind path is 42 km without the consideration of variability in surface roughness. Consistent with the larger range in spatial SBCC, the attenuation rate is higher in hot sea breeze days being 0.9 °C·h /km. The corresponding estimated penetration distance is 29 km. This means that the cooling effect covers nearly the whole metropolitan area of Adelaide.

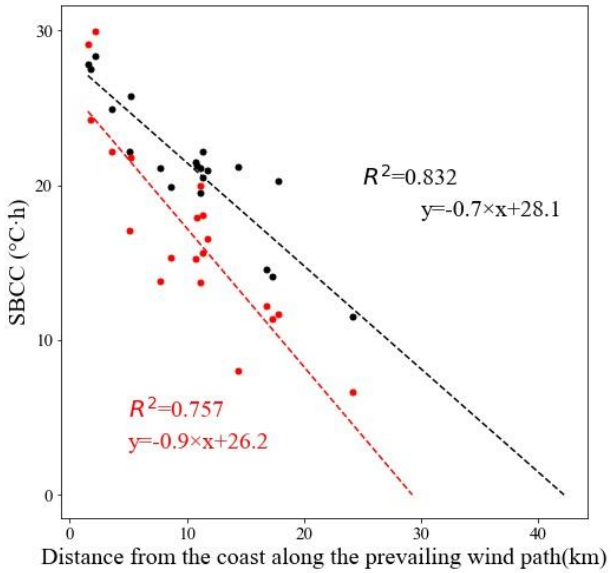

Figure 3. 7 The relationship between the distance from the coast along the prevailing wind path and SBCC averaged over all sea breeze days (black) and hot sea breeze days (red) from December 2010 to March 2013 for individual sites in metropolitan Adelaide.

Synoptic background is an important factor influencing the interaction between sea breezes and the local environment. In order to explore the mechanism leading to the higher attenuation rate of sea breeze cooling during hot sea breeze days, I analyse synoptic types

during all sea breeze days and hot sea breeze days respectively using JC classification method (Jenkinson and Collison, 1977). The results are shown in Figure 3.8. For all sea breeze days, the most frequent type is anti-cyclone (A: 24 days, 20.7%), followed by three directional flows (E: 12 days, 10.3%; SE: 12 days, 10.3%; S: 14 days, 12.1%). However, more than 40% of hot sea breeze days experience eastern and south-eastern directional flows (E: 7 days, 24.1%; SE: 6 days, 20.7%). Only one hot sea breeze day has an anti-cyclone pattern (3.4%). In addition, for hybrid types that combine directional flows and cyclonic/anti-cyclonic patterns, the directional components are also dominated by easterly patterns in hot sea breeze days. Attention needs to be paid that E and SE here mean the direction of background synoptic wind. Large-scale synoptic wind is significantly related to large-scale atmospheric circulation at the spatial scale of hundreds of kilometres and is hardly affected by topography, such as location of the coast. Therefore, synoptic winds can be E or SE when the sea is on the west.

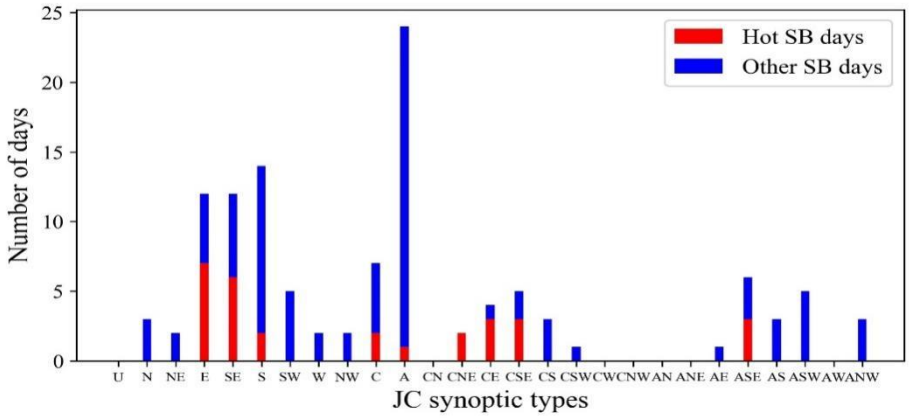

Figure 3. 8 Distribution of JC synoptic types during hot sea breeze days and other sea breeze days.

In the southern hemisphere, the Coriolis Force moves the horizontal airflow towards the left, so the typical easterly and south-easterly synoptic patterns lead to northerly and north-easterly winds in Adelaide. In fact, a large area of dry land where the air temperature is extremely high in summer is located to the northeast of metropolitan Adelaide. Winds blowing from this area can contribute to high temperature in Adelaide and counteract the sea breeze cooling effect to a certain extent. Therefore, the large-scale synoptic patterns explain the faster weakening process of sea breeze cooling during hot sea breeze days.

The penetration distance of sea breeze cooling shown here is conceptually different from that of a sea breeze, although they are relevant. The latter has been investigated in the literature. Salvador and Mill'an (2003) have proposed a method using observed data (Azorin- Molina et al., 2011) to calculate the inland penetration distance of a sea breeze. With this method, the sea-breeze penetration distance is calculated by multiplying a fixed wind speed and a specific time interval. This method has been widely used in studies on sea breezes with estimated sea-breeze penetration distances of up to 300 km (Khan et al., 2018). Salvador's method does not consider the weakening effect of the sea breeze during its inland penetration. Cloud-lines extracted from satellite observations have proven to identify sea breeze fronts well and this can be used in the analysis of sea breeze penetration (Hadi et al., 2002; Ferdiansyah et al., 2020). However, it should be noted that sea breezes interact with the underlying land cover, thus their properties (e.g., temperature) change during the penetration. In cities, high-rise buildings can contribute to the upwelling of low-level air and rapidly change temperature of the air mass (Allegrini and Carmeliet, 2017). Due to these interactions, the properties of a sea breeze change along its path. Specifically, temperature of the sea breeze gradually gets closer to that of the surrounding atmosphere. There can be locations where the cooling power disappears while the sea breeze still exists. Therefore, the penetration distance of sea breeze cooling power is different from that of the sea breeze itself. Without using the measurements of air temperature throughout a coastal area, the estimated sea-breeze penetration distances from these methods do not represent the coverage area of sea breeze cooling. In order to have a better understanding of the effects of sea breezes on thermal environment and relevant variables such as energy consumption, the penetration distance of sea breeze cooling is adopted in this study.

It should be noted that 225° is set as the prevailing sea breeze direction in this study. In fact, this angle is a statistical value based on local weather condition during sea breeze days in Adelaide. In real conditions, the prevailing wind path might vary slightly case by case. Therefore, potential uncertainties of the calculated distances from the coast exist.

3.3.6 Mapping SBCC in metropolitan Adelaide

As has been mentioned in Sect. 3.3.4, there is a clear decreasing pattern of SBCC values during the inland penetration of sea breeze cooling and the magnitudes of SBCC are supposed to be affected by terrain effects. A multiple linear regression of spatial SBCC per

event with geographical variables is performed. In this study, elevations at the onshore points (**Z**) and the distances from the coast along the prevailing wind paths (**D**) of the 20 sites in this study are utilized as independent variables. The former one is chosen because topography on the coast may impact sea breeze cooling. In this study, elevation at the onshore point is defined as the mean elevation of the corresponding coastal raster with 30-m width along the prevailing wind path of each site. The result demonstrates that both variables are statistically significant in explaining the spatial variability of SBCC with the *p* values of t-tests being 0.00 for the distance from the coast and 0.03 for elevation at the onshore point, respectively. With the increase of inland distance and elevation at the onshore point, there will be a smaller SBCC. According to the regression result, the two variables together explain 87.6% of the spatial variability of the temporally average SBCC. Overall, the multiple linear regression suggests that SBCC distribution in Adelaide can be estimated using this regression function: SBCC ($^{\circ}$C·h) = - 0.7 (°C·h/km) × **D** (km) – 0.3 (°C·h /m) × **Z** (m) + 31.7 (°C·h). The negative relation between SBCC and elevation at the onshore point is reasonable as higher elevation can resist the inland penetration of the sea breeze.

3.4 Conclusions

The sea breeze has the potential to cool the local environment and therefore mitigate the urban heat in summer. In this study, I analyse sea breeze cooling capacity (SBCC) and propose a new method to estimate its inland penetration using observed data from the Adelaide urban heat island monitoring network.

In the study period of 364 summer days from December 2010 to March 2013, I have identified 116 days as sea breeze days. During the process of sea breeze cooling, wind direction changes from southeast to southwest in the morning, and it gradually returns to southeast in the afternoon. Averaged over all sea breeze days, the cooling arrival time ranges from 9:29 to 10:36 for individual sites, while the corresponding retreat time ranges from 16:14 to 18:36. The SBCC value is 21.3 °C·h per event averaged spatially in Adelaide summer. As for the spatial distribution of SBCC values, there is a decreasing pattern from coast to inland. Averaged over hot sea breeze days, SBCC values are particularly smaller in most of the sites and the differences are gradually getting larger from coast to inland.

On the basis of the negative relationship between SBCC values and distances from the coast, a new method for estimating the penetration distance of sea breeze cooling has been proposed and applied. It is important to note that the penetration distance of sea breeze cooling calculated here is conceptually different from that of a sea breeze, although they are relevant. The result shows that the penetration distance of sea breeze cooling is estimated to be about 42 km along the prevailing wind path (225°). For hot sea breeze days, the corresponding distance declines to about 29 km. With the analysis of Jenkinson and Collison (JC) synoptic types in hot sea breeze days and other sea breeze days, it has been found that the large-scale synoptic patterns can explain this phenomenon. In addition, the result from multiple linear regression shows that the distance from the coast along the prevailing wind path (225°) and elevation at the onshore point together explain 87.6% of the spatial variability of the temporally average SBCC in the study area.

References

Allegrini J, Carmeliet J. Coupled CFD and building energy simulations for studying the impacts of building height topology and buoyancy on local urban microclimates. Urban Climate. 2017 Sep 1;21:278-305.

Arrillaga JA, Yagüe C, Sastre M, Román-Cascón C. A characterisation of sea-breeze events in the eastern Cantabrian coast (Spain) from observational data and WRF simulations. Atmospheric Research. 2016 Nov 15;181:265-80.

Azorin-Molina C, Chen D. A climatological study of the influence of synoptic-scale flows on sea breeze evolution in the Bay of Alicante (Spain). Theoretical and applied climatology. 2009 May;96(3):249-60.

Azorin‐Molina C, Chen D, Tijm S, Baldi M. A multi‐year study of sea breezes in a Mediterranean coastal site: Alicante (Spain). International Journal of climatology. 2011 Mar 15;31(3):468-86.

Bastin S, Drobinski P, Dabas A, Delville P, Reitebuch O, Werner C. Impact of the Rhône and Durance valleys on sea-breeze circulation in the Marseille area. Atmospheric research. 2005 Mar 1;74(1-4):303-28.

Broderick C, Fealy R. An analysis of the synoptic and climatological applicability of circulation type classifications for Ireland. International Journal of Climatology. 2015 Mar;35(4):481-505.

Chen F, Miao S, Tewari M, Bao JW, Kusaka H. A numerical study of interactions between surface forcing and sea breeze circulations and their effects on stagnation in the greater Houston area. Journal of Geophysical Research: Atmospheres. 2011 Jun 27;116(D12).

Coumou D, Rahmstorf S. A decade of weather extremes. Nature climate change. 2012 Jul;2(7):491-6.

Dandou A, Tombrou M, Soulakellis N. The influence of the city of Athens on the evolution of the sea-breeze front. Boundary-Layer Meteorology. 2009 Apr;131(1):35-51.

Estoque MA. The sea breeze as a function of the prevailing synoptic situation. Journal of Atmospheric Sciences. 1962 May;19(3):244-50.

Ferdiansyah MR, Inagaki A, Kanda M. Detection of sea-breeze inland penetration in the coastal-urban region using geostationary satellite images. Urban Climate. 2020 Mar 1;31:100586.

Freitas ED, Rozoff CM, Cotton WR, Dias PL. Interactions of an urban heat island and sea-breeze circulations during winter over the metropolitan area of São Paulo, Brazil. Boundary-layer meteorology. 2007 Jan;122(1):43-65.

Furberg M, Steyn DG, Baldi M. The climatology of sea breezes on Sardinia. International Journal of Climatology: A Journal of the Royal Meteorological Society. 2002 Jun 30;22(8):917-32.

Guan H, Kumar V, Clay R, Kent C, Bennett J, Ewenz C, Hopkins G, Simmons CT. Temporal and spatial patterns of air temperature in a coastal city with a slope base setting. Journal of Geophysical Research: Atmospheres. 2016 May 27;121(10):5336-55.

Hadi TW, Horinouchi T, Tsuda T, Hashiguchi H, Fukao S. Sea-breeze circulation over Jakarta, Indonesia: A climatology based on boundary layer radar observations. Monthly Weather Review. 2002 Sep;130(9):2153-66.

He BJ. Potentials of meteorological characteristics and synoptic conditions to mitigate urban heat island effects. Urban climate. 2018 Jun 1;24:26-33.

He BJ, Ding L, Prasad D. Outdoor thermal environment of an open space under sea breeze: A mobile experience in a coastal city of Sydney, Australia. Urban Climate. 2020 Mar 1;31:100567.

Huang M, Gao Z, Miao S, Xu X. Characteristics of sea breezes over the Jiangsu coastal area, China. International Journal of Climatology. 2016 Oct;36(12):3908-16.

Jenkinson AF, Collison FP. An initial climatology of gales over the North Sea. Synoptic climatology branch memorandum. 1977;62:18.

Kala J, Lyons TJ, Abbs DJ, Nair US. Numerical simulations of the impacts of land-cover change on a southern sea breeze in south-west Western Australia. Boundary-layer meteorology. 2010 Jun;135(3):485-503.

Khan B, Abualnaja Y, Al‐Subhi AM, Nellayaputhenpeedika M, Nellikkattu Thody M, Sturman AP. Climatology of sea breezes along the Red Sea coast of Saudi Arabia. International Journal of Climatology. 2018 Jul;38(9):3633-50.

Khan SM, Simpson RW. Effect of a heat island on the meteorology of a complex urban airshed. Boundary-Layer Meteorology. 2001 Sep;100(3):487-506.

Kim YH, Baik JJ. Daily maximum urban heat island intensity in large cities of Korea. Theoretical and Applied Climatology. 2004 Dec;79(3):151-64.

Lapola DM, Braga DR, Di Giulio GM, Torres RR, Vasconcellos MP. Heat stress vulnerability and risk at the (super) local scale in six Brazilian capitals. Climatic Change. 2019 Jun;154(3):477-92.

Lopes A, Lopes S, Matzarakis A, Alcoforado MJ. The influence of the summer sea breeze on thermal comfort in Funchal (Madeira): A contribution to tourism and urban planning. Meteorologische Zeitschrift. 2011;5(20):553-64.

Masselink G, Pattiaratchi CB. Characteristics of the sea breeze system in Perth, Western Australia, and its effect on the nearshore wave climate. Journal of Coastal Research. 2001 Jan 1:173-87.

Meir T, Orton PM, Pullen J, Holt T, Thompson WT, Arend MF. Forecasting the New York City urban heat island and sea breeze during extreme heat events. Weather and Forecasting. 2013 Dec 1;28(6):1460-77.

Miller ST, Keim BD, Talbot RW, Mao H. Sea breeze: Structure, forecasting, and impacts. Reviews of geophysics. 2003 Sep;41(3).

Naor R, Potchter O, Shafir H, Alpert P. An observational study of the summer Mediterranean Sea breeze front penetration into the complex topography of the Jordan Rift Valley. Theoretical and applied climatology. 2017 Jan;127(1):275-84.

Neumann J. Land breezes and nocturnal thunderstorms. Journal of Atmospheric Sciences. 1951 Feb;8(1):60-7.

Ohashi Y, Kida H. Local circulations developed in the vicinity of both coastal and inland urban areas: A numerical study with a mesoscale atmospheric model. Journal of Applied Meteorology. 2002 Jan;41(1):30-45.

Ookouchi Y, Wakata Y. Numerical simulation for the topographical effect on the sea-land breeze in the Kyushu island. Journal of the Meteorological Society of Japan. Ser. II. 1984;62(6):864-79.

Papanastasiou DK, Melas D. Climatology and impact on air quality of sea breeze in an urban coastal environment. International Journal of Climatology: A Journal of the Royal Meteorological Society. 2009 Feb;29(2):305-15.

Pattiaratchi C, Hegge B, Gould J, Eliot I. Impact of sea-breeze activity on nearshore and foreshore processes in southwestern Australia. Continental Shelf Research. 1997 Nov 1;17(13):1539-60.

Pattison I, Lane SN. The relationship between Lamb weather types and long-term changes in flood frequency, River Eden, UK. International Journal of Climatology. 2012 Nov 15;32(13):1971-89.

Poljak G, Prtenjak MT, Kvakić M, Strelec Mahović N, Babić K. Wind patterns associated with the development of daytime thunderstorms over Istria. InAnnales Geophysicae 2014 Apr 14 (Vol. 32, No. 4, pp. 401-420). Copernicus GmbH.

Ribeiro FN, de Oliveira AP, Soares J, de Miranda RM, Barlage M, Chen F. Effect of sea breeze propagation on the urban boundary layer of the metropolitan region of Sao Paulo, Brazil. Atmospheric Research. 2018 Dec 1;214:174-88.

Salvador RO, Millán M. Análisis histórico de las brisas en Castellón. Tethys. 2003;2:37-51.
Sarricolea P, Meseguer-Ruiz O, Martín-Vide J, Outeiro L. Trends in the frequency of synoptic types in central-southern Chile in the period 1961 - 2012 using the Jenkinson and Collison synoptic classification. Theoretical and Applied Climatology. 2018 Oct;134(1):193-204.

Sasaki Y, Matsuo K, Yokoyama M, Sasaki M, Tanaka T, Sadohara S. Sea breeze effect mapping for mitigating summer urban warming: For making urban environmental climate map of Yokohama and its surrounding area. Urban climate. 2018 Jun 1;24:529-50.

Shen L, Zhao C. Dominance of shortwave radiative heating in the sea-land breeze amplitude and its impacts on atmospheric visibility in Tokyo, Japan. Journal of Geophysical Research: Atmospheres. 2020 Apr 27;125(8):e2019JD031541.

Shen L, Zhao C, Ma Z, Li Z, Li J, Wang K. Observed decrease of summer sea-land breeze in Shanghai from 1994 to 2014 and its association with urbanization. Atmospheric Research. 2019 Oct 1;227:198-209.

Smoyer-Tomic KE, Kuhn R, Hudson A. Heat wave hazards: an overview of heat wave impacts in Canada. Natural hazards. 2003 Mar;28(2):465-86.

Trewin B, Vermont H. Changes in the frequency of record temperatures in Australia, 1957 - 2009. Aust Meteorol Oceanogr J. 2010 Jun 1;60:113-9.

Wang S, Zhu J. Amplified or exaggerated changes in perceived temperature extremes under global warming. Climate Dynamics. 2020 Jan;54(1):117-27.

Yamamoto Y, Ishikawa H. Influence of urban spatial configuration and sea breeze on land surface temperature on summer clear-sky days. Urban Climate. 2020 Mar 1;31:100578.

Yamato H, Mikami T, Takahashi H. Impact of sea breeze penetration over urban areas on midsummer temperature distributions in the Tokyo Metropolitan area. International Journal of Climatology. 2017 Dec;37(15):5154-69.

Yoshikado H. Numerical study of the daytime urban effect and its interaction with the sea breeze. Journal of Applied Meteorology (1988-2005). 1992 Oct 1:1146-64.

Zhang K, Zhao C, Fan H, Yang Y, Sun Y. Toward understanding the differences of PM2. 5 characteristics among five China urban cities. Asia-Pacific Journal of Atmospheric Sciences. 2020 Nov;56(4):493-502.

Chapter 4 Characteristics and cooling effects of sea breezes in Australian cities

Abstract

The sea breeze is an important phenomenon that can mitigate urban heat of coastal cities. However, a systematic understanding of sea breeze cooling over various cities of different environment is limited. In this study, I propose to perform a comparative analysis of the basic characteristics and cooling effects of sea breezes at various Australian cities. The results show that a large diversity in frequency of sea breeze events exists among the five coastal cities of Australia ranging from 17% to 56%, which are mainly controlled by the large-scale synoptic patterns of surrounding areas. From the analysis of SBCC in three selected cities with regular topographies, there are also significant declining trends of SBCC values and maximum temperature reductions during sea breeze events with the penetration distances being 43.3 km, 41.0 km and 26.6 km for Perth, Adelaide, and Melbourne, respectively. With respect to the temporal variations of SBCC for the three selected cities, frequency of days with anti-cyclone systems is positively related to seasonal cooling of sea breezes for coastal sites, with the R^2 value being 0.80.

In the thesis, this chapter makes the contribution on the comparison and attribution of sea breeze cooling among cities and it focuses more on the impacts of large-scale synoptic backgrounds. The results are helpful in understanding the characteristics and influencing factors of sea breeze cooling and can be useful for further studies in estimating the sea breeze cooling magnitudes in other coastal cities.

4.1 Introduction

The sea breeze is fuelled by the contrast of surface heating of the lower boundary layer between land and sea during the daytime. This phenomenon was identified hundreds of years ago, and it has been found to exert influences on local environment (Miller et al., 2003a). According to observations from weather radars, the sea breeze circulation may extend about 100 km from the coastline (Suresh, 2007). Increased concentration of air pollutants (PM 2.5, NOx …) has been observed in many regions due to the passage of a sea breeze front (Augustin et al., 2020; Mavrakou et al., 2012). More importantly, lower temperatures can be detected in areas where sea breezes can penetrate (Sasaki, et al., 2018).

Local factors pose multiple effects on the characteristics of sea breezes. During the daytime, mountains take effects on sea breezes by two major approaches: mechanical forcing of sea breeze circulation and intensification induced by climbing valley breezes. In addition, convergence and wind direction of the sea breeze are modulated by shape of the coastline. According to a numerical simulation, the offshore wind is stronger with a concave coast compared to a convex coast (Arritt et al., 1989). For urban areas, the distribution of high-rise buildings can lead to specific sea breeze paths. With the commonly used approach of least cost path methodology, sea breezes have been found to be separated into multiple groups with different wind directions resulting from the effects of buildings clusters and complex terrains, which have been validated by on-site measurements in the city of Dalian, China (Guo et al., 2018). Meanwhile, the cooling magnitude induced by sea breezes has been found to be negatively related to the averaged building height, but positively related to the diversity of building heights in a specific area according to Chapter 2.

Large-scale synoptic patterns play important roles in the formation, extent and intensity of sea breezes. Specifically, strong offshore winds prevent the formulation of sea breezes. With stronger opposing wind, the associated marine air mass is shallower (Frizzola et al., 1963). On the central New England coast, sea breezes account for 80% of occurrences of the synoptic type with northeasterly wind, while two other synoptic types with southwesterly or northwesterly winds generate no sea breeze events (Miller et al., 2003b). The impacts of large-scale winds also depend on the relative locations and orientations of coastlines with respect to the wind directions driven by large-scale synoptic patterns. For example, observations revealed that the intensified sea breezes appear near western coast over the Florida Peninsula under south-western synoptic patterns (Lericos et al., 2002).

In Australia, the major cities are located in the coastal areas, mostly along the southern or eastern coastlines. For these cities, sea breezes demonstrate significant effects on the local climate and environment and relevant characteristics have been investigated in last decades. Masselink et al. (2001) collected wind data at Perth Airport and found that Perth experiences frequent and strong sea breezes. Specifically, the maximum wind speed sometimes reaches 10 m/s at 10-metre height. It has also been found that the wind directions range from south to southwest during sea breezes in this city. In Melbourne, Abbs (1986) revealed that sea breezes are composed of winds blowing both from Port Phillip Bay and Bass Strait. Correspondently, the prevailing wind directions during sea breezes vary among different locations of the coastal area. In Sydney, it is shown that sea breezes can mitigate excessive heat and decrease the temperature difference across the greater Sydney area into less than 1 ℃ (Hirsch et al., 2021). Jiang et al. (2017) further investigated the effect of the interaction between sea breezes and synoptic types on air quality of Sydney. In addition, Pazandeh Masouleh et al. (2016) noted that the maximum sea breeze intensities in summer months have a comparatively stronger southerly component than those in other seasons by analysing wind data in the city of Adelaide.

As has been introduced above, the properties, structures and impacts of sea breezes on local environment have been well investigated in major Australian cities and other coastal cities in the world. Meanwhile, the understanding of their cooling abilities is limited. In chapter 2, I introduced the metric of sea breeze cooling capacity and analysed its spatial patterns at different spatial scales in the city of Adelaide. However, it is still uncertain what are the magnitudes of sea breeze cooling in other coastal cities of Australia and what are the influencing factors that lead to the differences among these cities. Therefore, I propose to perform a comparative analysis of the basic characteristics and cooling effects of sea breezes in major coastal cities of Australia in summer using weather data during Dec, 2002 – Mar, 2020.

4.2 Study areas and data

4.2.1 Study areas

In this chapter, I focus on the major Australian cities and five coastal cities are selected. The basic information (population and climate type) of these cities is shown in Table 4.1. The city of Perth is near Indian Ocean and embraces a straight coastline from north to south. There is a

low escarpment named the Darling Scarp on the east, while Rottnest Island is located to the west of the metropolitan area (Figure 4.1(b)). Melbourne is located on the northern coast of the Port Phillip Bay and the coastline near the greater Melbourne area is in concave shape. The topography is relatively flat over this city (Figure 4.1(d)). The greater Sydney area is located on a coastal basin with the Blue Mountain to the west and the Tasman Sea on the east. On the north of the city locates Hornsby Plateau where the elevation is evidently higher. Inside the metropolitan area, Port Jackson Bay and Botany Bay lie on the north and south of the CBD area of Sydney, respectively (Figure 4.1(e)). The greater Brisbane area is on the east of the Great Dividing Range. Meanwhile, the Taylor and D'Aguilar ranges extend into this city. Moreton Island and North Stradbroke Island are located to the east of the metropolitan Brisbane (Figure 4.1(f)). In summary, topographies of Sydney and Brisbane are slightly more complicated compared to those of other cities. As for the topography in Adelaide, more introductions are presented in Sect. 2.3.1.

Table 4. 1 Basic information of five cities in this multi-city analysis

City	Population	Climate type
Perth	2.0 million	Mediterranean climate
Adelaide	1.5 million	Mediterranean climate
Melbourne	5.1 million	Humid subtropical climate
Sydney	5.3 million	Humid subtropical climate
Brisbane	2.3 million	Humid subtropical climate

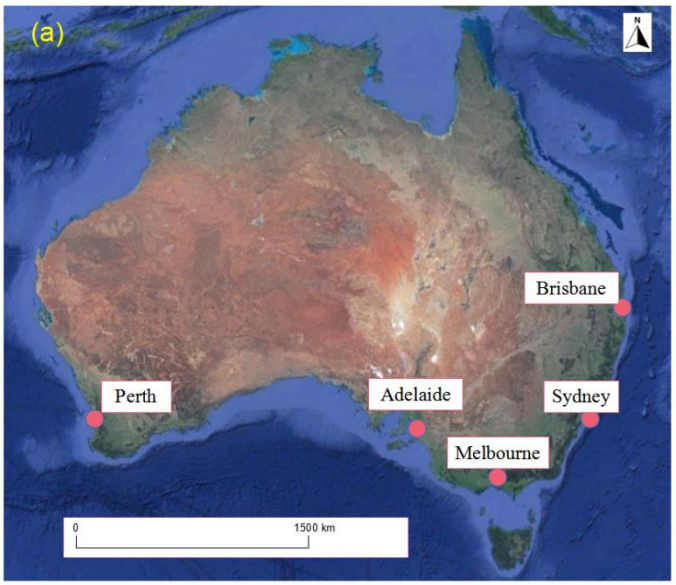
(a)
Brisbane
Perth
Adelaide
Sydney
Melbourne
0
1500 km

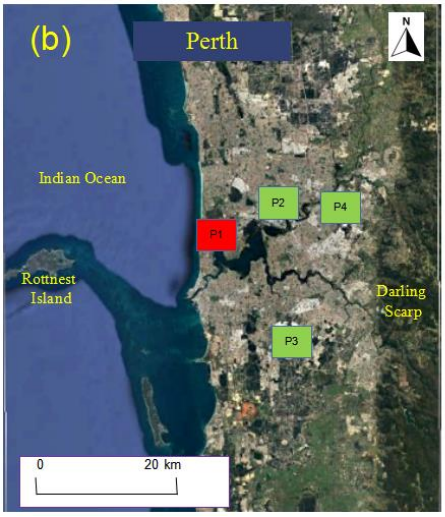
(b)
Perth
Indian Ocean
P2
P4
P1
Rottnest Island
Darling Scarp
P3
0
20 km

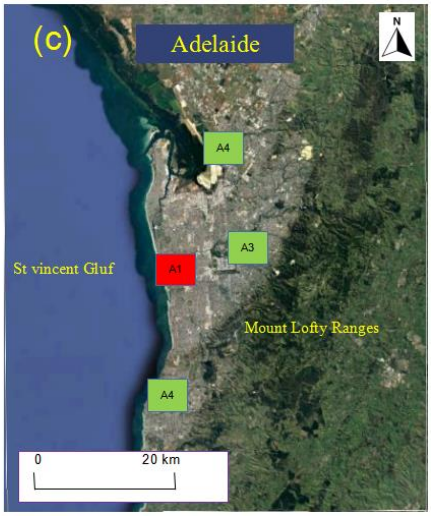
(c)
Adelaide
A4
A3
St vincent Gluf
A1
Mount Lofty Ranges
A4
0
20 km

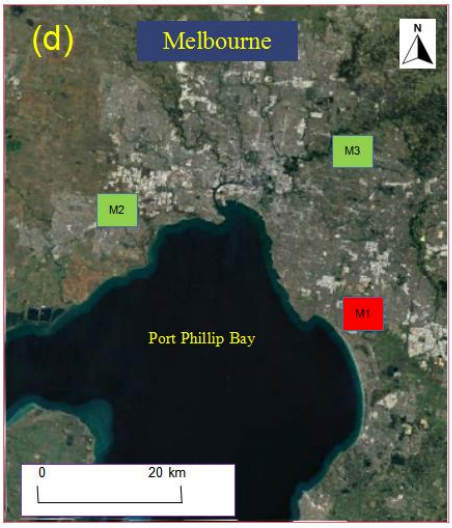
(d)
Melbourne
M3
M2
M1
Port Phillip Bay
0
20 km

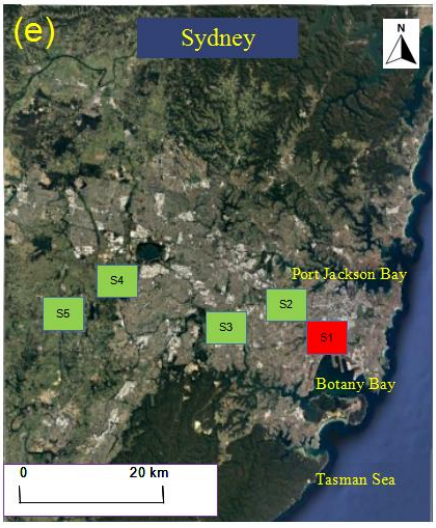
(e)
Sydney
S4
Port Jackson Bay
S5
S2
S3
S1
Botany Bay
0
20 km
Tasman Sea

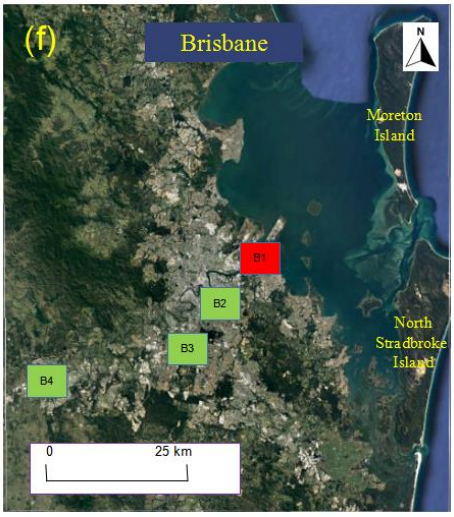

Figure 4. 1 Map of the selected coastal cities of Australia in this study (a) and the distribution of sites for individual cities (b-f).

4.2.2 Data

According to previous studies, sea breezes are most common in hot seasons (Masselink et al., 2001; Pazandeh Masouleh, 2015). Therefore, data in summer (December, January, February and March) are used in this research and the corresponding months from December 2002 to March 2020 are adopted to be the period for further analysis. Totally, 72 months are selected.

In this study, weather data are provided by Bureau of Meteorology, Australia (BOM). The meteorological variables used in this study contain instantaneous air temperature, specific humidity, wind speed and wind direction and the corresponding temporal resolution is 30 minutes. In the metropolitan area, there are more than six BOM sites in each city. In order to have a satisfactory analysis of sea breeze characteristics of these cities, there should be no missing data for each site during the 18 summer seasons. Accordingly, four, four, three, five and four sites satisfy this standard in Perth, Adelaide, Melbourne, Sydney and Brisbane. Overall, weather data from 20 sites of five Australian cities (Perth, Adelaide, Melbourne, Sydney and Brisbane) are used for analysing the characteristics and the cooling effects of sea breezes (Figure 4.1). The detailed information of the selected sites is shown in Table 4.2.

In addition, 30-metre DEM data provided by Department for Environment and Water, South Australia are applied. In this study, they are used to calculate the distances towards the coastline for individual coastal sites.

Table 4. 2 Information of BOM sites used in the analysis of sea breeze cooling, including locations and geographic coordinates.

City	ID	Station Name	Latitude	Longitude
Perth	P1	Swanhourne	31° 57’21’’	115° 45’42’’
Perth	P2	Perth_metro	31° 55’9’’	115° 52’22’’
Perth	P3	Jandakot_aero	32° 6’3’’	115° 52’45’’
Perth	P4	Perth_airport	31° 55’38’’	115° 58’35’’
Adelaide	A1	Adelaide_Airport	34° 57’8’’	138° 31’10’’
Adelaide	A2	Noarlunga	35° 9’30’’	138° 30’20’’
Adelaide	A3	Kent_Town	34° 55’15’’	138° 37’17’’
Adelaide	A4	Parafield_Airport	34° 47’51’’	138° 37’41’’
Melbourne	M1	Moorabbin_aiport	37° 58’47’’	145° 5’46’’
Melbourne	M2	Laverton_raaf	37° 51’23’’	144° 45’23’’
Melbourne	M3	Viewbank	37° 44’26’’	145° 5’49’’
Sydney	S1	Sydney_airport_amo	33° 56’47’’	151° 10’23’’
Sydney	S2	Canterbury_racecourse	33° 54’20’’	151° 6’48’’
Sydney	S3	Bankstown_airport	33° 55’3’’	150° 59’1’’
Sydney	S4	Horsley_park	33° 51’3’’	150° 51’24’’
Sydney	S5	Badgreys_creek	33° 53’48’’	150° 43’41’’
Brisbane	B1	Brisbane_aero	27° 23’30’’	153° 7’45’’
Brisbane	B2	Brisbane	27° 28’50’’	153° 2’20’’
Brisbane	B3	Archerfield	27° 34’17’’	153° 0’25’’
Brisbane	B4	Amberly amo	27° 37’46’’	152° 42’39’’

4.3 Results

4.3.1 Frequency of sea breeze days of major Australian cities

Using the standards listed in Sect. 2.3.3, I have estimated the frequencies of sea breeze days for the five cities during the study period. In each city, the site closest to the coast is selected for the frequency analysis because these sites experience the most frequent sea breezes of the corresponding cities. Ultimately, the sites of P1, A1, M1, S1, B1 are used. As is shown in Figure 4.2, a large range of sea breeze frequency exists among different coastal cities of Australia. In Perth, sea breeze days appear in more than 56% of summer days. Adelaide is

placed second, with the frequency being 40%. In contrast, the corresponding proportions in Sydney and Brisbane are lower than 25%, being 22% and 17% respectively.

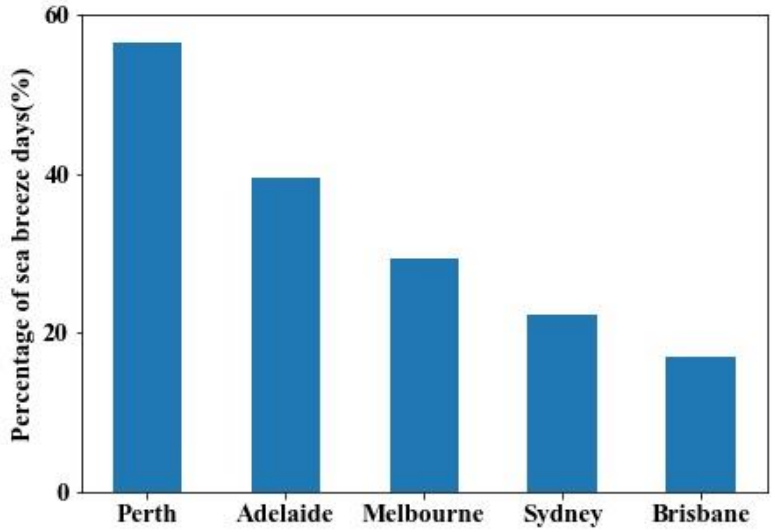

Figure 4. 2 Percentages of sea breeze days in summer (December 2002 - March 2020) for five selected coastal cities of Australia.

In order to attribute the variation of sea breeze frequencies to large-scale synoptic patterns of the five selected cities, Jenkinson and Collison method is used in the classification of synoptic backgrounds. Figure 4.3 shows the correlation between frequencies of sea breeze days and days when anti-cyclone systems exist (synoptic types belonging to A, AN, ANE, AE, ASE, AS, ASW, AW, ANW) for individual years. A clear positive correlation is demonstrated with the R^2 value being 0.57. For the city of Brisbane, the sea breeze frequencies range from 11% to 23%, while days with anti-cyclone systems occupy 17% to 42% of summer days. In contrast, Perth has the most sea breeze days among these cities with the frequencies ranging from 48% to 65%. The corresponding frequencies of days with anti-cyclone systems are also the highest in this city (49% - 75%). In summary, the diversity in frequencies of sea breeze events can largely be explained by synoptic backgrounds.

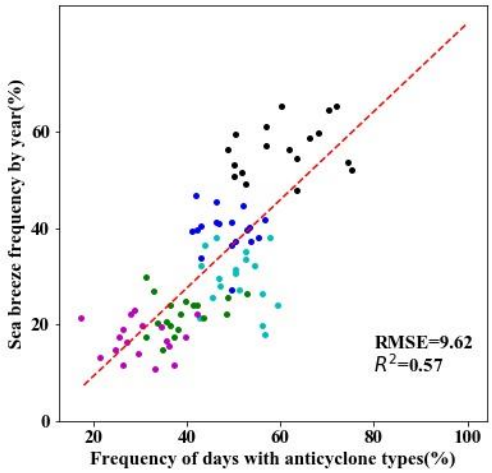

Figure 4. 3 The relationship between sea breeze frequencies by year and proportions of days with anti-cyclone systems (JC types of A; AN; ANE; AE; ASE; AS; ASW; AW; ANW) of individual years for the 5 selected coastal cities. The colours of black, blue, cyan, green and magenta indicate data from Perth, Adelaide, Melbourne, Sydney and Brisbane, respectively.

.

4.3.2 Wind patterns during sea breeze days

Wind speed and wind direction during sea breeze days are investigated for a better understanding of the wind processes affected by sea breezes. Results for the five cities are shown in Figure 4.4. Overall, wind directions are within small ranges and wind speeds are significantly higher during daytime when sea breezes blow over the metropolitan area.

Specifically, more than 90% of wind directions are within 180° - 240° for the coastal site (P1, Swanhourne) at 16:00 in Perth. At site P2 (Perth_metro), the corresponding proportion drops to 73%. For the other two inland sites, only less than 53% of wind directions are within this range. Similar spatial characteristics of wind condition appears in the city of Melbourne. For the two sites which are less than 9 km towards the coast, most of wind directions are concentrated within small ranges. Specifically, 74% of wind directions at site M1 (Moorabbin_aiport) are within 190° - 250° and 60% of wind directions at site M2 (Laverton_raaf) are within 130° - 190° at 14:00. In contrast, for the inland site M3 (Viewbank), wind directions are relatively scattered. As for Adelaide, wind speeds are mostly concentrated within the range of 2 – 6 m/s, while more than 66% of winds blow from 210° to 260° at 14:00 for site A1 (Adelaide_Airport). Meanwhile, for the inland site of Kent_Town (site A3), the corresponding proportion is only 48%, 18% lower. It should be noted that site A2 (Noarlunga) and A4 (Parafield_Airport) show atypical characteristics of wind patterns during sea breezes. For site A2, most of wind directions are distributed relatively scattered between 180° and 300°.

This can be explained by the mountain on the east. When sea breezes blow in this area, the return flow from the mountain can resist the penetration of sea breezes. Additionally, although site A4 is more than 15 km towards the coast along the prevailing wind path, the wind directions of this site are still limited in a small range, which is more similar to the wind pattern of coastal sites. This phenomenon is likely to be resulted from the bay located nearby (Figure 4.1(c)) as airflows from the bay can contribute to the development of sea breezes. Overall, in a place where the topography is relatively flat, the intensity of sea breezes is evidently weakened with the increased distance from the coast.

However, for the city of Sydney and Brisbane, the conditions are different. In Sydney, wind directions are spread in northeast and south at coastal sites. Specifically, 47% and 24% of wind directions at 16:00 at site S1 (Sydney_airport_amo) are within 30° - 80° and 130° - 180°, respectively. In contrast, wind directions between the two ranges (80° - 130°) only account for 17%. From the DEM data of Sydney, it can be clearly seen that two bays exist in the south-eastern and north-eastern part of the metropolitan area, respectively. During daytime, the temperature differences between the two bays and the city centre of Sydney are likely to cause sea breezes blowing from these bays with different directions. Furthermore, they can interact with the sea breeze coming from the coastline facing Tasman Sea at a larger scale. Therefore, sea breeze observations from sites in Sydney are not similar to the general rule that wind directions are within small ranges. Correspondingly, the spatial patterns of characteristics and cooling powers of sea breezes may be irregular.

In Brisbane, there is also a wide distribution of wind direction during sea breezes, mostly within the range of 20° - 150°. From the satellite map of Brisbane, Moreton Island and North Stradbroke Island are located to the north-east of the city. They are probable to impair the formation of the sea breeze. In addition, the shape of coastline is curving, and multiple hills are located inside the metropolitan area of Brisbane. Therefore, the interaction between sea breezes and complex topography is probable to lead to the irregular characteristics of sea breezes inside the city.

In consideration of the different wind patterns of sea breezes among the selected cities, Perth, Adelaide and Melbourne where the topographies are relatively regular are selected in the following analysis. For Sydney and Brisbane, because of the irregular sea breeze characteristics caused by topographies, the cooling effects induced by sea breezes are not further investigated. It should be noted that although there are some sites of Adelaide where the sea breeze

characteristics are not typical, I still choose Adelaide in the further analysis because the topography is relatively regular and there is a clear spatial pattern of SBCC in Adelaide according to Chapter 3.

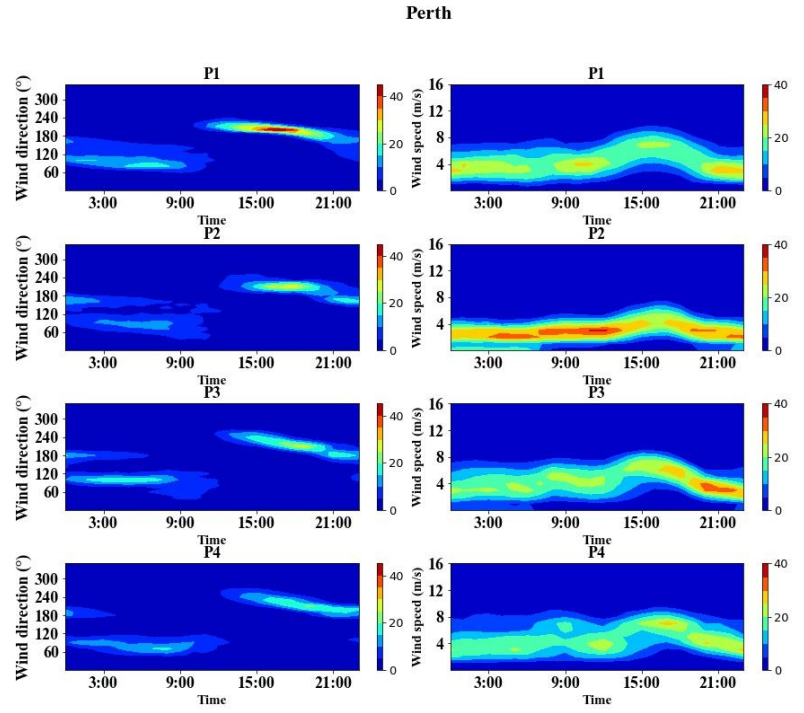

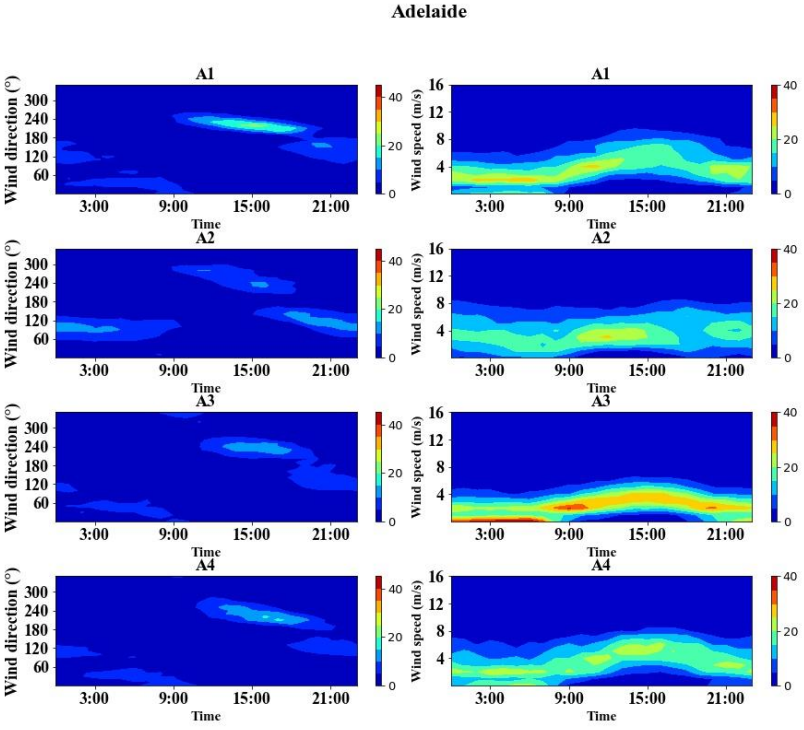

Melbourne

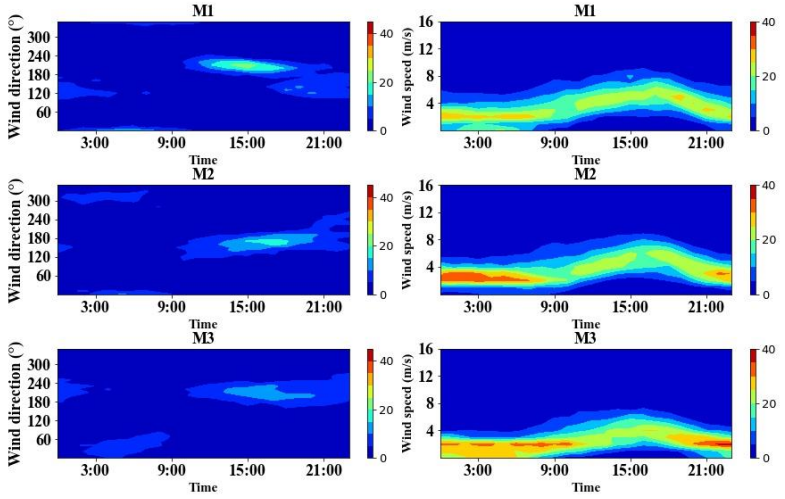

Sydney

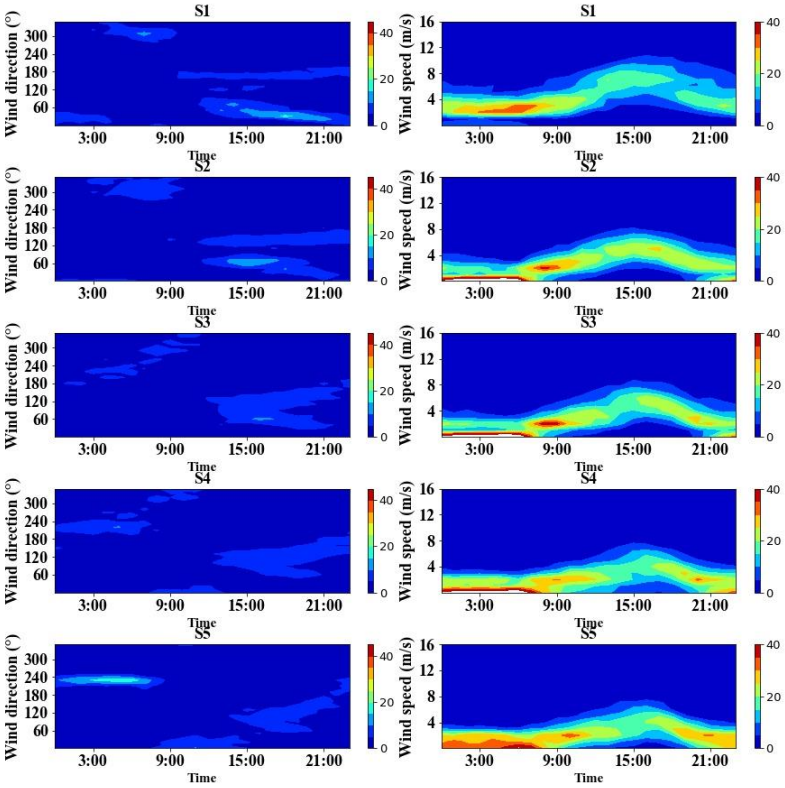

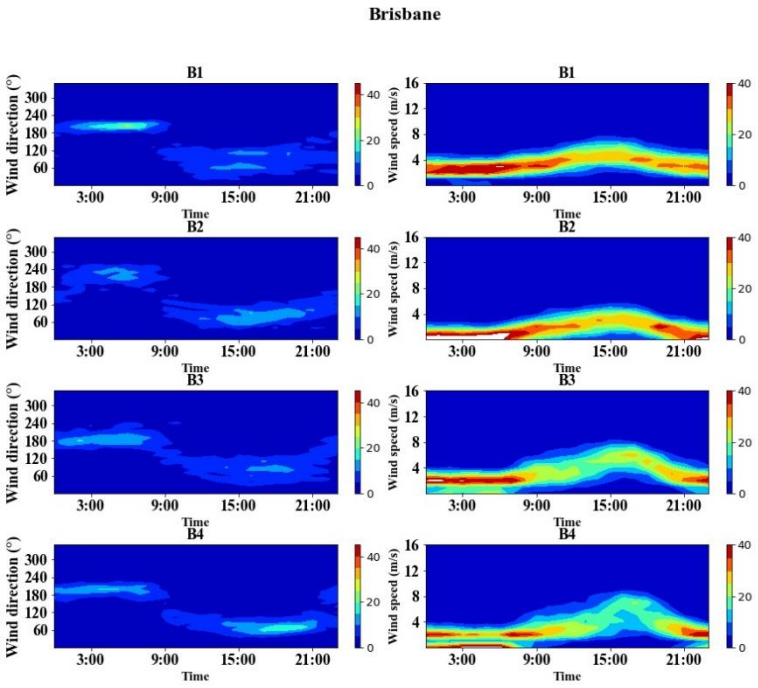

Figure 4. 4 Patterns of hourly wind direction/wind speed frequency (%) during sea breeze days of December 2002 - March 2020 with an interval of 10° for individual sites of the five selected coastal cities.

4.3.3 Diurnal cycle of air temperature for individual sites of Australian cities

Figure 4.5 shows the diurnal changes in air temperatures for different sites of the three cities during sea breeze days. Different colour depths of lines represent different distances to the coast from the corresponding site. For each city, a large diversity of air temperature is shown among sites. In Perth, the coastal site P1 shows a clearly lower air temperature than other sites, especially during daytime. At 14:00, air temperature of site P1 is 4 °C lower than that at site P4. Correspondingly, the temperature differences among sites are much smaller during nighttime. At 22:00, the averaged air temperature is 22.0 °C at the coastal site (P1) and it is only 0.8 °C lower at site P4. Similar patterns of air temperature appear in other cities. In Adelaide, the temperature difference between the coastal site (A1) and the inland site (A4) changes from 3.2 °C to 0.4 °C during 14:00 - 22:00. In Melbourne, air temperatures at 14:00 at the two sites which are close to the coast (M1 and M2) are 23.7 °C and 24.1 °C respectively. The value is about 2 °C higher at site M3. In contrast, the corresponding temperature difference at 22:00 is less than 0.6 °C. Overall, the results demonstrate that there is a clearly increasing trend of air temperature from coast to inland, especially during the daytime. This can be attributed to the weakening cooling powers of sea breezes during the penetration process.

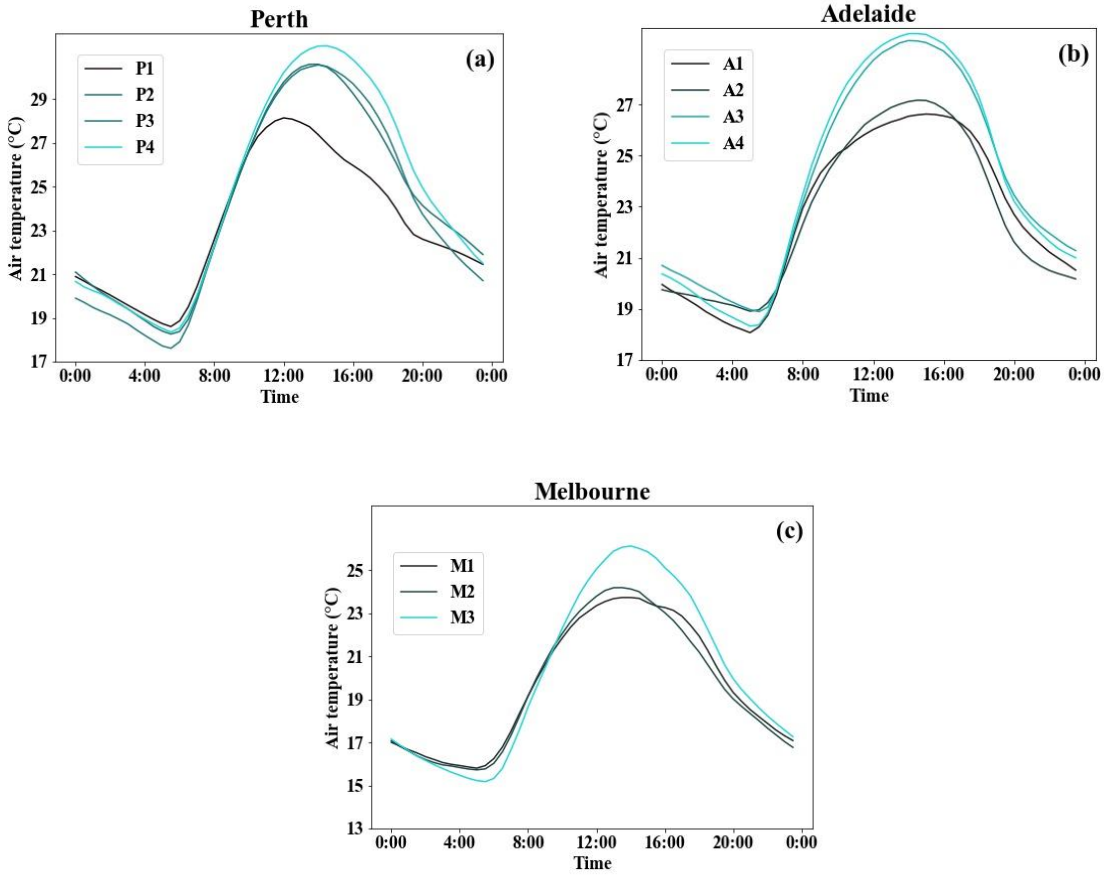

Figure 4. 5 Averaged diurnal cycles of air temperature in summer days during December 2002 - March 2020 for individual sites at (a) Perth, (b) Adelaide, (c) Melbourne. The colour depths represent different distances towards the coast for individual sites. Lines of shallow colours indicate results of inland sites and lines of deep colours indicate results of coastal sites.

4.3.4 Magnitude of temperature reduction of sea breeze cooling

The maximum temperature reduction of sea breeze cooling (dT_{max}) is defined as the maximum temperature difference between the adjusted reference temperature curve and observed temperature curve in a sea breeze event. With the reduced intensity of the sea breeze, the maximum temperature reduction of sea breeze cooling declines during the sea breeze penetration (Figure 4.6). In Melbourne, dT_{max} values are 3.8 °C and 3.1 °C at site M1 and M2 averaged over all sea breeze days, while the corresponding magnitude at the most inland site (M3) is 1.8 °C. In Perth and Adelaide, the ranges of dT_{max} values are 1.9 °C – 4.6 °C and 3.0 °C - 4.1 °C, respectively.

Similar to Chapter 3, I have also analysed the temperature reduction in hot sea breeze days and the definition of a hot sea breeze day here is the same as that in Chapter 3. The results reveal larger contrasts of dT_{max} values between coastal sites and inland sites for the three cities during

hot sea breeze days. In Melbourne, the temporally average dT_{max} values are 4.7 °C and 3.3 °C at site M1 and M2 and it is only 1.2 °C at site M3. The contrast between site M3 and M1 is 3.5 °C, 1.5 °C larger than that during all sea breeze days. In Perth and Adelaide, the contrasts of temperature reductions among sites are 4.5 °C and 2.3 °C in hot sea breeze days.

Figure 4. 6 Spatial patterns of maximum temperature reduction (°C) averaged over the study period (summer sea breeze days during December 2002 - March 2020) for Perth (a,b), Adelaide (c,d) and Melbourne (e,f) in all sea breeze days (a,c,e) and hot sea breeze days (b,d,f), respectively.

4.3.5 Spatial pattern of SBCC for major Australian cities and its influencing factors

Figure 4.7 shows the spatial patterns of event SBCC and seasonal SBCC for the three selected cities. For each site, the seasonal SBCC is the SBCC value averaged over all 18 summers (from December to March next year). The results reveal that large contrasts of SBCC exist in all three cities. In Perth, the temporally average SBCC during the study period is 32.0 °C·h per event (2190.8 °C·h per season) at the coastal site (P1) and the corresponding magnitude is 9.3 °C·h per event (638.5 °C·h per season) at site P4. Here a season represents a continuous period from December to March next year. In Adelaide, the temporally average SBCC at the coastal site (A1) is 25.2 °C·h per event (1206.8 °C·h per season). At site A3, it rapidly drops to 17.3 °C·h per event (829.1 °C·h per season). Correspondent to the wind patterns during sea breeze days, temporally average SBCC at site A2 and A4 are 17.0 °C·h and 18.6 °C·h per event (813.5 °C·h and 890.7 °C·h per season), respectively. The important role of mountains and waterbodies in determining sea breeze cooling is clearly demonstrated from the two sites. Similar spatial patterns can also be found in Melbourne, in which M1 being the site with the largest cooling (24.4 °C·h per event, 867.8 °C·h per season) and M3 the site with the smallest cooling (8.5 °C·h per event, 302.5 °C·h per season). In summary, the decreasing patterns of SBCC from coast to inland exist for the three coastal cities of Australia.

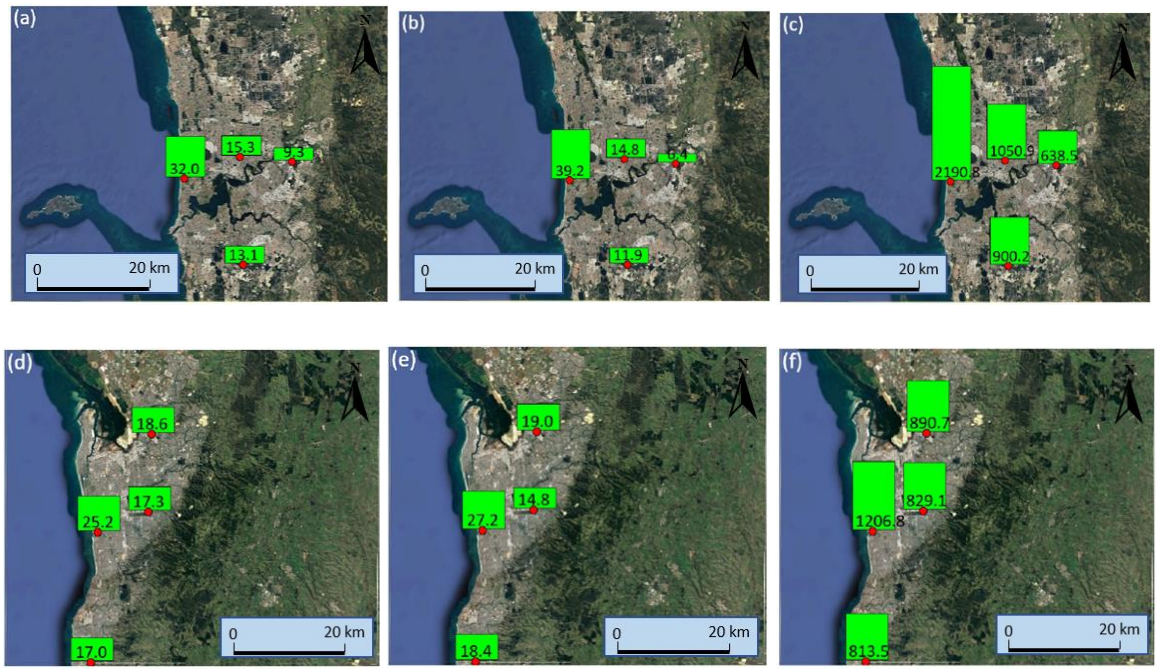

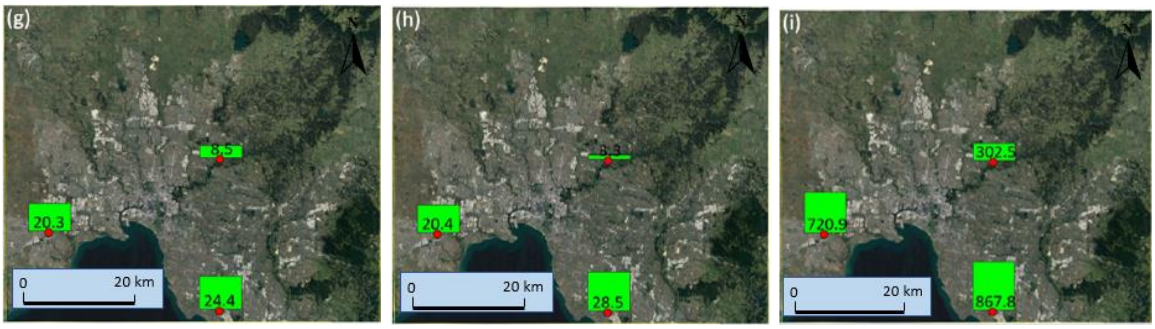

Figure 4. 7 Spatial patterns of SBCC (°C·h) averaged over the study period (summer sea breeze days during December 2002 - March 2020) for Perth (a,b,c), Adelaide (d,e,f) and Melbourne (g,h,i), respectively. The averaged event SBCC values are shown in subplots (a,d,g) for all sea breeze days and (b,e,h) hot sea breeze days. The subplots (c,f,i) represent seasonal SBCC values for all sea breeze days.

Consistent with the spatial pattern of dT_{max}, there is also a larger diversity of the temporally average SBCC values in each city during hot sea breeze days compared to those of all sea breeze days. In Perth, it is 39.2 °C·h per event at the coastal site (P1) and it drops to 6.4 °C·h at site P4. Correspondently, the site-to-site contrast is 32.8 °C·h. In Adelaide and Melbourne, the contrasts of temporally averaged SBCC per event among sites are 12.4 °C·h. and 25.2°C·h, respectively.

4.3.6 Penetration distance of sea breeze cooling

From the spatial patterns of temporally average SBCC, sea breeze cooling magnitudes decrease along the penetration path. In Chapter 3, I have detected a linear relationship between the distances from the coast and SBCC values in metropolitan Adelaide and therefore the penetration distance of sea breeze cooling for a city can be estimated according to this relationship. According to Figure 4.8, the distances are 43.3 km, 41.0 km and 26.6 km for Perth, Adelaide and Melbourne, respectively. In hot sea breeze days, the corresponding distances decrease to 36.3 km, 28.8 km and 20.3 km. In Chapter 3, I have analysed the relation between the distance towards the coast and SBCC and the results are shown as the blue dotted lines in subplots (c) and (d) of Figure 4.8. The similarity of these two lines with the red dashed lines calculated by BOM data confirms the reliability of the result in this multi-city analysis although much less sites have been used.

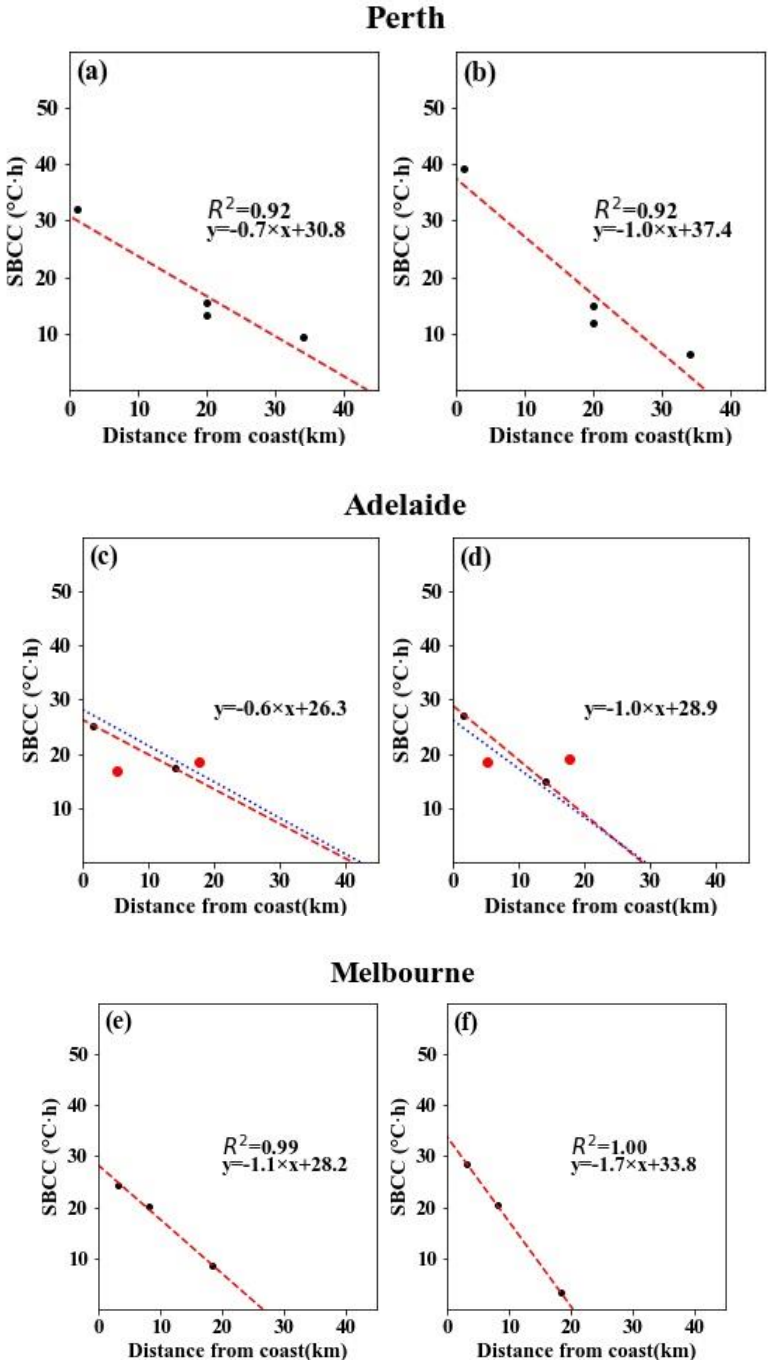

Figure 4. 8 Estimation of penetration distances of sea breeze cooling according to the relationship between distance from the coast and SBCC for three cities in all sea breeze days (a,c,e) and hot sea breeze days (b,d,f), respectively. The two red dots represent two sites which are significantly influenced by surrounding topography. The blue dotted lines in subplots (c) and (d) show the relation between SBCC and distance towards the coast using data from the Adelaide urban heat island monitoring network in Chapter 3.

4.3.7 Temporal variations of seasonal sea breeze cooling for individual sites and the influencing factors

In order to investigate the temporal patterns of sea breeze cooling in Australian cities, inter-annual variations of seasonal SBCC of all sites in the three selected cities are explored.

According to Figure 4.9 and Table 4.3, there is no significant trend of seasonal SBCC in most of the sites. As an exception, a significant decrease appears at the coastal site of Perth (site P1) with the slope being -26.1 °C·h/year and the corresponding *p* value being 0.03. In addition, seasonal SBCC at site M3 shows a significant increasing trend with the slope being 7.9 °C·h/year and the corresponding *p* value being 0.04.

Meanwhile, linear regressions of SBCC with potential influencing factors are performed using seasonal values at individual sites for the corresponding variables. It is likely that the cooling is mostly influenced by the background synoptic characteristics and mesoscale driving forces of the coastal areas. Meanwhile, the characteristics on land (topography, land cover and urban structure) can be additional influencing factors of the inland areas. Therefore, the sites in the analysis are separated into two groups: coastal sites and inland sites. The sites that are nearest to the coast for individual cities (P1, A1 and M1) are assigned as the coastal sites, while the remaining sites are defined as the inland sites. In this study, I adopt temperature difference between land and sea surface and frequency of days with anti-cyclone systems as potential influencing factors for analysing the temporal variability of SBCC.

Results of these regressions show that temperature difference between land and sea has limited effects on sea breeze cooling for both types of sites (Figure 4.10). Meanwhile, the large-scale synoptic patterns are significantly related to sea breeze cooling only for the coastal sites with the R^2 value being 0.80. Conversely, the corresponding relationship is weak for the inland sites. It reveals the key roles of land cover and topography in influencing sea breeze cooling for inland areas.

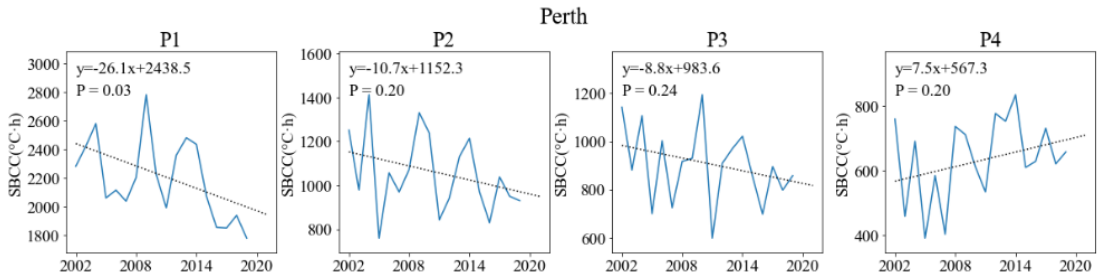

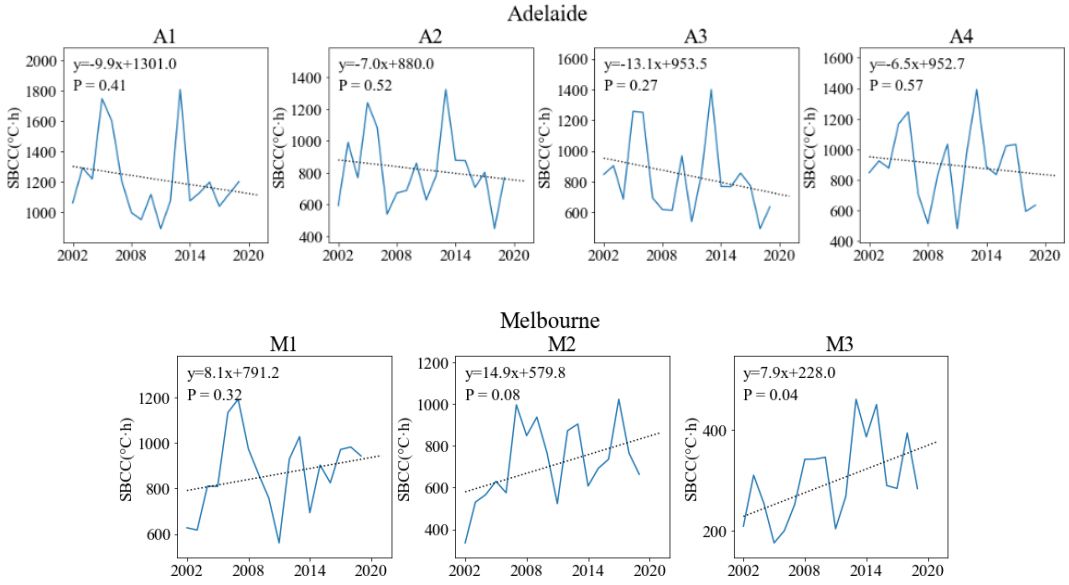

Figure 4. 9 Inter-annual variations of SBCC for coastal sites of the three selected Australian cities.

Table 4. 3 Result of significance analysis of SBCC trends during the study period. Grey colour indicates sites without significant trends of seasonal SBCC. Red and blue colours indicate sites with significantly negative and positive trends of seasonal SBCC, respectively.

	Site 1	**Site 2**	**Site 3**	**Site 4**
Perth				
Adelaide				
Melbourne				

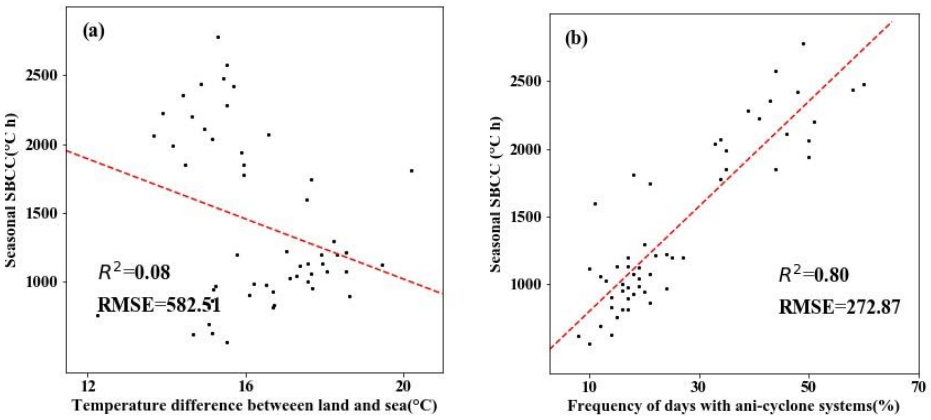

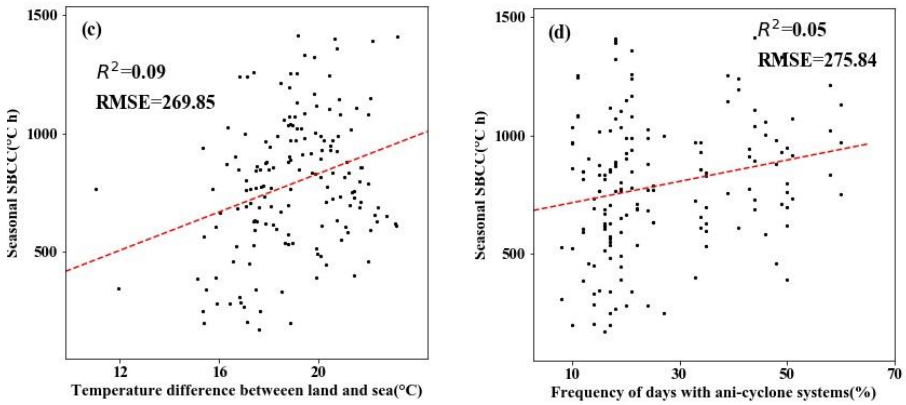

Figure 4. 10 The relationship between seasonal SBCC and climate background (temperature difference between land and sea and frequency of days with anti-cyclone systems) for coastal sites (a,b) and inland sites (c,d) respectively.

4.4 Discussion

Driven by the positive temperature differences between land and sea, the occurrences of sea breezes are significantly influenced by the background weather which is shaped by synoptic patterns of the surrounding area. Among the five Australian cities selected, there is a large variation in sea breeze frequency varying from 17% to 56%. Meanwhile, the frequency of synoptic patterns with anti-cyclone systems shows a positive relation with the sea breeze frequency. This is reasonable as high-pressure systems are more likely to dominate the metropolitan areas and hence the air temperatures over the land increase faster during days with anti-cyclone systems than that during other days. Consequently, a larger probability of positive land - sea temperature contrast can be generated. In addition, with high-pressure systems, the large-scale background wind is relatively weak and hence local-scale atmospheric systems are probable to control the weather during these days. Observations show that the mean wind speed during daytime at an inland station is less than 5 m/s under high-pressure systems for most of mesoscale breezes (Laird et al., 2001). Similar characteristics can also be found in other coastal cities in the world. In Jiangsu, China, anti-cyclone type is the most frequent synoptic type among all types except the unknown type during sea breeze days (Huang et al., 2016). In Alicante, Spain, the anti-cyclone type occupies more than 30% of sea breeze days (Azorin-Molina et al., 2011). Overall, the synoptic backgrounds play significant roles in influencing the formation of sea breeze days in coastal cities of Australia.

Sea breezes can also develop during days with other types of systems (e.g., cyclone systems) at a lower probability. For example, a thermal low-pressure region around Iberian Peninsula leads to a low gradient of air pressure at sea surface level and sea breezes can also develop in this environment (Hoinka et al., 2003). A weak pressure gradient occurs under NE type (the type that contributes to northeasterly airflows) when subtropical high pressure moves north in Alicante (Luchetti et al., 2017).

4.5 Conclusions

The sea breeze is an important atmospheric phenomenon in mitigating excessive heat during summer for coastal cities and a comparative analysis of the cooling effects induced by sea breezes is contributory in understanding the mechanism of sea breeze cooling. In this study, I analyse the temporal and spatial patterns of basic characteristics and cooling effects of sea breezes in major Australian cities. The study period includes all summer days from December 2002 to March 2020.

The results show that there is a relatively large diversity in frequency of sea breeze events ranging from 17% to 56% among the five major cities (Perth, Adelaide, Melbourne, Sydney and Brisbane). According to the linear regression, the sea breeze frequency is significantly related to the frequency of days with anti-cyclone systems, with the R^2 being 0.57. Therefore, it can be derived that large-scale synoptic patterns play an important role in determining the sea breeze frequency. There are also large inconsistencies of wind patterns of sea breeze days among these cities. Specifically, in Perth, Adelaide and Melbourne, wind speeds are evidently higher and wind directions are within small ranges during daytime when sea breezes happen in most of the sites. However, for the cities of Sydney and Brisbane, the temporal patterns of wind speeds and wind directions are atypical, which is considered to be resulted from complex topographies of the two cities.

For the three cities with regular topographies (Perth, Adelaide, and Melbourne), comparisons of air temperatures among multiple sites demonstrate the key role of the distance towards the coast on air temperature for coastal cities which can be attributed to the weakening power of sea breezes. This has been confirmed by the declining trends of SBCC and maximum temperature reductions during sea breeze events. Specifically, temporally average dT_{max} values range from 1.9 °C to 4.6 °C in Perth, from 3.0 °C to 4.1 °C in Adelaide and from 1.8 °C to 3.8 °C in Melbourne. The SBCC values per event range from 9.3 °C·h to 32.0 °C·h

in Perth, from 17.0 °C·h to 25.2 °C·h in Adelaide and from 8.5 °C·h to 24.4 °C·h in Melbourne. According to the declining trends of SBCC values during sea breeze events, the penetration distances of sea breeze cooling are estimated to be 43.3 km, 41.0 km and 26.6 km for Perth, Adelaide and Melbourne, respectively.

With respect to the inter-annual variations of seasonal SBCC for the three selected cities, it is found that the effects of temperature difference between land and sea are limited. Meanwhile, frequency of days with anti-cyclone systems is positively related to the seasonal cooling of sea breezes for coastal sites. For inland sites, the corresponding relation is weak which is derived to be resulted from the effects of local factors on land along penetration paths.

References

Abbs DJ. Sea-breeze interactions along a concave coastline in southern Australia: Observations and numerical modeling study. Monthly weather review. 1986 May;114(5):831-48.

Arritt RW. Numerical modelling of the offshore extent of sea breezes. Quarterly Journal of the Royal Meteorological Society. 1989 Apr;115(487):547-70.

Augustin P, Billet S, Crumeyrolle S, Deboudt K, Dieudonné E, Flament P, Fourmentin M, Guilbaud S, Hanoune B, Landkocz Y, Méausoone C. Impact of sea breeze dynamics on atmospheric pollutants and their toxicity in industrial and urban coastal environments. Remote Sensing. 2020 Jan;12(4):648.

Azorin-Molina C, Chen D. A climatological study of the influence of synoptic-scale flows on sea breeze evolution in the Bay of Alicante (Spain). Theoretical and applied climatology. 2009 May;96(3):249-60.

Azorin‐Molina C, Chen D, Tijm S, Baldi M. A multi‐year study of sea breezes in a Mediterranean coastal site: Alicante (Spain). International Journal of climatology. 2011 Mar 15;31(3):468-86.

Frizzola JA, Fisher EL. A series of sea breeze observations in the New York City area. Journal of Applied Meteorology and Climatology. 1963 Dec;2(6):722-39.

Grau A, Jiménez MA, Cuxart J. Statistical characterization of the sea‐breeze physical mechanisms through in‐situ and satellite observations. International Journal of Climatology. 2021 Jan;41(1):17-30.

Guo F, Zhang H, Fan Y, Zhu P, Wang S, Lu X, Jin Y. Detection and evaluation of a ventilation path in a mountainous city for a sea breeze: The case of Dalian. Building and Environment. 2018 Nov 1;145:177-95.

Hirsch AL, Evans JP, Thomas C, Conroy B, Hart MA, Lipson M, Ertler W. Resolving the influence of local flows on urban heat amplification during heatwaves. Environmental Research Letters. 2021 Jun 10;16(6):064066.

Hoinka KP, Castro MD. The Iberian peninsula thermal low. Quarterly Journal of the Royal Meteorological Society: A journal of the atmospheric sciences, applied meteorology and physical oceanography. 2003 Apr;129(590):1491-511.

Huang M, Gao Z, Miao S, Xu X. Characteristics of sea breezes over the Jiangsu coastal area, China. International Journal of Climatology. 2016 Oct;36(12):3908-16.

Jiang N, Scorgie Y, Hart M, Riley ML, Crawford J, Beggs PJ, Edwards GC, Chang L, Salter D, Virgilio GD. Visualising the relationships between synoptic circulation type and air quality in Sydney, a subtropical coastal‐basin environment. International Journal of Climatology. 2017 Mar;37(3):1211-28.

Laird NF, Kristovich DA, Liang XZ, Arritt RW, Labas K. Lake Michigan lake breezes: Climatology, local forcing, and synoptic environment. Journal of Applied Meteorology. 2001 Mar;40(3):409-24.

Lericos TP, Fuelberg HE, Watson AI, Holle RL. Warm season lightning distributions over the Florida peninsula as related to synoptic patterns. Weather and Forecasting. 2002 Feb;17(1):83-98.

Luchetti NT, Nieto Ferreira R, Rickenbach TM, Nissenbaum MR, McAuliffe JD. Influence of the North Atlantic Subtropical High on wet and dry sea-breeze events in North Carolina, United States.

Masselink G, Pattiaratchi CB. Seasonal changes in beach morphology along the sheltered coastline of Perth, Western Australia. Marine Geology. 2001 Feb 15;172(3-4):243-63.

Mavrakou T, Philippopoulos K, Deligiorgi D. The impact of sea breeze under different synoptic patterns on air pollution within Athens basin. Science of the total environment. 2012 Sep 1;433:31-43.

Miller ST, Keim BD, Talbot RW, Mao H. Sea breeze: Structure, forecasting, and impacts. Reviews of geophysics. 2003a Sep;41(3).

Miller ST, Keim BD. Synoptic-scale controls on the sea breeze of the central New England coast. Weather and forecasting. 2003b Apr;18(2):236-48.

Pazandeh Masouleh Z. *Identification of sea breezes, their climatic trends and causation, with application to the Adelaide coast* (Doctoral dissertation).

Pazandeh Masouleh Z, Walker DJ, Crowther JM. Sea breeze characteristics on two sides of a shallow gulf: study of the Gulf St Vincent in South Australia. Meteorological Applications. 2016 Apr;23(2):222-9.

Suresh R. Observation of sea breeze front and its induced convection over Chennai in southern peninsular India using Doppler weather radar. InAtmospheric and oceanic 2007 (pp. 1511-1525). Birkhäuser Basel.

You C, Fung JC, Tse WP. Response of the sea breeze to urbanization in the Pearl River Delta Region. Journal of Applied Meteorology and Climatology. 2019 Jul 1;58(7):1449-63.

Chapter 5 Variation of sea breeze cooling induced by the interaction between urban structure and wind speed

Abstract

The understanding of the combined effects of urban structure and wind speed on thermal environment is limited. In particular, it is not clear what the magnitude of the influence of urban structures on wind cooling can be. In this study, I analyse the quantitative effects of urban structure (building height, canyon orientation) and wind speed on air temperature and thermal comfort level based on the ENVI-met simulation of a typical sea breeze day in the coastal city of Adelaide, Australia. Results show a reduction of averaged air temperature from 27.16 °C to 26.92 °C with an increase of building height from 4 metres to 12 metres. Meanwhile, air temperature has been found to change nonlinearly with canyon orientation. With the increased building height, the cooling induced by stronger wind decreases. This indicates the contrasting effects of building height on air temperature by shading and wind cooling.

In this thesis, this chapter makes the contribution on the quantitative effects of urban structure and background wind speed on the thermal environment, taking the sea breeze as the wind background. It has implications for urban designs of cities with different types of prevailing winds.

5.1 Introduction

The United Nations reports that about 4.2 billion people lived in cities on earth in 2018 and the number is estimated to rise to 5.5 billion by 2035 (United Nations, 2018). With the increasing number of residents living in cities, the climate and environment of urban areas have become the focus of many studies. In particular, much attention has been paid on the negative effects of urban heat island under global warming. In fact, urban climate is more or less the consequence of human modifications and therefore appropriate urban designs make remarkable contributions in improving the thermal environment of urban areas. For example, based on the analysis on land surface temperature in Dalian, China, Yang et al. (2020) proposed an appropriate layout of local climate zone that distinctly mitigates the accumulated urban heat island intensity. In Guangzhou, a simulation revealed that adding grey infrastructures (artificial shading facilities) is more efficient than planting vegetation of the same coverage area in heat mitigation for parks and squares (Jing et al., 2020). Therefore, specific planning strategies should be adopted for individual local climate zones to make the best of measures of urban cooling.

Traditional approaches in mitigating urban heat island include reducing the net absorption of solar radiation, enhancing ventilation in the urban canopy and active cooling (e.g., increasing evapotranspiration from leaf surfaces and evaporation from open water bodies and surfaces). The effects of ventilation on the thermal environment of urban areas have been widely reported. If the wind comes from a cooler area, air temperature would decrease and consequently the heat stress would be eliminated to a certain extent. Among all the variables related to ventilation, wind speed has received much attention. Giannaros et al. (2012) investigated air temperature in the Thessaloniki metropolitan area of Greece for a whole year and concluded that the intensity of hourly urban heat island is largely weakened when wind speed is higher than 4 m/s by summarizing continuous hourly data for a whole year. By analysing observation data from a monitoring network, an average reduction of 0.14 °C in urban heat island induced by 1 m/s increase of wind speed is detected in Melbourne (Morris et al., 2001).

Urban structure comprises the 3-dimensional characteristics (shapes, layouts and sizes) of buildings and the relative locations of these buildings to the surrounding streets and open areas. It can largely influence the airflow inside the urban canopy and typical geometrical parameters have been used as potential factors in investigating the effects of urban structure

on ventilation. According to simulation results, the increase of frontal area density of an urban area can lead to a reduction of in-canopy wind velocity (Bentham et al., 2003). In addition, the diversity of building heights facilitates vertical mixing of the lower atmosphere and accordingly affects urban ventilation (Wang et al., 2021). As for the shape of buildings, a computational fluid dynamics (CFD) simulation revealed that the 'L'-shaped building array performs better in distributing pollutants than the 'U'-shaped building array (Llaguno-Munitxa et al., 2017). In addition, air change rate per hour drops and the ventilation is worsened in urban canopy if urban size is expanded from 390 m to 5 km according to a simulation (Lin et al., 2014). There can also be a large variety of ventilation effects among different layouts of buildings. Using a large-eddy simulation in a typical high-density urban area, Wang et al. (2018) revealed that the larger parallel-to-perpendicular street width ratio makes rectangular layout performs better in inducing airflow compared to square layout.

In fact, urban structure also alters the absorption of solar radiation and influences the exchange of longwave radiation at pedestrian level. Therefore, it is an important factor in the mitigation of urban heat island. For example, aspect ratio is the ratio of street width to the average height of surrounding buildings of a street canyon. In the city of Thessaloniki, Chatzidimitriou et al. (2017) revealed that the increase of aspect ratio from 0.7 to 3.0 can reduce physiological equivalent temperature (PET) by 7 °C in winter daytime. The cooling effect of increasing aspect ratio has also been found to be relatively smaller in cloudy days compared to sunny days according to observations in Sri Lanka (Rohinton et al., 2006). In contrast to aspect ratio, the ratio of street length to the average height of surrounding buildings takes limited effects on the movement of airflow and thermal performance at microscale (Oke et al., 2004). As for the spatial layout and orientation of buildings, enclosing-form building layout is found to be unfavourable in improving thermal comfort during summer in residential areas of Xi'an, China (Yang et al., 2020). Strømann-Andersen et al. (2011) also demonstrated an increase of up to 30% in energy consumption resulted from an unreasonable layout of urban canyon.

Table 5. 1 Representative researches on the application of ENVI-met in simulating urban microclimate.

Classification of research objects	Scenario settings	Year	City	Main findings	Reference

Urban structure	Settings with different aspect ratios and L/H (length/height) ratios	2015, 2016	Sao Paulo, Brazil,	Canyons with a higher aspect ratio improve the thermal comfort at the pedestrian level, especially in the summer, while an increase in the L/H ratio had no significant effect on the thermal comfort.	Muniz-Gäal et al., 2020
	Different building heights and building densities	2018	Nanjing, China	Building heights and building densities play the most important role in thermal comfort.	Peng et al., 2020
	Five urban forms	2000	De Bilt, Netherlands	Duration of direct sun and mean radiant temperature, which are influenced by urban form, play the most important role in thermal comfort	Taleghani et al., 2015
Vegetations	Plants with different LAIs	2018	Chongqing, China	Tree species with low LAI had a greater cooling effect on the surrounding waterfront thermal environment.	Shi et al., 2020
	Different arrangements and species of trees	2016	Wuhan, China	The impact of vegetation on both heat environment and ventilation depended on tree arrangement, LAI, crown width and tree height	Zhang et al., 2018
	Different land covers of vegetations (trees and grasses)	2018	Cairo, Egypt	Trees are ineffective in the decreasing of air temperature and the reduction of energy in buildings while they are effective in enhancing thermal performance	Aboelata et al., 2020
Mixture of multiple elements	Adding different proportions of green, blue and grey infrastructures	2019	Guangzhou, China	The cooling is strongest for adding grey infrastructures in the square and park and for green infrastructures in residential districts.	Li et al., 2019

Despite that both urban structure and background wind speed are responsible in shaping the urban thermal environment, the combined effects of both variables are still not well understood. According to Chapter 2, sea breezes blow in about 1/3 of in Adelaide summer and they have been found to significantly reduce air temperature of the urban area. In this study, ENVI-met, a widely used urban microclimate model, is used to analyse the effects of

urban structure (building height, canyon orientation) and wind speed on air temperature and thermal comfort in a typical sea breeze event based on the coastal city of Adelaide. Particular attention is paid on the effect of urban structure on wind cooling induced by sea breezes. This study aims to provide a satisfactory plan to create a climate-friendly urban design for coastal cities.

5.2 Data and Methods

5.2.1 Introduction of ENVI-met model

ENVI-met is a 3-dimensional theoretical model used for simulating the interaction of multiple processes inside the urban canopy (Tsoka et al., 2018). It contains atmospheric, vegetation and surface modules. The simulations are based on high spatial resolutions of 0.5 - 10 metres and therefore the continuous changes of meteorological variables inside a small area can be demonstrated in detail. If there are good consistencies between simulations and observations for one or several measurement points in a real urban area, this model can further be used in evaluating the effects of surface elements on local climate by adopting different settings of input variables.

Studies have shown that ENVI-met model performs well in estimating air temperature, relative humidity and mean radiant temperature under different climate conditions (Li et al., 2020; Muniz-Gäal et al., 2020). Until now, this model has been used in many studies in understanding the effects of urban characteristics on microclimate. Research questions mainly include: (1) the effects of adding urban vegetations such as trees and grasses; (2) the effects of using cool materials of land and building surfaces; (3) the effects of waterbodies such as ponds, lakes and fountains; (4) the effects of the combined application of multiple measures (Fahmy et al., 2009; Kruger et sl., 2011; Ng et al., 2012). In addition, indexes such as Predicted Mean Vote, Physiological Equivalent Temperature can also be calculated by the "Bio-met" module inside ENVI-met simulation software. They are helpful in evaluating the thermal comfort levels of urban areas (Taleghani et al., 2015).

5.2.2 Study area

The interested area in this chapter is Hawthorn, a suburb located about 4 km to the south of the Adelaide CBD. This area is composed of multiple single or double-story residential

houses arranged in rows. The heights of these houses are mostly less than 10 metres. Around most of the houses, grasses are planted in backyards to improve the living environment of residents. Along the sidewalks are white cedar (Melia azedarach) trees with the average height being about 10 metres. In summary, the study area presents a regular urban structure and is representative of suburban areas for Australian cities. Therefore, the suburb of Hawthorn is suitable for an urban simulation at microscale.

5.2.3 Setup for ENVI-met validation

Two simulation files need to be prepared for the initialization of ENVI-met modelling: (1) a domain file describing the 3-dimensional spatial pattern and properties of buildings and other land surface elements (e.g., trees, grasses); (2) a file of initial boundary condition with background weather data configured, such as air temperature, relative humidity, wind speed and wind direction.

To maintain the robustness of the modelling, the minimum heights of the 3-dimensional domains should be higher than twice of the maximum building heights inside the corresponding areas. In this study, the maximum building heights are less than 13 metres in the case-study areas. Correspondently, the vertical sizes of the domains are set to be 32 metres. Based on two typical suburban areas of Hawthorn, i.e. Jeffery and Rugby, two domains of 400 m × 400 m × 32 m are set as domains for the model validation. Considering the computer capacity and simulation time, the corresponding spatial resolutions are 5 m × 5 m × 1.6 m (Figure 5.1). Similar resolutions have been used in other studies (Sun et al., 2017; Li et al., 2020).

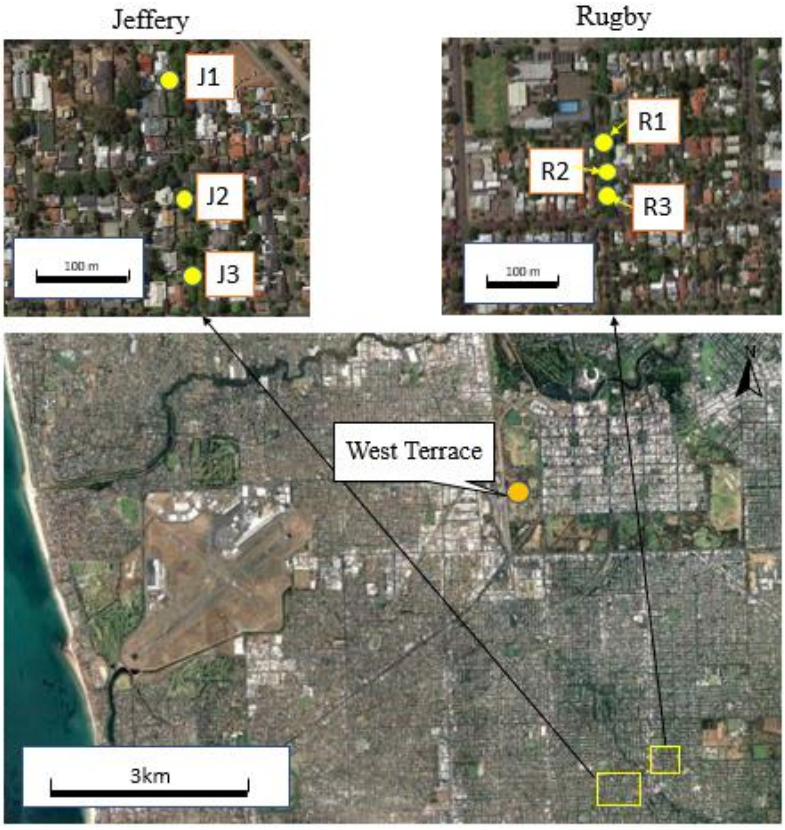

Figure 5. 1 Locations of six measurement sites on Jeffery and Rugby Streets.

West Terrace weather station of BOM (Bureau of Meteorology, Australia) is about 5 kilometres to the north of Hawthorn and its surrounding environment is relatively flat. Here, weather data from this station on February 13rd, 2020 (air temperature, relative humidity, wind speed and wind direction) with the time interval of 1 hour are used as the input boundary condition for the evaluation of ENVI-met in the city of Adelaide. The data are derived from Bureau of Meteorology, Australia.

Vegetation plays an important role in shaping the micro-climate of surrounding areas mainly by transpiration and wind blocking effects. In the simulation, a standard tree model is configurated based on properties of white cedar (*Melia azedarach*) trees in Hawthorn. For an accurate description of the effects of urban vegetations on microclimate, leaf area density (LAD) is used to describe the 3-dimensional characteristics of vegetations in ENVI-met modelling. Leaf area density is defined as the ratio of leaf surface to the volume of air in a specific space. Different from leaf area index (LAI) which only focuses on 2-dimensional processes, LAD considers the vertical distribution of leaf density of a tree. On the basis of the on-site measurement of typical trees in Hawthorn, the vertical pattern of LAD of the standard

tree is assessed and shown in Table 5.2. Additionally, I use default values of the corresponding materials (reinforced brick for walls and tile for roofs) in ENVI-met as standard thermal properties of building materials in the simulation.

Table 5. 2 Vertical distribution of leaf area density (LAD) of the standard tree in ENVI-met simulation.

Height (m)	LAD (m^2/m^3)
2 - 3	0.5
3 - 5	0.7
5 - 6	0.9
6 - 8	1.1
8 - 9	0.9
9 - 10	0.7

5.2.4 Field measurement

In order to evaluate the accuracy of ENVI-met model in simulating urban microclimate of the metropolitan Adelaide, data of air temperature and relative humidity from field-based measurements are used. They were collected by six Maxim Thermochron Ibutton Sensors at 4-metre height with an interval of 60 minutes on two streets in Hawthorn (Jeffery Street and Rugby Street) (Figure 5.1). These sensors are covered by naturally ventilated radiation shields to avoid the influences of sunlight and rain. In this study, February 13rd, 2020 is selected as the study period for the evaluation of ENVI-met model as it is a typical sea breeze day of Adelaide. From data provided by the reference weather station (West Terrace), the maximum and minimum air temperatures of this day are 29.5 °C and 17.9 °C respectively.

5.2.5 Model evaluation

With the model setup described in Sect. 5.2.3, simulations have been performed on Jeffery Street and Rugby Street. The modelling results of air temperature and relative humidity are then compared to the on-site measurements to evaluate the performance of ENVI-met in Adelaide. The evaluation is based on coefficient of determination (R^2) and root mean square error (RMSE) and the corresponding results are shown in Figure 5.2 and Figure 5.3.

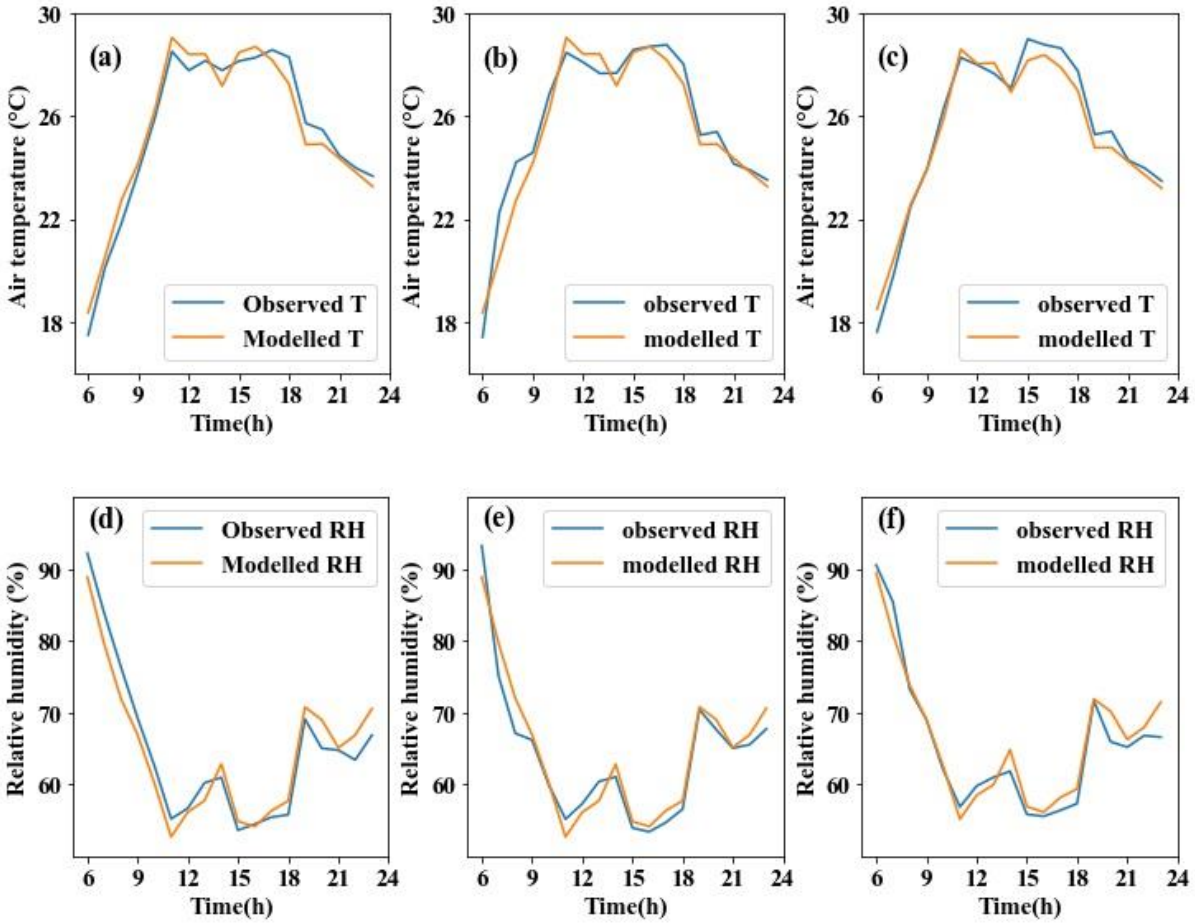
(a)
Observed T
Modelled T
Air temperature (°C)
Time(h)
(b)
observed T
modelled T
(c)
observed T
modelled T
(d)
Observed RH
Modelled RH
Relative humidity (%)
(e)
observed RH
modelled RH
(f)
observed RH
modelled RH

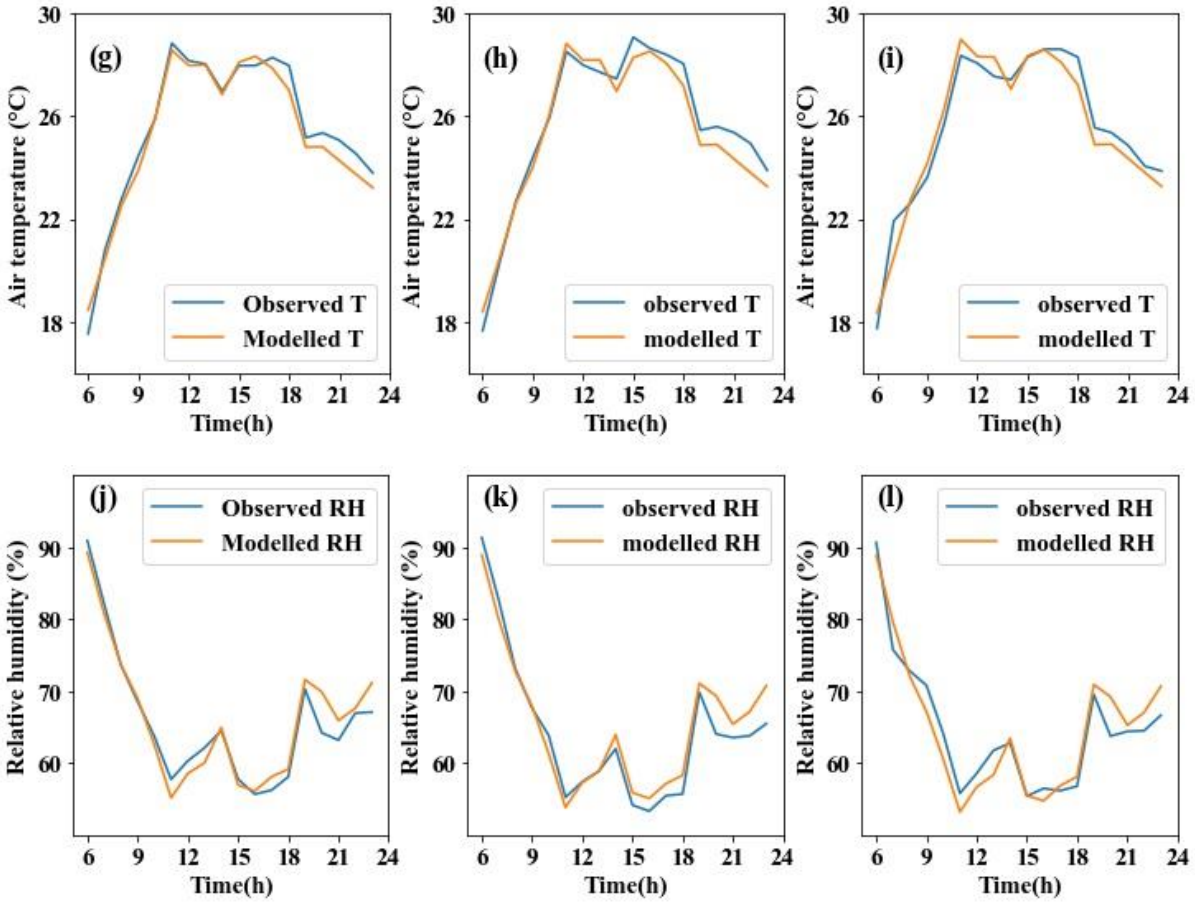

Figure 5. 2 Comparisons of simulation results with observations on 13rd, February for 6 sites on Jeffery (J1, J2 and J3) and Rugby Street (R1, R2 and R3).

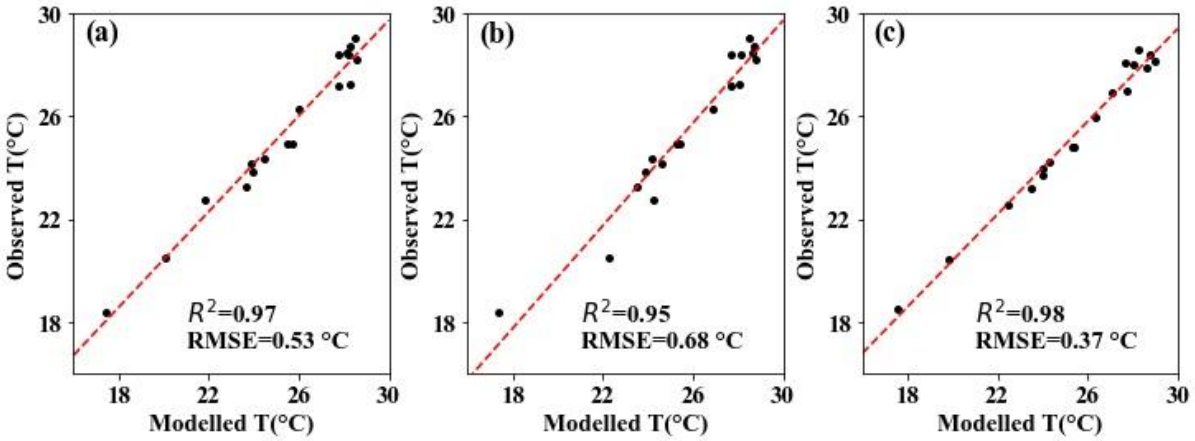

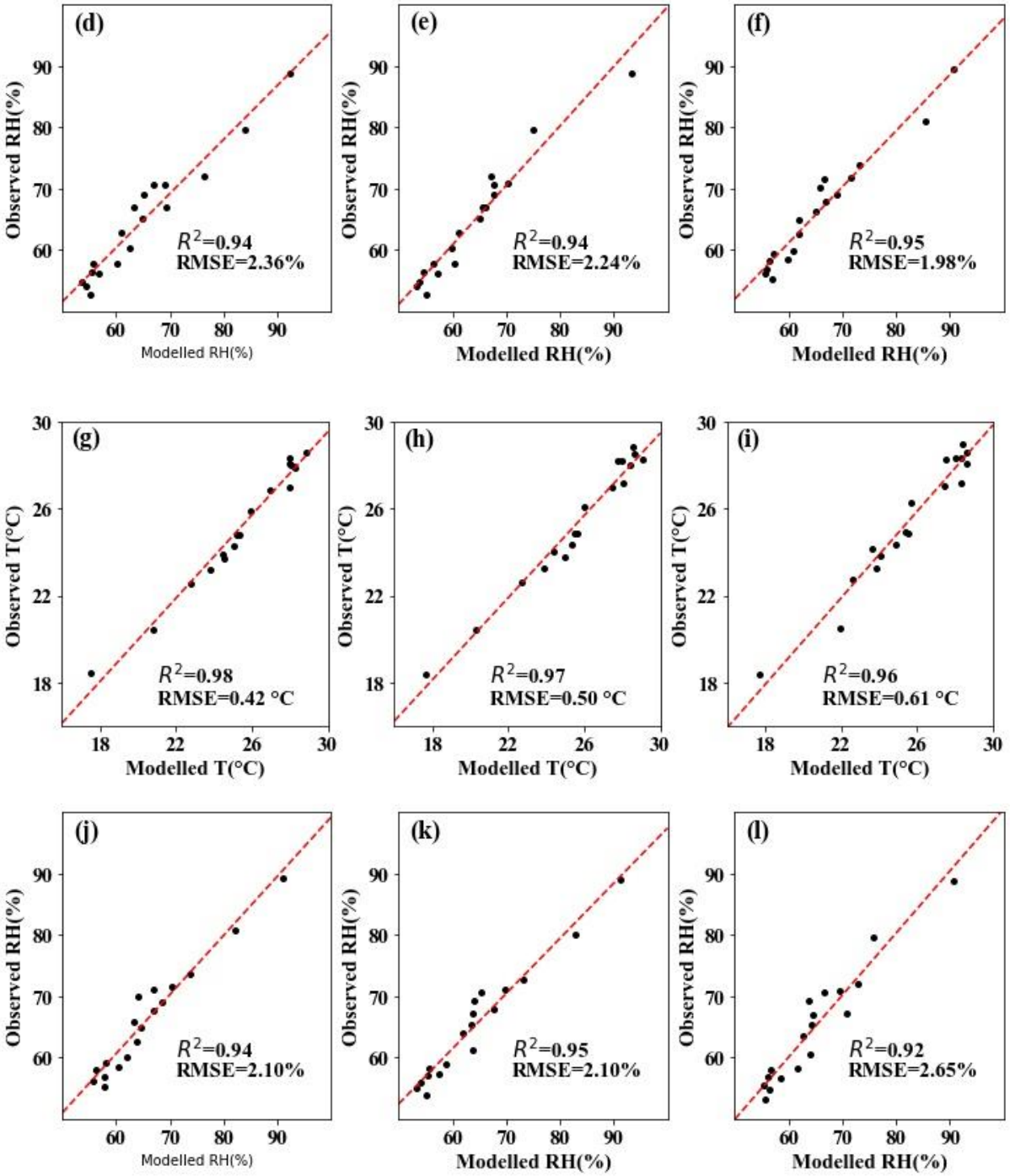

Figure 5. 3 Scatter plots showing the linear regressions of simulation results with observations on 13rd, February for six sites on Jeffery (a-f) and Rugby Streets (g-l).

According to Figure 5.2, the simulated results are highly correlated with observations for the 6 sites on both streets. By comparing simulated and observed air temperature on Jeffery Street, the R^2 values of the linear regressions are 0.97, 0.95 and 0.98 and the corresponding RMSE values are 0.53 °C, 0.68 °C and 0.37 °C for site J1, J2 and J3, respectively. On Rugby

Street, the R^2 values are 0.98, 0.97 and 0.96 and the RMSE values are 0.42 °C, 0.50 °C and 0.61 °C for air temperature at site R1, R2 and R3, respectively. This model also performs well in simulating relative humidity with the R^2 values of all linear regressions being higher than 0.9 (Figure 5.3).

In real urban environment, air temperature is affected by multiple local factors and some of them are not considered in ENVI-met model, such as anthropogenic heat generated from car emissions and indoor activities. Therefore, it is reasonable that there are some slight differences between observations and simulations. Overall, the evaluation confirms the accuracy of ENVI-met in simulating urban microclimate in the metropolitan Adelaide.

5.2.6 Scenario analysis

With the consideration of the spatial pattern of houses and typical sizes of surface elements (vegetations, streets and houses), multiple scenarios are designed for our controlled simulation. In this scenario analysis, the model runs from 6:00, 13rd, Feb, 2020 to 0:00, 14th, Feb, 2020 with a time interval of 1 hour and the input meteorological data are taken from West Terrace weather station. For each scenario, a domain with the size of 400 m × 400 m × 32 m is established. It is made up of 5 m × 5 m × 1.6 m grids. The domain is divided into four square blocks of the same size and the side length of each block is therefore 200 metres. Inside each block, two rows of houses are distributed in arrays and the distances between neighbouring arrays are set to be 30 metres. The width of each house is set as 20 metres. In order to generate domains with the surface properties being similar to those of Hawthorn, the distribution of vegetation is set on the basis of the typical spatial pattern of Hawthorn. Specifically, standard trees are set in arrays near sidewalks of the streets.

In this study, I propose to analyse air temperature and thermal comfort under multiple scenarios with different settings of building height, canyon orientation and wind speed. In this way, the roles of urban structure and wind condition on thermal environment could be well understood. In suburban Adelaide, street canyons are commonly arranged in rows with E – W, N – S, NW – SE or NE – SW orientations. In addition, studies have demonstrated different characteristics of air advection under heterogeneous patterns of street canyons compared to those under homogeneous patterns (Cheng et al., 2021; Camelli et al., 2006). Therefore, canyons with mixed orientations have also been considered. Consequently, six

types of canyon orientations are designed: (1) E – W; (2) N – S; (3) NW – SE; (4) NE – SW; (5) Combination of N – S and E – W orientations; (6) Combination of NE – SW and NW – SE orientations. Meanwhile, the heights of houses in suburban Adelaide are mostly lower than 13 metres. Therefore, I set four levels of building heights in this scenario analysis, including 4 metres, 8 metres and 12 metres and a mixed level combining 4-metre and 12-metre buildings.

According to Sect. 4.3.2, the averaged wind speed is about 4 m/s in the coastal area of Adelaide during sea breeze events. The value decreases to about 2 m/s when the influences of sea breezes disappear. Therefore, 2 m/s and 4 m/s are set as representative values of wind speed in our controlled modelling. Correspondently, the effects of urban characteristics on thermal behaviour can be well compared under different wind intensities during sea breezes.

Overall, four settings of building height, six settings of canyon orientation and two settings of wind speed are configurated in this scenario analysis (Figure 5.4). By permutation and combination with different settings of these three variables, 4 * 6 * 2 = 48 scenarios are configurated in total.

As is shown in Figure 5.4, I have assigned labels for representing different settings of building height, canyon orientation and wind speed. Correspondently, the name of a scenario is the combination of these labels. For example, for the scenario with 4-metre building height, E – W canyon orientation and 4 m/s wind speed, the name is ‘A=4’.

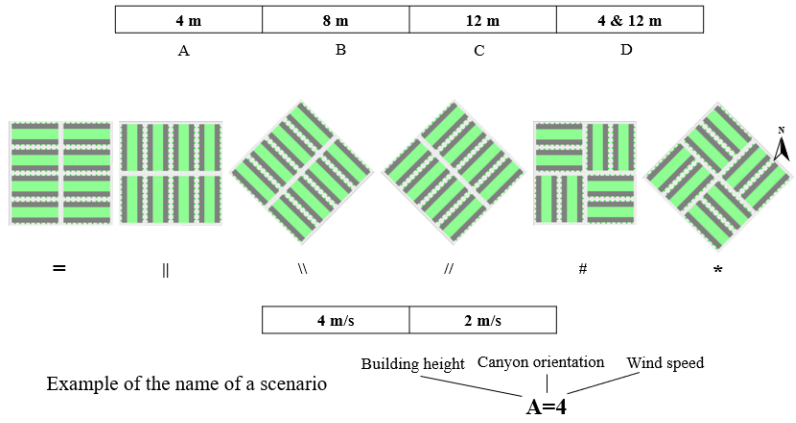

Figure 5. 4 *Settings of building height, canyon orientation and wind speed in the ENVI-met simulation in this study. White colour represents road areas, grey colour represents building areas, light green areas represent vegetation areas and deep green dots represent trees.*

5.2.7 Thermal comfort index

Thermal comfort or heat stress of residents relies on multiple meteorological factors and physical conditions of humans. Dozens of criteria have been proposed which are appropriate for different synoptic backgrounds. Particularly, physiological equivalent temperature (PET) has been widely used in evaluating the thermal comfort level of urban areas. PET is defined as the air temperature at which the heat balance of human body is achieved under a typical indoor setting. This index has the advantage that it is effective in all seasons and climate types, and it considers the physiological aspects of human bodies . The input variables of its calculation include air temperature, mean radiant temperature, wind speed, relative humidity, and geographic location. In this study, the index of PET is adopted to analyse the thermal comfort levels under individual scenarios. They are calculated by ENVI-met package BioMet. The detailed calculation method of this index has been introduced by Höppe (1999). Thermal comfort is a subjective perception and residents in different climate zones have various ideas on whether the environment is comfortable or not with the same PET value. Therefore, I propose to use a standard to classify thermal comfort levels in the study area. In this study, the standard proposed by Kenawy et al. (2018) based on a study in Melbourne is adopted as the climate of Melbourne is similar to that of Adelaide. Specifically, the thermal comfort levels are classified into four groups: (1) slightly warm (25 °C – 30 °C); (2) warm (30 °C – 35 °C); (3) hot (35 °C – 40 °C); (4) very hot (> 40 °C).

5.3 Results

5.3.1 Diurnal variation of mean air temperature

Figure 5.5 is plotted to demonstrate the diurnal variations of mean air temperatures of all 48 scenarios. For all scenarios, there are rapid increases of air temperatures since 6:00 (ranging from 18.19 °C to 18.69 °C). Unlike most cities in which the temperatures peak in the afternoon, in this sea breeze day the maximum air temperatures appear at about 11:00 (ranging from 27.75 °C to 29.53 °C). From 11:00 to 14:00, there is a temperature reduction by about 1.5 – 3 °C because of the cooling effect from prevailing sea breezes. With the weakening of sea breeze cooling, the temperatures increase again from 14:00 to 16:00. After this period, air temperatures drop rapidly resulted from the reduced absorbed net radiation.

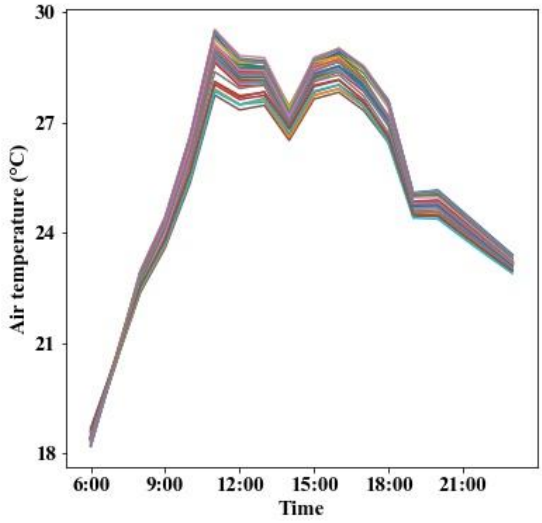

Figure 5. 5 Temporal variations of mean air temperatures of all 48 scenarios during 6:00 – 23:00

There are temperature contrasts of more than 0.9 °C among the 48 scenarios during 10:00 - 18:00 (Figure 5.6). In contrast, the corresponding contrasts are relatively small in most of the nighttime. Specifically, the differences between the 25^{th} and 75^{th} percentiles of the temperature distributions for all the scenarios are less than 0.15 °C during 19:00 - 23:00 when there is limited sunlight. In fact, caused by shadows of buildings and trees, there is a large contrast of absorbed net radiation in different locations during the daytime rather than nighttime. Therefore, it can be derived that the spreads of air temperatures among scenarios are largely explained by different absorption ratios of solar radiation during the daytime. According to the meteorological data of this day, sea breeze cooling is strongest at 14:00. As there is a relatively large variation in air temperature among scenarios at this time point, 14:00 is selected in the following analyses.

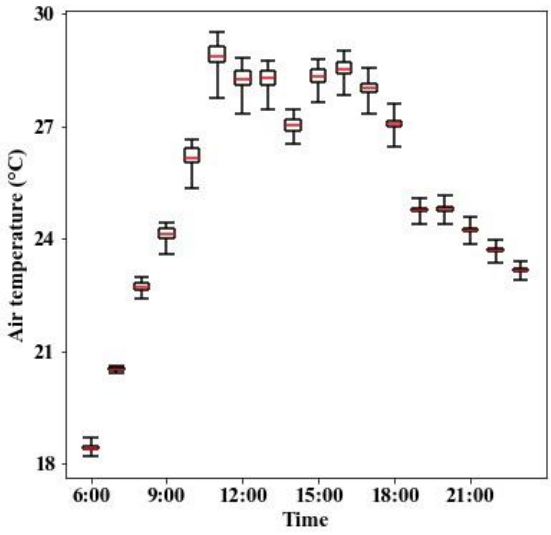

Figure 5. 6 Boxplots showing the diurnal variations of air temperatures of the case-study area aggregated over all 48 scenarios.

5.3.2 Distribution of air temperature of individual scenarios

The spatial patterns of air temperature at 14:00 for all 48 scenarios configurated in this study can be seen from Figure A.4 and Figure 5.7 shows the corresponding boxplots. It should be noted that the values are obtained at the height of 1.4 metres as it is close to the pedestrian level. Summarized over all scenarios, air temperatures range from 25.73 °C to 28.43 °C at this time point. For scenarios with the same building height and canyon orientation, 4 m/s wind shows markedly better effect in cooling air than 2 m/s wind. In addition, building height and canyon orientation both play significant roles in affecting air temperature inside the area. In order to analyse the significance of the effects of environmental factors on air temperature, a N-way ANOVA analysis is performed. The result shows that the *p* values of the three variables in this ANOVA analysis are all zero and therefore these variables influence air temperature significantly during the study period.

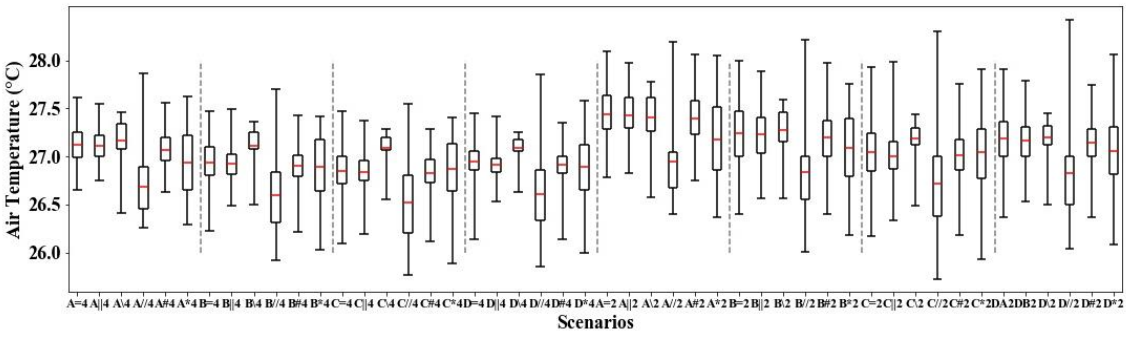

Figure 5. 7 Boxplots showing the distributions of air temperatures of individual scenarios at 14:00 (1.4-metre height). In each boxplot, the boundaries of the lower whisker and upper whisker represent the minimum and maximum value, respectively. The horizontal line inside each box represents the mean value of the distribution of air temperature. The box is drawn from the 25th percentile to the 75th percentile of the distribution.

There are three factors considered in this scenario analysis. In order to quantify the effect of a single factor on air temperature during sea breezes, I aggregate air temperatures over all scenarios with each setting of the factor together in the following analysis. For example, the result of 'A (4m)' is the aggregation of results over all 12 scenarios with 4-metre building height.

Figure 5.8 shows the distributions of air temperatures for the four settings of building height. According to the result, a declining trend of air temperature with increased building height is demonstrated, which is considered to be mainly resulted from stronger shading effect with higher buildings. For scenarios with 4-metre building height, the averaged air temperature is 27.16 ℃. The value decreases to 27.02 ℃ with 8-metre buildings and 26.92 ℃ with 12-metre buildings. For scenarios with mixed building heights (4 and 12 metres), the mean air temperature over all scenarios is 26.99 ℃, which is slightly lower than that of 8-metre height. This implies that heterogeneous building height is more likely to cool the urban environment than homogeneous building height with the same settings of building density. This is reasonable as different building heights inside an area can contribute to the convection of air and enhance the penetrative effects of sea breeze cooling. For the purpose of examining the significances of differences induced by building height, one-way ANOVA analyses are performed among the four groups of scenarios. The result shown in Table 5.3 reveals that the *p* value of the ANOVA analysis is less than 0.05 for each pair of groups. Therefore, it can be derived that any change in building height in this scenario setting results in significant variation in thermal environment.

Table 5. 3 The *p* values of individual pairs of groups aggregated over scenarios with different building heights.

p value	4m	8m	12m	4&12m
4m	/	0.00	0.00	0.00
8m	/	/	0.00	0.00
12m	/	/	/	0.00
4&12m	/	/	/	/

It should also be noted that the minimum air temperature inside the area drops faster than the maximum air temperature with the increase of building height. Specifically, the difference of minimum air temperature between groups of scenarios with 4-metre and 12-metre building height is 0.35 °C, while the corresponding contrast is only 0.19 °C for the maximum air temperature.

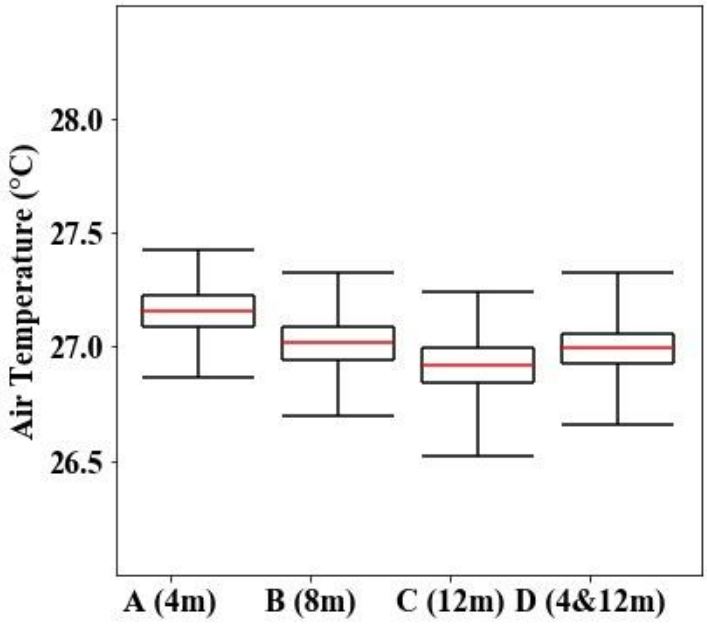

Figure 5. 8 Boxplots showing the quantitative effects of building height on air temperature. Each boxplot indicates the distribution of air temperature aggregated over scenarios of all wind speeds and canyon orientations for each building height (4-metre, 8-metre, 12-metre, 4-metre & 12-metre) at 14:00 (1.4-metre height). In each boxplot, the boundaries of the lower whisker and upper whisker represent the minimum and maximum values. The horizontal line inside each box represents the mean value of the distribution of air temperature. The box is drawn from the 25th percentile to the 75th percentile of the distribution.

The simulation results can also be classified into six groups with different canyon orientations. For canyons with E – W and N – S orientations, the mean air temperatures within the case-study area are similar, being 27.09 °C and 27.08 °C, respectively (Figure 5.9). The temperature is the highest with NW – SE canyon orientation, being 27.19 °C. This is because the arrays of houses are orthogonal to the direction of the prevailing sea breezes and the existence of these houses can stop the penetration of wind towards the leeward area. Therefore, the cooling effect of wind is limited in a small area. Meanwhile, the mean air temperature with NE – SW canyon orientation is lower than those with other three homogenous orientations, being only 26.72 °C. The difference of averages among other five canyon orientations is 0.10°C, while the difference between NE – SW and the lowest of the other five orientations is 0.36°C, more than three times larger. For this canyon orientation, a large positive scatter of the temperature distribution is observed. This can be explained by the excessively high temperatures of tiny areas between neighbouring corridors (Figure A.4). With strong winds penetrating through the corridors, the airflows inside these tiny areas are hardly affected by the neighbouring corridors. Therefore, the temperatures are likely to be high in these areas. It is also important to note that the mean air temperature changes nonlinearly with canyon orientation. When canyon orientation changes from N – S to NE – SW, there is a temperature drop of 0.36 °C, while an increase of 0.11 °C is detected from N – S to NW – SE. For the group of scenarios with heterogeneous canyon orientations combining N – S and E – W, the mean air temperature of 27.06 °C is lower than those with homogeneous orientations of N – S and E – W, respectively. However, this phenomenon does not appear for the group with the heterogeneous orientations combining NW – SE and NE – SW as the averaged air temperature is 27.00 °C. Therefore, I can conclude that the effect of heterogenous orientations relies on the specific components of canyon orientations.

The same as the analysis of four groups with diverse building heights, one-way ANOVA analyses have also been performed for all the pairs of groups with different canyon orientations. As all the *p* values for individual pairs are less than 0.05 (Table 5.4), it can be derived that any change in canyon orientation in this scenario setting can lead to evident variation of air temperature.

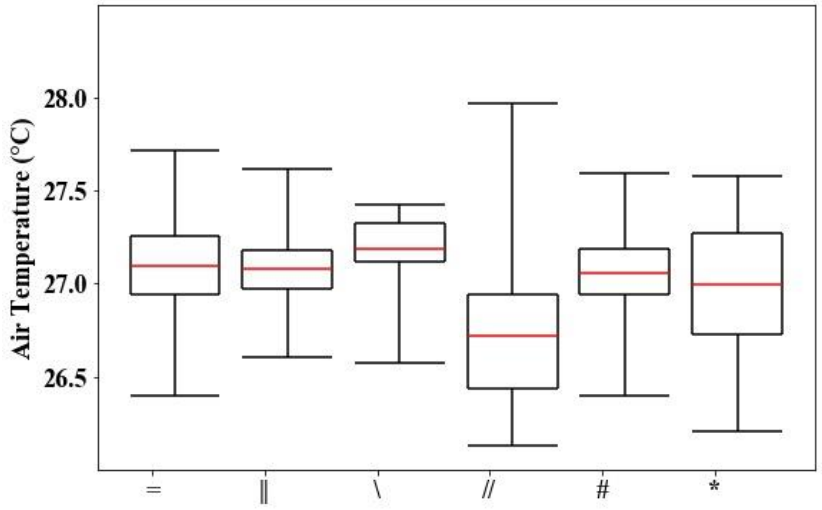

Figure 5. 9 Boxplots showing the quantitative effects of canyon orientation on air temperature. Each boxplot indicates the distribution of air temperature aggregated over scenarios of all wind speeds and building heights for each canyon orientation (E – W, N – S, NW – SE, NE – SW, E – W & N – S, NW – SE & NE - SW) at 14:00 (1.4-metre height). In each boxplot, the boundaries of the lower whisker and upper whisker represent the minimum and maximum values. The horizontal line inside each box represents the mean value of the distribution of air temperature. The box is drawn from the 25th percentile to the 75th percentile of the distribution.

Table 5. 4 The *p* values of individual pairs of groups aggregated over scenarios with different building heights.

p value	‖	=	//	\\	#	*
‖	/	0.00	0.00	0.00	0.00	0.00
=	/	/	0.00	0.00	0.00	0.00
//	/	/	/	0.00	0.00	0.00
\\	/	/	/	/	0.00	0.00
#	/	/	/	/	/	0.00
*	/	/	/	/	/	/

Wind speed is a key factor in influencing air temperature. Figure 5.10 shows the distribution of air temperature for scenarios with 4 m/s wind and 2 m/s wind respectively. According to this figure, the averaged air temperature for scenarios with 2 m/s wind is 27.14 °C and it drops to 26.91 °C with 4 m/s wind. Thus, a temperature reduction of 0.23 °C is detected for this 2 m/s increase of wind speed. As for the maximum air temperature, the corresponding cooling magnitude is stronger as the temperature contrast between the two groups of

scenarios is 0.28 °C. According to the one-way ANOVA analysis, this difference is significant ($p<0.05$).

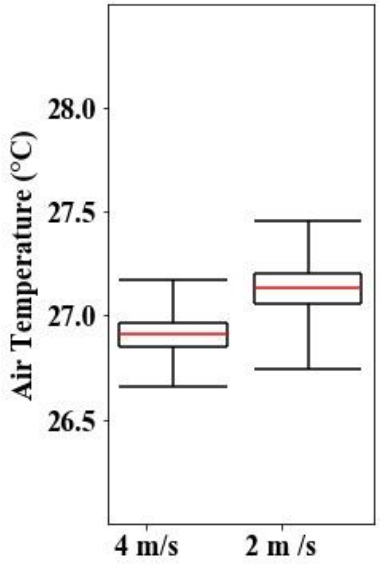

Figure 5. 10 Boxplots showing the quantitative effects of wind speed on air temperature. Each boxplot indicates the distribution of air temperature aggregated over scenarios of all canyon orientations and building heights for each canyon orientation (2 m/s and 4 m/s) at 14:00 (1.4-metre height). In each boxplot, the boundaries of the lower whisker and upper whisker represent the minimum and maximum values. The horizontal line inside each box represents the mean value of the distribution of air temperature. The box is drawn from the 25th percentile to the 75th percentile of the distribution.

In addition to shielding solar radiation, varying building density of urban environment takes effect on airflow inside the urban canopy. Therefore, the magnitude of sea breeze cooling is influenced by building height. Sea breeze cooling can be demonstrated by subtracting simulation result aggregated over all scenarios with 4 m/s wind from that with 2 m/s wind. The result in Figure 5.11 reveals a declining trend of sea breeze cooling with increasing building height from 4 metres to 12 metres. With 4-metre buildings, mean air temperature drops from 27.30 °C to 27.02 °C with the increased wind speed and the corresponding cooling is 0.28 °C. Meanwhile, the cooling magnitude is 0.25 °C with 8-metre buildings and 0.17 °C with 12-metre buildings. Therefore, increased building height can not only generate cooling by increasing the shading area of cities, but also impair cooling by resisting the penetration of cooler winds from surrounding areas. It shows that the enhanced cooling from increased shading controls the process if wind is not strong enough. It can also be derived that the reduced cooling from wind blocking effect is likely to prevail over the shading effect if wind speed is higher than a threshold or the sunlight is not strong enough.

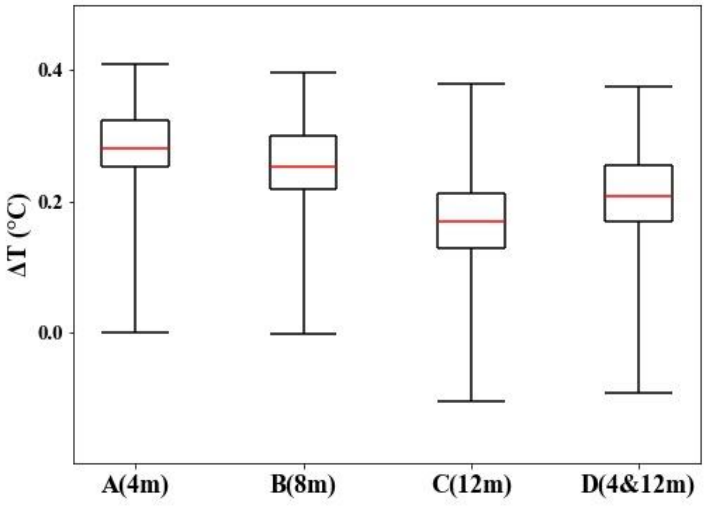

Figure 5. 11 Boxplots showing the quantitative effects of building height on sea breeze cooling induced by the increase of wind speed from 2 m/s to 4 m/s. Each boxplot indicates the distribution of air temperature aggregated over scenarios of all wind speeds and canyon orientations for each canyon orientation (2 m/s and 4 m/s) at 14:00 (1.4m height).

There are also differences in sea breeze cooling among multiple groups of scenarios with different canyon orientations. According to Figure 5.12, for scenarios with E – W and N – S orientations, the averaged magnitudes of sea breeze cooling are similar, being 0.27 ℃ to 0.26 °C, respectively. The cooling power of scenarios with NE – SW canyon orientation is slightly lower, being 0.23 ℃. The minimum cooling (0.15 ℃) appears under scenarios with NW – SE orientation which is orthogonal to the prevailing wind direction of sea breezes. For two scenarios with heterogeneous canyon orientations, the magnitudes of sea breeze cooling are 0.26 ℃ and 0.20 ℃.

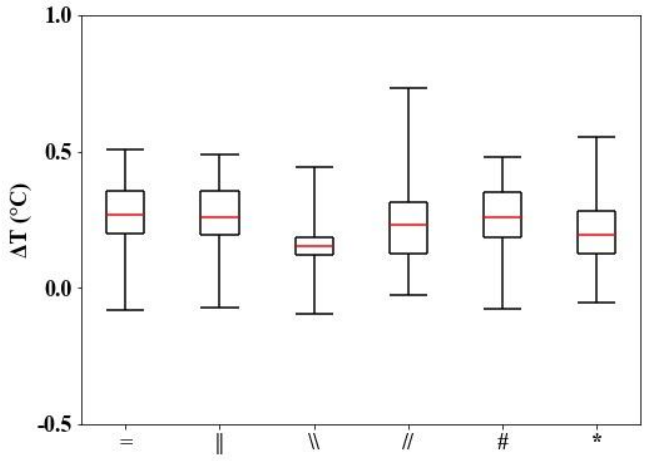

Figure 5. 12 Boxplots showing the quantitative effects of canyon orientation on sea breeze cooling induced by the increase of wind speed from 2 m/s to 4 m/s. Each boxplot indicates the distribution of air temperature aggregated over scenarios of all wind speeds and building heights for each canyon orientation (2 m/s and 4 m/s) at 14:00 (1.4m height).

5.3.3 Distribution of thermal comfort level of individual scenarios

The effects of environmental variables on the distribution of thermal comfort levels inside the case-study area are also estimated by comparing the aggregating scenarios. The spatial patterns of PET at 14:00 for all 48 scenarios are shown in Figure A.5 and the distributions of PET levels with different settings of building height, canyon orientation and wind speed are estimated in this analysis. The percentages in columns represent the area proportions of comfort levels of individual settings. According to Figure 5.13, there is a notable drop of the proportion of "very hot" area from 28% to 16% with the increase of building height from 4 to 12 metres. Correspondently, the proportion of "warm" area increases from 0% to 10%. This confirms that the cooling induced by increased building height can be reflected in the improvement of residents' thermal comfort levels.

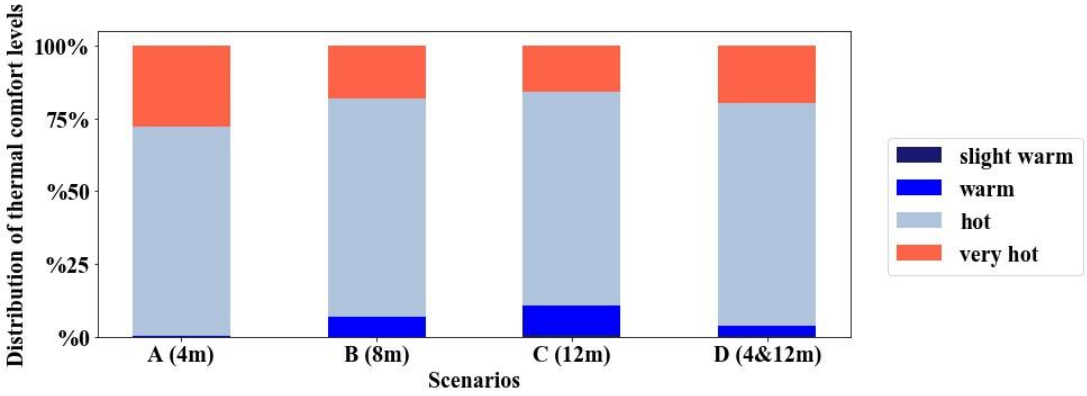

Figure 5. 13 Bars showing the quantitative effects of building height on thermal comfort level. Each bar indicates the distribution of thermal comfort level aggregated over scenarios of all wind speeds and canyon orientations for each building height (4-metre, 8-metre, 12-metre, 4-metre &12-metre) at 14:00 (1.4-metre height).

According to the bars shown in Figure 5.14, "very hot" areas occupy 7% and 8% of the whole case-study area on average for E – W and N – S canyon orientations, respectively. However, for scenarios with NW – SE orientation, more than 70% of the area is classified as "very hot". Therefore, it can be concluded that the high temperatures caused by the resistance of wind penetration can largely deteriorate the comfort level of local residents during heatwave events. It is also important to note that a much larger proportion of "slightly warm" area (9%) is generated in scenarios with the canyon orientation parallel to the prevailing wind direction (NE – SW). The corresponding ratios are all less than 2% for other three homogenous canyon orientations. Overall, this result confirms the key role of canyon orientation in improving thermal comfort during hot days. To enhance the cooling from ventilation effect of urban areas, canyon orientation should be arranged to be as parallel to the prevailing wind direction as possible.

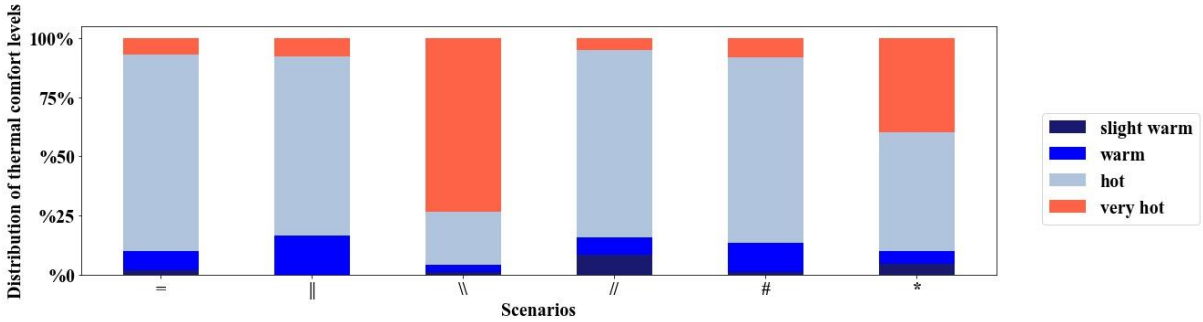

Figure 5. 14 Bars showing the quantitative effects of canyon orientation on thermal comfort level. Each bar indicates the distribution of thermal comfort level aggregated over scenarios of individual canyon orientations.

A comparison of PET values between scenarios with different wind speed also reveals a large contrast (Figure 5.15). About 54% of the area is classified as “very hot” with 2 m/s wind, while the percentage drops to only 6% with 4 m/s wind. Correspondently, the proportion of “warm” area increases from 2% to 7% with the increase of background wind speed.

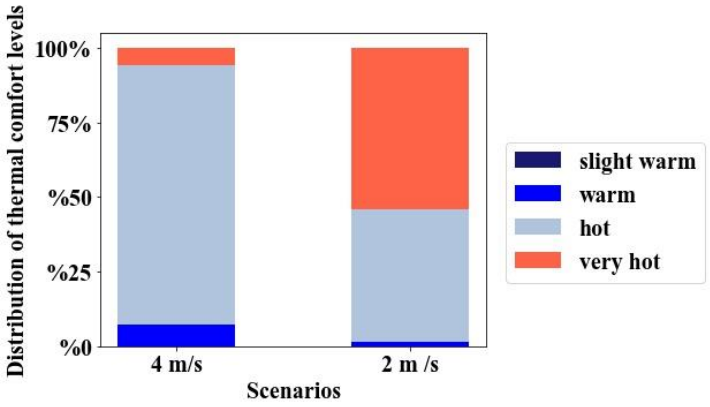

Figure 5. 15 Bars showing the quantitative effects of wind speed on thermal comfort level. Each bar indicates the distribution of thermal comfort level aggregated over scenarios of individual wind speeds.

5.4 Discussion

5.4.1 The effects of urban structure and wind speed on air cooling

Optimizing urban structure and promoting ventilation have long been seen as potential approaches in improving the urban thermal environment. It is important to have a good understanding of the quantitative effects of these factors on air temperature and thermal comfort levels.

Previous researches have observed the competing effects of increased building height on urban thermal environment. Because of the reduced solar radiation absorbed, increased building height is expected to cool the urban area. For example, an increase of height/width ratio from 0.5 to 2 can cool the urban air by nearly 1 °C in Sao Paulo, Brazil (Muniz-Gäal et al., 2020). On the other hand, higher obstacles can enhance the resistance of wind penetration inside the city and is not beneficial for ventilation cooling of urban areas. At city scale, it has been observed that limited wind speed is linked to buildings with larger frontal area indexes (Wong et al., 2013). The understanding of the combined consequences of the two contrasting effects is limited. In this study, it is revealed that the shading cooling prevails over the wind

cooling in a typical sea breeze day of Adelaide. Results also show that the relative role of wind cooling is strengthened with the increase of wind speed. Therefore, it can be derived that wind cooling could be stronger than shading cooling when the wind speed reaches a threshold or the shading effect is limited. Due to the limitation of data availability, the threshold has not been estimated in this study. In future studies, it's necessary to have a further look at the respective effects of wind cooling and shading cooling with different settings of urban structure.

The results also demonstrate that there is a non-linear change of air temperature with canyon orientation. This is expected to be caused by different types of the interactions of prevailing winds with buildings. If there is a large difference between the prevailing wind direction and canyon orientation, wind cooling effects of the local environment are similar among different setups of canyon orientation. In contrast, thermal environment can be largely improved even with a small change in canyon orientation if the canyon orientation is close to the prevailing wind direction.

5.4.2 Implications for urban planning

The focus of this study is to understand the roles of urban structure and wind condition in urban thermal environment, and it aims to provide insights on urban planning. According to the results, the background weather conditions should be seriously considered before creating a climate-friendly urban design. For most cities without significant background wind conditions, appropriate increase of building heights can mitigate urban heat at penetration level by reflecting more solar radiation. Meanwhile, for cities with prevailing wind settings, more attention should be paid on the utilization of ventilation. In the process of urban design, the main wind path should be well designed as buildings had better be distributed parallelly to the prevailing wind path. This is particularly important for high-density cities.

5.5 Conclusions

In urban design, urban structure is an important factor worthy of further consideration. An appropriate urban design can mitigate heat excess and improve the thermal environment during hot days. However, the combined effects of wind condition and urban structure on urban climate are not well understood. In this study, I select the coastal city of Adelaide to investigate

the effects of these environmental factors on thermal environment in a sea breeze event based on simulation results of ENVI-met model. Particular attention is paid on the effect of urban structure on wind cooling induced by sea breezes.

Comparisons of simulation results with observations show that ENVI-met performs well in simulating micro-climate of the metropolitan Adelaide. Differences in air temperatures and thermal comfort levels have been detected with various settings of environmental variables, especially during the daytime. According to the comparison among all 48 scenarios at 14:00, building height, canyon orientation and wind speed all have significant influences on air temperature inside the area. A reduction of mean air temperature from 28.43 °C to 25.73 °C is detected with an increase of building height from 4 metres to 12 metres, which is mainly resulted from the enhanced shading effect of buildings. Meanwhile, air temperature changes nonlinearly with canyon orientation. When canyon orientation varies from N – S to NE – SW, there is a temperature decrease of 0.36 °C. With the change from N – S to NW – SE, an increase of 0.11 °C is identified. The existence of temperature differences among canyon orientations can be largely explained by the different extents of wind penetration inside the area. In addition, change in wind speed from 2 m/s to 4 m/s causes a temperature reduction of 0.23 °C on average.

The magnitude of sea breeze cooling is influenced by urban structure. Specifically, the mean cooling magnitude induced by increasing wind speed (from 2 m/s to 4 m/s) is negatively related to the averaged building height. With 4-metre buildings, the cooling is 0.28 °C, the corresponding value drops to 0.17 °C with 12-metre buildings. This shows the contrasting effects of increased building height on thermal environment of urban areas. On one hand, larger shading area is expected to reduce air temperature. On the other hand, resistance of wind penetration from building surfaces can decrease wind cooling. Overall, the shading effect plays the dominant role in this scenario analysis. With respect to canyon orientation, NW – SE which is orthogonal to the prevailing wind direction of sea breezes shows a much lower magnitude of cooling (0.15 °C).

The impacts of urban structure and wind speed on thermal comfort levels have also been investigated. Specifically, the proportion of “very hot” area changes from 28% to 16 % with the increase of building height from 4 to 12 metres. An averaged contrast of 48% of “very hot” area is found between scenarios with 2 m/s wind and 4 m/s wind. The result also highlights the key role of canyon orientation in improving thermal comfort during hot days. To enhance the

cooling from ventilation effect, canyon orientation should be arranged to be as parallel to the prevailing wind direction as possible.

In urban planning, appropriate layouts of buildings and street canyons are important in cities with sea breezes or other prevailing winds. However, it should be noted that this study is on the basis of a typical sea breeze event of the coastal city of Adelaide. In future research works, more attention should be paid on different background wind conditions, such as valley breezes or large-scale synoptic winds.

References

Aboelata A. Vegetation in different street orientations of aspect ratio (H/W 1: 1) to mitigate UHI and reduce buildings' energy in arid climate. Building and Environment. 2020 Apr 1;172:106712.

Bentham T, Britter R. Spatially averaged flow within obstacle arrays. Atmospheric Environment. 2003 May 1;37(15):2037-43.

Camelli F, Lohner R, Hanna S. VLES study of flow and dispersion patterns in heterogeneous urban areas. In44th AIAA Aerospace Sciences Meeting and Exhibit 2006 Jan (p. 1419).

Chatzidimitriou A, Yannas S. Street canyon design and improvement potential for urban open spaces; the influence of canyon aspect ratio and orientation on microclimate and outdoor comfort. Sustainable cities and society. 2017 Aug 1;33:85-101.

Cheng WC, Liu CH, Ho YK, Mo Z, Wu Z, Li W, Chan LY, Kwan WK, Yau HT. Turbulent flows over real heterogeneous urban surfaces: Wind tunnel experiments and Reynolds-averaged Navier-Stokes simulations. InBuilding Simulation 2021 Oct (Vol. 14, No. 5, pp. 1345-1358). Tsinghua University Press.

Davis RE, McGregor GR, Enfield KB. Humidity: A review and primer on atmospheric moisture and human health. Environmental research. 2016 Jan 1;144:106-16.

DESA U. World Urbanization Prospects: The 2018 Revision, online ed. New York: Population Division, UN DESA. 2018.

Emmanuel R, Johansson E. Influence of urban morphology and sea breeze on hot humid microclimate: the case of Colombo, Sri Lanka. Climate research. 2006 Apr 26;30(3):189-200.

Fahmy M, Sharples S. On the development of an urban passive thermal comfort system in Cairo, Egypt. Building and Environment. 2009 Sep 1;44(9):1907-16.

Giannaros TM, Melas D. Study of the urban heat island in a coastal Mediterranean City: The case study of Thessaloniki, Greece. Atmospheric Research. 2012 Nov 15;118:103-20.

Höppe, P. (1999). The physiological equivalent temperature–a universal index for the biometeorological assessment of the thermal environment. International journal of Biometeorology, 43(2), 71-75.

Kenawy I, Elkadi H. The outdoor thermal benchmarks in Melbourne urban climate. Sustainable cities and society. 2018 Nov 1;43:587-600.

Krüger EL, Minella FO, Rasia F. Impact of urban geometry on outdoor thermal comfort and air quality from field measurements in Curitiba, Brazil. Building and Environment. 2011 Mar 1;46(3):621-34.

Li G, Ren Z, Zhan C. Sky View Factor-based correlation of landscape morphology and the thermal environment of street canyons: A case study of Harbin, China. Building and Environment. 2020 Feb 1;169:106587.

Li J, Wang Y, Ni Z, Chen S, Xia B. An integrated strategy to improve the microclimate regulation of green-blue-grey infrastructures in specific urban forms. Journal of Cleaner Production. 2020 Oct 20;271:122555.

Lin M, Hang J, Li Y, Luo Z, Sandberg M. Quantitative ventilation assessments of idealized urban canopy layers with various urban layouts and the same building packing density. Building and environment. 2014 Sep 1;79:152-67.

Llaguno-Munitxa M, Bou-Zeid E, Hultmark M. The influence of building geometry on street canyon air flow: validation of large eddy simulations against wind tunnel experiments. Journal of Wind Engineering and Industrial Aerodynamics. 2017 Jun 1;165:115-30.

Morris CJ, Simmonds I, Plummer N. Quantification of the influences of wind and cloud on the nocturnal urban heat island of a large city. Journal of Applied Meteorology and Climatology. 2001 Feb 1;40(2):169-82.

Muniz-Gäal LP, Pezzuto CC, de Carvalho MF, Mota LT. Urban geometry and the microclimate of street canyons in tropical climate. Building and Environment. 2020 Feb 1;169:106547.

Ng E, Chen L, Wang Y, Yuan C. A study on the cooling effects of greening in a high-density city: An experience from Hong Kong. Building and environment. 2012 Jan 1;47:256-71.

Oke TR. Initial guidance to obtain representative meteorological observations at urban sites.

Peng LL, Jiang Z, Yang X, He Y, Xu T, Chen SS. Cooling effects of block-scale facade greening and their relationship with urban form. Building and Environment. 2020 Feb 1;169:106552.

Shi D, Song J, Huang J, Zhuang C, Guo R, Gao Y. Synergistic cooling effects (SCEs) of urban green-blue spaces on local thermal environment: A case study in Chongqing, China. Sustainable Cities and Society. 2020 Apr 1;55:102065.

Strømann-Andersen J, Sattrup PA. The urban canyon and building energy use: Urban density versus daylight and passive solar gains. Energy and buildings. 2011 Aug 1;43(8).

Taleghani M, Kleerekoper L, Tenpierik M, Van Den Dobbelsteen A. Outdoor thermal comfort within five different urban forms in the Netherlands. Building and environment. 2015 Jan 1;83:65-78.

Tsoka S, Tsikaloudaki A, Theodosiou T. Analyzing the ENVI-met microclimate model's performance and assessing cool materials and urban vegetation applications - A review. Sustainable cities and society. 2018 Nov 1;43:55-76.

Wang W, Ng E. Large-eddy simulations of air ventilation in parametric scenarios: comparative studies of urban form and wind direction. Architectural Science Review. 2018 Jul 4;61(4):215-25.

Wang W, Wang X, Ng E. The coupled effect of mechanical and thermal conditions on pedestrian-level ventilation in high-rise urban scenarios. Building and Environment. 2021 Mar 15;191:107586.

Wong MS, Nichol JE. Spatial variability of frontal area index and its relationship with urban heat island intensity. International Journal of Remote Sensing. 2013 Feb 10;34(3):885-96.

Yang J, Wang Y, Xiu C, Xiao X, Xia J, Jin C. Optimizing local climate zones to mitigate urban heat island effect in human settlements. Journal of Cleaner Production. 2020 Dec 1;275:123767.

Yang S, Zhou D, Wang Y, Li P. Comparing impact of multi-factor planning layouts in residential areas on summer thermal comfort based on orthogonal design of experiments (ODOE). Building and Environment. 2020 Sep 1;182:107145.

Zhang L, Zhan Q, Lan Y. Effects of the tree distribution and species on outdoor environment conditions in a hot summer and cold winter zone: A case study in Wuhan residential quarters. Building and Environment. 2018 Feb 15;130:27-39.

Chapter 6 Concluding remarks

6.1 Conclusions

In the context of climate change and continuous urbanization over the world, there is an increasing need of improving thermal environment of urban areas. In coastal cities, the sea breeze plays a non-negligible role in shaping urban climate. By exploring the effect of sea breezes on air temperature and the corresponding influencing factors, this study aims at providing insights on urban planning of coastal cities. The summary of each chapter is shown as follows.

In Chapter 2, the metric of Sea Breeze Cooling Capacity (SBCC) is proposed by being considered as the difference between air temperature of a sea breeze day and that of the average of non-sea breeze days. In the Adelaide Central Business District (CBD), I have revealed the temporal and spatial patterns of SBCC and examined their associations with environmental variables using data from the Adelaide urban heat island monitoring network during 2010 - 2013. A large contrast in SBCC is found between western and eastern parts of the Adelaide CBD. This demonstrates the attenuation of the cooling power as the sea breeze passes around high-rise buildings. There is a key finding that the inter-event variability of SBCC can be explained by specific humidity and wind speed, while the spatial variability is primarily affected by Frontal Area Index (FAI), Terrain Ruggedness Index (TRI), distance towards the coast and temperature prior to the sea breeze onset. It should be noted that sea breeze cooling can be enhanced by the increased diversity of building heights, while mean building height, as intuitively expected, reduces SBCC. Based on the relationship between urban structure and SBCC, a potential change of sea breeze cooling inside the Adelaide CBD has been predicted.

Overall, I made a comprehensive observation analysis of sea breeze cooling capacity and explored its interactions with urban structure. The Adelaide CBD is a dense urban area widely covered by high-rise buildings. Therefore, the results demonstrate that the arrangement of buildings with different heights is important for high-density areas of coastal cities as it is strongly related to the heat mitigation from sea breeze cooling of these areas.

In Chapter 3, the basic characteristics and cooling abilities of sea breezes are investigated inside the whole metropolitan area of Adelaide. According to the result, a delaying trend of arrival time and an advanced trend of cessation time of sea breeze cooling are clearly shown

from coast to inland. Correspondently, a decreasing trend of SBCC is identified and the average value is estimated to be 21.3 °C·h.

There is a new finding that SBCC values averaged over hot sea breeze days are particularly smaller (sea breeze days with maximum temperatures above the 75th percentile of all sea breeze days) compared to that averaged over other sea breeze days in most of the sites. The differences are gradually getting larger from coast to inland. Correspondently, the mean penetration distance in hot sea breeze days is only 29 km, about 13 km lower than that in all sea breeze days. Attention needs to be paid that the penetration distance of sea breeze cooling shown here is conceptually different from that of a sea breeze, although they are both relevant. Based on the analysis of synoptic background of the surrounding area, this difference can be explained by a higher proportion of days with systems of directional flows from east or south-east in hot sea breeze days of Adelaide.

In addition, result from a multiple linear regression indicates that the distance from the coast and elevation at the onshore point account for 88% of the spatial variability of the temporally average SBCC totally. Overall, these results can contribute to a better understanding of the spatial pattern of sea breeze cooling in coastal cities where a large number of people reside.

As there is no study that systematically compares basic characteristics and cooling magnitudes of sea breezes among multiple cities, investigations on sea breezes of major Australian cities have been performed in Chapter 4. It reveals a large diversity in frequency of sea breeze events among the five coastal cities (Perth, Adelaide, Melbourne, Brisbane and Sydney) ranging from 17% to 56%, which can be explained by different frequency of days with anti-cyclone systems. Results also show that topography of the metropolitan area significantly influences wind patterns. For the three cities with regular topographies (Perth, Adelaide and Melbourne), frequency of days with anti-cyclone systems has significant effects on the magnitudes of seasonal SBCC of coastal sites, with the R^2 being 0.80. In contrast, the corresponding relation is weak for inland sites, which is considered to be resulted from the effects of land surfaces. Overall, the study in Chapter 4 of this thesis for the first time compares the characteristics and cooling effects of sea breezes among cities. It reveals the importance of synoptic backgrounds in influencing sea breezes.

Finally, ENVI-met, a commonly used micro-climate model, is used to explore the quantitative effects of urban structure and wind speed on air temperature and thermal comfort level in a typical sea breeze day of Adelaide. According to the comparison among all 48

scenarios at 14:00, building height, canyon orientation and wind speed all have significant influences on air temperature inside the case-study area. Meanwhile, mean air temperature has been found to change nonlinearly with canyon orientation. The result also highlights the key role of canyon orientation in improving thermal comfort during hot days. To enhance the cooling from ventilation effect, canyon orientation should be arranged to be as parallel to the prevailing wind direction as possible.

It is important to note that this study reveals the contrasting effects of increased building height on thermal environment. More shading areas are expected to reduce air temperature, but the resistance of wind penetration from larger building surfaces can generate less wind cooling. With 4-metre buildings, the cooling magnitude caused by the increase of wind speed from 2 m/s to 4 m/s is 0.28 °C, while the corresponding magnitude decreases to 0.17 °C with 12-metre buildings.

Overall, this thesis for the first time proposes the metric of Sea Breeze Cooling Capacity and performs a quantitative analysis of sea breeze cooling and the impact factors at different spatial scales. It is helpful for a systematic understanding of the cooling effect induced by sea breezes. The key findings increase the knowledge on the mitigation of heat stress of urban areas.

Key findings of this thesis include: 1) Increase in the diversity of building heights can strengthen sea breeze cooling; 2) Sea breeze cooling in hot days attenuates faster than that in other days along the ventilation path in Adelaide, which is supposed to be resulted from large-scale synoptic backgrounds; 3) When comparing multiple cities, frequency of days with anti-cyclone systems is positively related to seasonal cooling of sea breezes for coastal sites; 4) With the increased building height, the cooling induced by stronger wind decreases.

These findings can provide new insights for policymaking towards climate-friendly urban design to utilize the sea breeze. For example, an incremental heterogeneity of building heights and a decline in average building height are preferred for urban planning of cities with regular winds. The results are also helpful in further investigations on public health and energy consumption. However, the urban characteristics of the study area are relatively simple as there are few buildings with the height being higher than 100 metres. The climate types of major Australian cities are Mediterranean climate and humid subtropical climate. The wind cooling in other climate types still needs to be further investigated.

6.2 Recommendations for future studies

In Chapter 2 and 3, the spatial patterns of SBCC in Adelaide have been analysed at different scales. In fact, the metropolitan area of Adelaide is mostly composed of a plain. For cities with more complicated topographies, such as Sydney and Brisbane, the wind analysis shows that the characteristics of sea breezes are inapparent. However, due to the limitation of observation data, sea breeze cooling in these cities has not been well investigated. Therefore, it is recommended to have further studies on the temporal and spatial patterns of temperature and sea breeze cooling using dense monitoring networks in coastal cities with different topographies. Specifically, the effects of curvature of coastline, mountains and bays should be precisely quantified.

In this study, the cooling magnitudes of sea breezes are concerned. In fact, the penetration distance of sea breeze cooling is different from that of a sea breeze itself although there are some relations between them. The inland penetration of the sea breeze cannot generate the cooling effect in some areas, especially those far from the coast or with complicated topographies. In the future work, it is recommended to have a more detailed analysis of the interaction between the air dynamics inside the urban canopy and the cooling effects during sea breezes. This is helpful for understanding the mechanism of sea breeze cooling.

Similar to sea breezes, other types of mesoscale winds exist inside or near cities, such as mountain-valley breezes. It is still not well understood how urban characteristics affect their interactions with urban climate. Therefore, long-term studies of the thermal environment in cities with frequent mesoscale winds can be a potential research topic.

Appendices

A1. Frontal area index (FAI) and Terrain ruggedness index (TRI)

Frontal area index (FAI) is defined as the ratio of total facet area perpendicular to the wind direction over the total plain area (Wong et al., 2010). Note that only the first windward facet is considered in the frontal area index as wind is almost blocked by the first windward buildings. The calculation of this index is given in Eq. (A.1):

$$\mathrm{FAI} = {A_{\mathrm{facets}}}\Big/{A_{\mathrm{plane}}} \tag{A.1}$$

where FAI is the frontal area index, A_{facets} is the total area of building facets perpendicular to the wind direction, and A_{plane} is the total plane area defined as the area of the square with a selected square size centred at the corresponding site. According to this definition, the larger FAI is, the larger part of wind will be blocked by buildings in a specific plane area, and thus the lower wind speed will be. Here I calculate FAI based on the southwesterly wind according to the major wind direction during sea breeze events in Adelaide. Terrain ruggedness index (TRI) is originally defined to quantify the heterogeneity of elevations inside a region and it has been widely used to explore the influence of topography on species distribution (Nellemann et al., 1995; Riley et al., 1999). In this study, I expand its application by using this index to demonstrate the diversity of building heights to quantify the relationship between urban structure and SBCC. To be specific, it is calculated as the standard deviation of the sub-grid heights inside a square centred at the corresponding site as shown in Eq. (A.2)

$$\mathrm{TRI} = \sqrt{\frac{1}{N}\sum(H_{i,j} - \bar{H})^2} \tag{A.2}$$

where $H_{i,j}$ is the building height of the corresponding grid inside the square shown in Figure A.1, H is the average building height of the square and N ($=n^2$) is the number of grids in the square.

$H_{1,1}$	$H_{1,2}$	$H_{1,3}$	...	$H_{1,n}$
$H_{2,1}$	$H_{2,2}$	$H_{2,3}$	...	$H_{2,n}$
$H_{3,1}$	$H_{3,2}$	$H_{3,3}$	...	$H_{3,n}$
...	...	...	...	...
$H_{n,1}$	$H_{n,2}$	$H_{n,3}$	...	$H_{n,n}$

Figure A. 1 Illustration of a square with different building heights in the calculation of TRI. n is the square size.

A2. The representativeness of the study period for climate in Adelaide

In order to validate the representativeness of our study period (summer days from December 2010 to March 2013, period A) for the climate in Adelaide, I perform an analysis of the weather condition for 15 years (summer days from December 2002 to March 2017, period B) in comparison with our study period. Based on the data from Adelaide Airport weather station, I calculate the averaged diurnal temperature fluctuation of sea breeze days and non-sea breeze days for the two periods, respectively. The result shown in Figure A.2 indicates that there is a good consistency between them. So, I conclude that the weather background during our study period can represent the climate in Adelaide well.

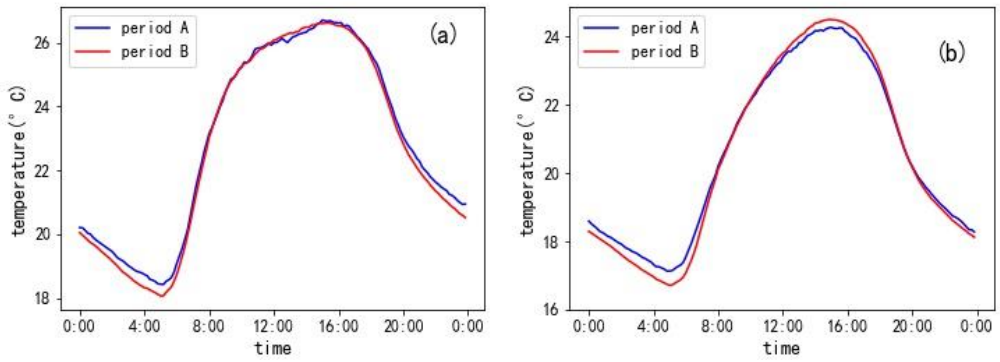

Figure A. 2 Averaged diurnal temperature fluctuation at Adelaide Airport station during period A (summer days from Dec 2010 to Mar 2013) and period B (summer days from Dec 2002 to Mar 2017) for sea breeze days(a) and non-sea breeze days(b), respectively

A3. Illustration of diurnal cycle of air temperature, wind direction and specific humidity in a selected day

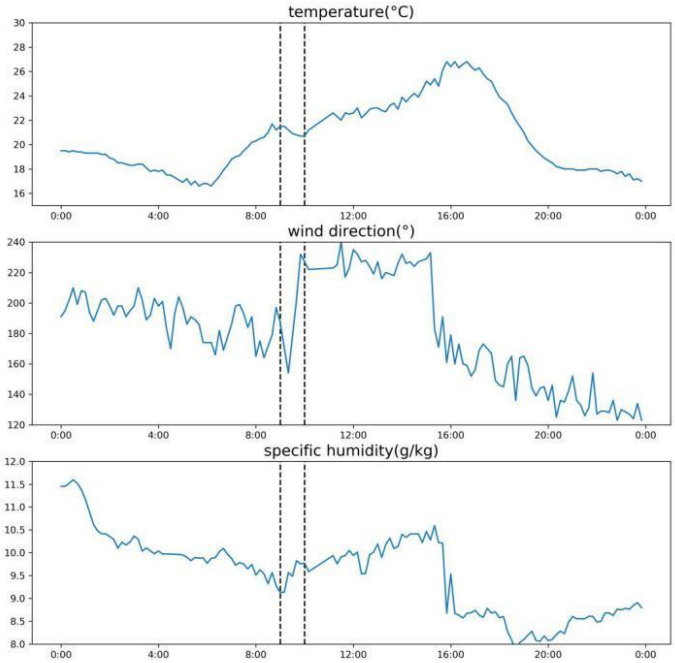

Figure A. 3 Diurnal cycle of air temperature, wind direction and specific humidity at a selected day (16th Feb 2012) at Adelaide Airport Station. The two vertical dashed lines represent time of sea breeze onset (9:00 LST) and one hour after the onset (10:00 LST).

A4. R-square of the regression of SBCC with urban structure and weather conditions using different square sizes for FAI and TRI

Table A. 1 R-square of the regression of SBCC with urban structure and weather conditions using different square sizes for FAI and TRI

Resolution(m)	50	70	90	110
R^2	0.64	0.79	0.76	0.73

A5. Spatial patterns of air temperature and PET at 14:00 for all 48 scenarios

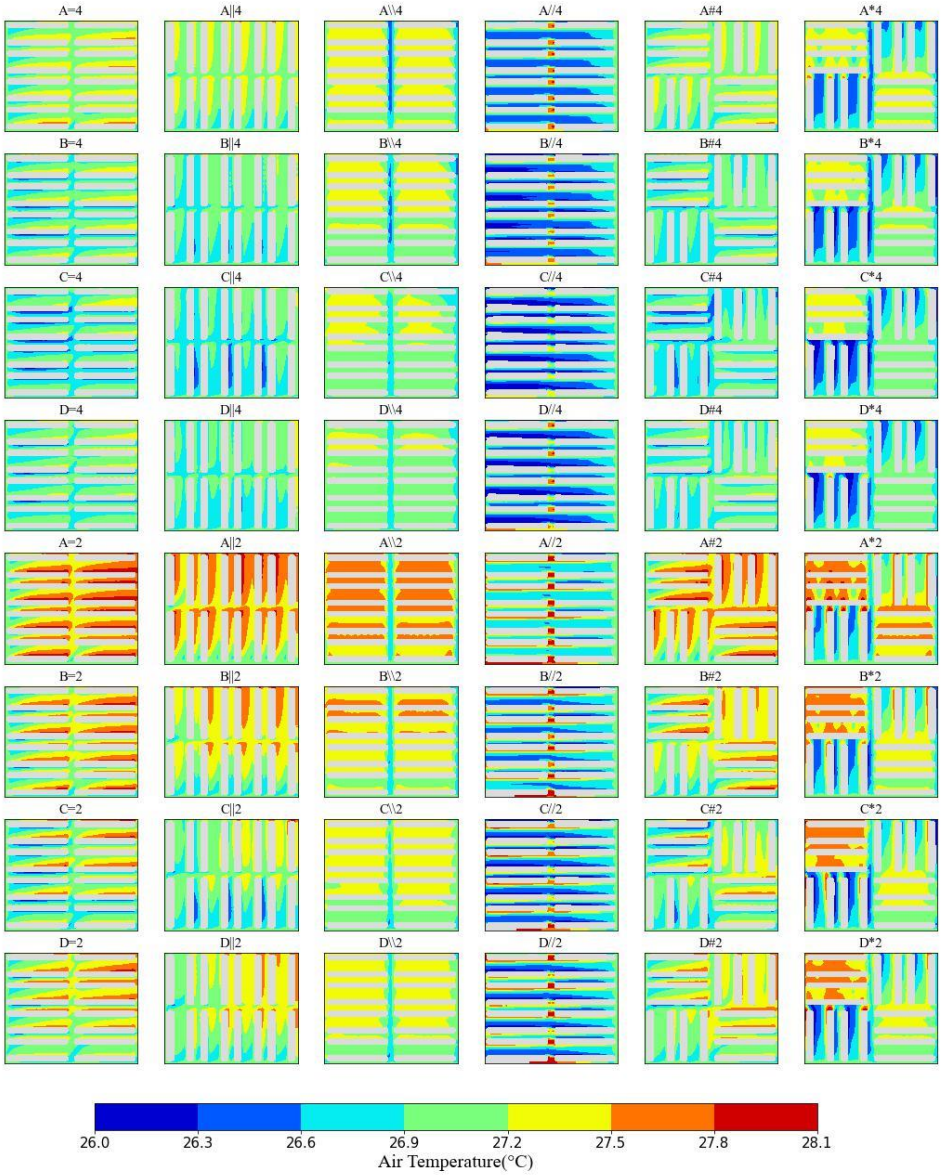

Figure A. 4 Spatial patterns of air temperature at 14:00 for all 48 scenarios configurated in the study of ENVI-met simulation in Chapter 5. The grey areas in the domains represent houses in the simulated areas.

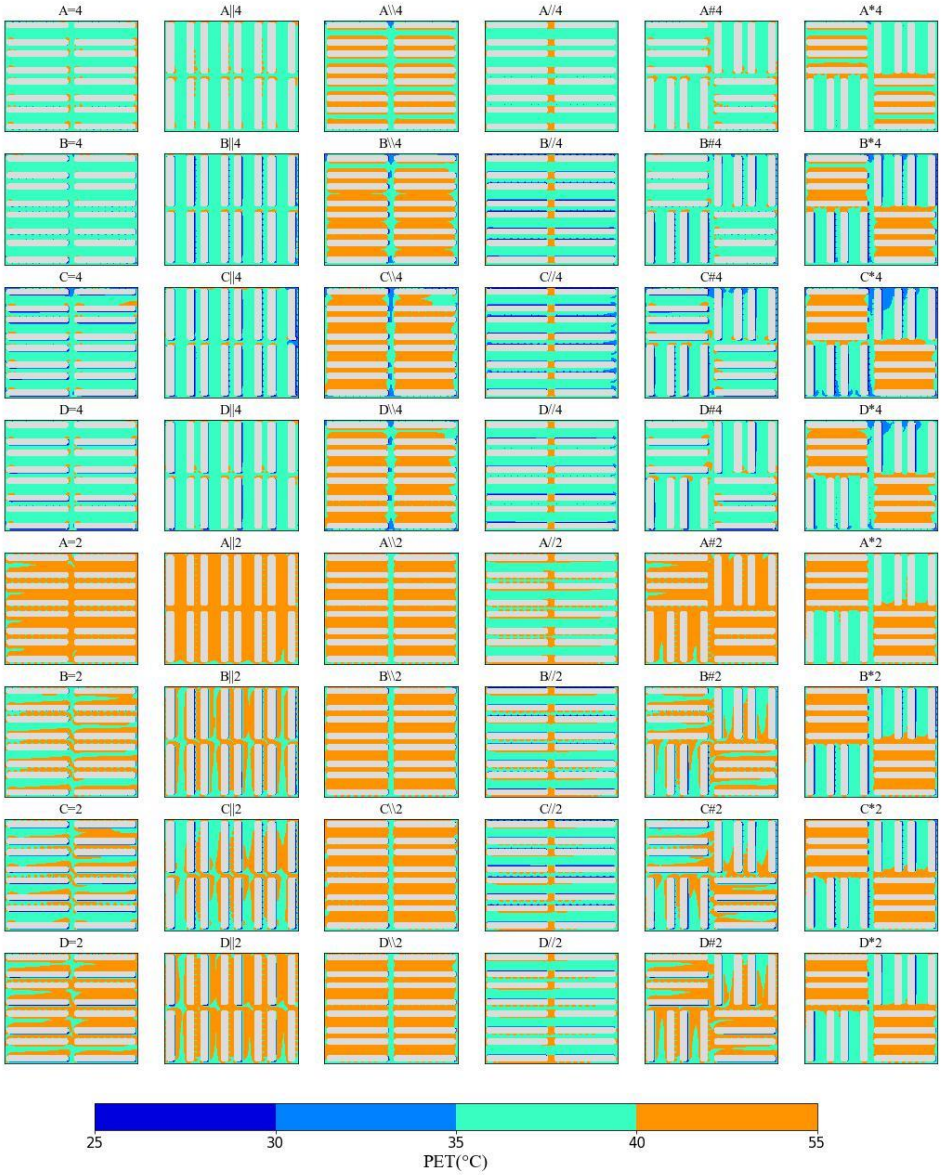

Figure A. 5 Spatial patterns of PET at 14:00 for all 48 scenarios configurated in the study of ENVI-met simulation in Chapter 5. The grey areas in the domains represent houses in the simulated areas.

References

Nellemann C, Fry G. Quantitative analysis of terrain ruggedness in reindeer winter grounds. Arctic. 1995 Jun 1:172-6.

Riley SJ, DeGloria SD, Elliot R. Index that quantifies topographic heterogeneity. intermountain Journal of sciences. 1999 Dec;5(1-4):23-7.

Wong MS, Nichol JE, To PH, Wang J. A simple method for designation of urban ventilation corridors and its application to urban heat island analysis. Building and Environment. 2010 Aug 1;45(8):1880-9.